Design, Modelling, and Control of an Ambidextrous Robot Arm

By

Mashood Mukhtar

A Thesis Submitted in Partial Fulfilment of the
Requirements for the Degree of
DOCTOR OF PHILOSOPHY

Department of Electronic and Computer Engineering
College of Engineering, Design and Physical Sciences
BRUNEL UNIVERSITY LONDON

July 2020

Abstract

This thesis presents the novel design of an ambidextrous robot arm that offers double range of motion as compared to dexterous arms. The proposed arm is unique in terms of design (ambidextrous feature), actuation (use of two different actuators simultaneously: Pneumatic Artificial Muscle (PAM) & Electric Motor)) and control (combined use of Proportional Integral Derivative (PID) with Neural Network (NN) for the hand and modified Multiple Adaptive Neuro-fuzzy Inference System (MANFIS) controller for the arm). The primary challenge of the project was to achieve ambidextrous behavior of the arm. Thus, a feasibility analysis was carried out to evaluate possible mechanical designs. The secondary aim was to deal with control issues associated with the ambidextrous design. Due to the ambidextrous nature of the design, the stability of such a device becomes a challenging task. Conventional controllers and artificial intelligence-based controllers were explored to find the most suitable one. Performances of all these controllers have been compared through experiments, and combined use of PID with NN was found to be the most accurate controller to drive the ambidextrous robot hand. In terms of ambidextrous robot arm control, a solution based on forward kinematic and inverse kinematic approach is presented, and results are verified using the derived equation in MATLAB. Since solving inverse kinematics analytically is difficult, Adaptive Neuro-Fuzzy Inference system (ANFIS) is developed using ANFIS MATLAB toolbox. When generic ANFIS failed to produce satisfactory results, modified MANFIS is proposed. The efficiency of the ambidextrous arm has been tested by comparing its performance with a conventional robot arm. The results obtained from experiments proved the efficiency of the ambidextrous arm when compared with a conventional arm in terms of power consumption and stability.

Dedication

This thesis is wholeheartedly dedicated to my beloved parents, who have been my source of inspiration and gave me strength when I thought of giving up, who continually provide moral, spiritual, emotional and financial support.

To my sisters, relatives, mentor and friends who shared their words of advice and encouragement to finish this thesis.

And lastly, I dedicated this book to the Almighty God Allah SWT, thank you for the guidance, strength, power of mind, for giving me a healthy life and opportunity to complete this thesis.

Declaration

I declare that this thesis is my own work and is submitted for the first time to the Post-Graduate Research Office. The study was originated, composed and reviewed by myself and my supervisors in the Department of Electronic and Computer Engineering, College of Engineering, Design and Physical Sciences, Brunel University London UK. All the information derived from other works has been properly referenced and acknowledged.

SIGNED:..... DATE:.....

Acknowledgements

I want to express my deep sense of gratitude and respect to my supervisor Dr Tatiana Kalganova for her excellent guidance, suggestion, support and the encouragement shown during these years. I consider myself extremely lucky to be able to work under the guidance of such a dynamic personality. I want to thank Dr Ali Mousavi for his support also for being my second supervisor. Big thanks go to Prof Stelarc, who played a key role from giving feedback to evaluating the work, his support, and encouragement.

The author thanks the Department of Electronic and Computer Engineering, Brunel University London for the received support and the staff of the Sustainable Electric Power (SEP) Laboratory for the help in the experimental part of the thesis.

An assemblage of this nature could not have been possible without reference to and inspiration from the works of others whose details are mentioned in the reference section. I acknowledge our indebtedness to all of them.

Special thanks to Dr Emre Akyürek for his initial support and guidance. I was not alone in this long but exciting journey, many people played important role namely Clement Fontaine, Nicoles Lesne and Maxime Degout. I thank them for their valuable support from solving mechanical issues with the structure to Solidworks design.

I want to acknowledge support from Festo for providing pneumatic muscles used for testing and Shadow Robot Company for their valuable feedback, advice and supplying material.

During my PhD, I met some of the brilliant minds in my field namely Dr Dhayaa

Khudher who was working on a robotic leg at Brunel University London. Discussion and time spent with him was very helpful in setting up my direction right.

Finally, I want to thank my family, friends and especially Kinza for supporting me in all those times whenever I felt down.

Contents

List of Figures

List of Tables

List of Acronyms

3D	Three-dimensional	12
AI	Artificial Intelligenc	7
AMO	Artificial Muscle Operated	18
AN	Adaptive Network	99
ANFIS	Adaptive Neuro-Fuzzy Inference System	5
BSC	Backstepping Control	5
CAD	Computer Aided Design	39
CT	Computerized Tomography	12
DH	Denavit Hardenberg	87
DOF	Degrees of Freedom	2
FIS	Fuzzy Inference System	98
FPGA	Field Programmer Gate Array	30
GWM	Great Wall Motors	15
HH	Human Hand	10
HIT	Harbin Institute of Technology	15
IFR	International Federation of Robotics	14

LSE	Least Square Error	103
MANFIS	Multiple Adaptive Neuro-fuzzy Inference System	ii
MCU	Microcontroller Unit	32
MF	Membership Function	100
MLP	Multi-Layer Perception	75
NN	Neural Network	ii, 5
PAM	Pneumatic Artificial Muscle	ii
PID	Proportional Integral Derivative	ii, 5
PPSC	Phasing Plane Switch Control	76, 77
PWM	Pulse Width Modulation	32
RBFN	Radial Basis Function Network	30
SCARA	Selective Compliance Assembly Robot Arm	20
SEP	Sustainable Electric Power	v
sPAM	series Pneumatic Artificial Muscles	31
UNECE	United Nations Economic Commission for Europe	14

List of Symbols

J	Jacobian matrix	98
$\dot{x}$	Velocity in task space	98
θ_f	The angle of each finger	78
f	Finger	77
G	Gravitational force	134
H	The floating base centripetal, coriolis	134
M	Inertia matrix	134
$\ddot{\theta}$	Joint acceleration	134
$\dot{\theta}$	Joint velocity	98
τ	Actuator torque	134

Chapter 1

Introduction

1.1 Introduction

The world is overwhelmed with incredible advances in engineering. Nearly all scientific disciplines including biomedical, art and engineering are seemed to be inspired by nature itself. These advancements have resulted in the production of many robots that are currently being used across various industries [1, 2]. The use of robots not only allows more productivity and safety at the workplace but also saves time and money. The history of robot development goes back to the ancient world [3]. Evolution of robot development started from a simple robot design idea and reached today at a point where most complicated and risky tasks are being handled by robots [4]. A robot arm plays an important role in determining a robot's capability as most of the tasks require some kind of end-effector to complete the task. The adroitness of the human hand to perform complicated operations has resulted in high demand across various industries. Literature reveals much work already completed on the design and control of robotic hands [5–7]. Robotic hands that can offer clever manipulating, grasping, lifting and sense of different objects have always been highly desirable in industry due to their wide scope in many applications such as

teleoperation, mobile robotics, industrial robots and biomedical robotics [8, 9]. This thesis relates to the design, development, modelling and control of the ambidextrous robot arm.

The ambidextrous arm that offers five Degrees of Freedom (DOF) is controlled using five servo motors and the system as a whole offers a unique combination where half of the system is actuated using pneumatic muscles and the rest with servo motors. The ambidextrous robot arm is interlinked with the modified version of pre-developed ambidextrous robot hand. The five finger ambidextrous robot hand offers a total of 14 DOF and it can bend its fingers in both ways left side and right side offering full ambidextrous functionality by using only twenty PAMs. Pneumatic systems are being widely used in many domestic, industrial and robotic applications due to their advantages such as structural flexibility, simplicity, reliability, safety and elasticity. A block diagram of how the ambidextrous robot arm project works is shown in Figure 1.1. To start a task, a user command is given to the Arduino unit. This command is checked internally if it meets the basic requirements of the system such as range of motion. Then, depending on the nature of the task, the robotic arm makes a move. Sensors incorporated on the ambidextrous robot arm provide valuable feedback and the system makes auto adjustments accordingly to complete the task efficiently in the shortest possible time.

Furthermore, a method for finding a neuro-fuzzy based solution to the inverse kinematics problem of the ambidextrous robot arm is investigated. For this purpose, the case of the ambidextrous robot arm is considered, for which computer simulation is performed in order to outline the effectiveness of the approach. By transforming the inverse kinematics problem to a fitting problem, the Adaptive Neuro-Fuzzy Inference System (ANFIS) is trained using the inverse mapping of the data provided by the forward kinematics and learns, with acceptable accuracy, the end-effector's localization to joint angles mapping.

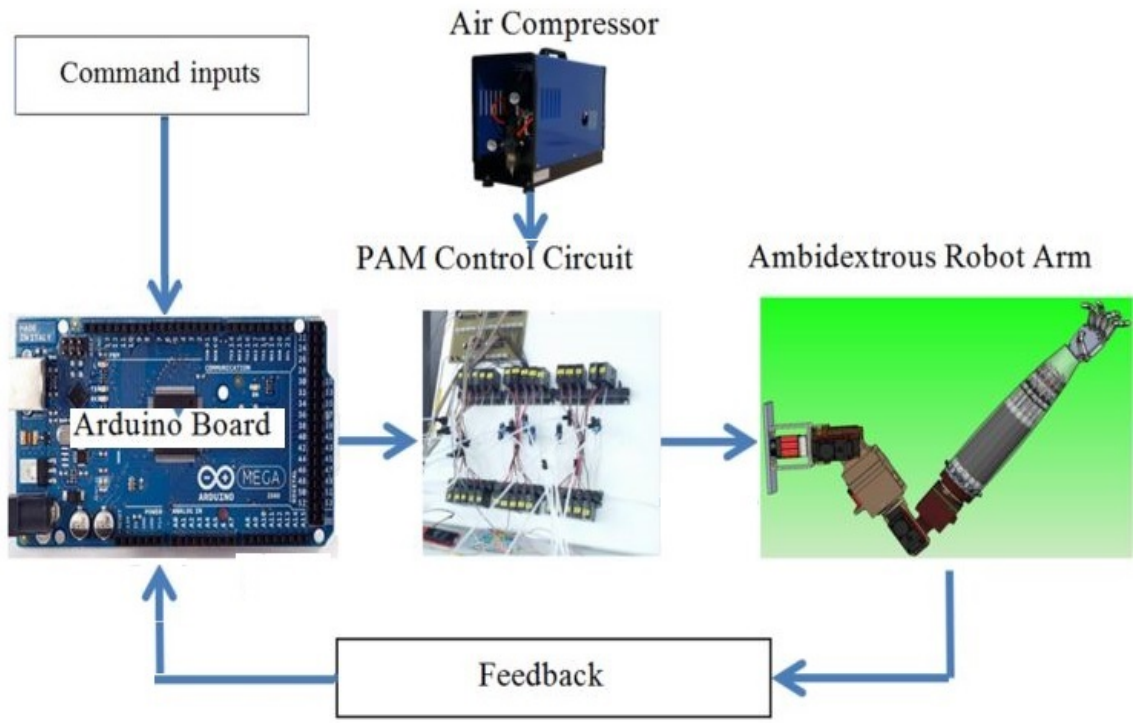

Figure 1.1: Overview of the project.

1.2 Problem Description and Motivation

Ambidextrous design offers greater flexibility in terms of the range of motion, power consumption and efficient use of time to complete a specific task. Systems that meet this criterion are in huge demand as they can not only save cost but also make the whole process more efficient. The ambidextrous robot arm is designed to increase the mechanical possibilities of an anthropomorphic arm. By combining the movements of the right and left arm, the ambidextrous robot arm can produce gestures that are impossible for a human counterpart.

The ambidextrous nature of the project make it appreciable from an artistic point of view too as the system attempts to break the physical constraints defined by Mother Nature. In addition to its artistic purpose, the ambidextrous robot arm can be used

in a situation where it is dangerous for humans to work such as in a radioactive environment, space exploration and dangerous situations. In the biomedical area use of such a unique mechanical model may be useful to overcome phantom limb pain experienced by amputees. Hand gesture recognition or electromyography is employed to offer users video feedback. An amputee can also use an exoskeleton glove for a better experience.

In the past, robotic systems were actuated using either pneumatic muscles, servo motors or hydraulic systems. The ambidextrous approach offers a unique set up where a hand is controlled using Festo PAM and the rest of the arm structure is actuated using servo motors. Control of such a unique actuation system is challenging task. So, to overcome this issue, a modified MANFIS controller is proposed. This thesis is focused on presenting the novel design structure of a robotic arm with ambidexterity, a unique actuation system (that employs PAMs to drive the ambidextrous robot hand and servo motors to control the robot arm respectively) and control of such a complex system using an artificial intelligence based method.

1.3 Aim and Objectives of the Thesis

The project aimed to design, develop and control an ambidextrous robotic arm system that was partially actuated by PAMs and servo motors. The critical part of the design process was breaking the physical constraints attached to each joint of a human arm and finding a controller that could be used to control such a device with an ambidextrous design.

In order to achieve this goal, a feasibility analysis was conducted to see if there was a possibility of breaking Mother Nature constraints on the human arm. As a result, many solutions were considered before finding a simple prototype that confirms the possibility of such a mechanical structure. A comprehensive design-flowchart was followed to move from prototype to the final ambidextrous robotic arm structure.

Furthermore, a Neural Network (NN) based controller was tested first on the ambidextrous robotic hand. Then, the NN controller was compared with the conventional controllers (Proportional Integral Derivative (PID), Bang-bang, Backstepping Control (BSC)). The ambidextrous robotic arm was designed and interlinked with the predesigned modified version of the ambidextrous robot hand. Control of such a device is a significant challenge in the robotics field. An attempt was made to overcome this challenge by first calculating forward and inverse kinematic problems of the arm and then exploring control using Adaptive Neuro-Fuzzy Inference System (ANFIS) based techniques. Finally, a controller that managed to control the ambidextrous structure satisfactorily was proposed.

1.4 Research Contributions

The ambidextrous robot arm project presented in this thesis brings several contributions to science:

- The main contribution of the thesis is to successfully design and implement an ambidextrous robot arm that offers double range of motion in most of the joints than its counterpart (dexterous robotic arms or human arm). The ambidextrous feature itself is unique in the robotics field and does not exist in the literature. This is the first time an ambidextrous robot arm of this nature has ever been designed and implemented.

- The proposed actuator system is unlike any other robotic arm actuator system; it allows the user to control the robot arm through the combined use of PAM and servo motors. The originality of the project is further confirmed by looking at the unique settings of actuators used in this project. In robotics, it is not a common practice to use PAMs as actuators due to PAMs feature of nonlinear effects, slow response time and time-varying parameters. Five servo motors actuate the ambidextrous robot arm, and twenty PAMs drive the ambidextrous

robot hand. So far, none of the robotic systems found in literature deployed such a combined actuation concept to drive the robot arm.

- Control of ambidextrous robot hand: Control of devices with ambidexterity feature is an extremely challenging task. NNs controller is tested on a uniquely designed ambidextrous robot hand and the best controller (combined use of PID with NN) has been identified.

- Control of ambidextrous robot arm: Since the design of the ambidextrous robot arm is unique, none of the controllers found in literature proved useful in controlling the ambidextrous robot arm, so the focus was diverted to find a solution from the range of artificial intelligence based controllers. After careful consideration and testing, a modified MANFIS controller was proposed and extensive guidance related to the setting of the controller was issued for a future researcher who wishes to control devices with an ambidextrous feature.

1.5 Organisation of the Dissertation

- Chapter 1 introduces the topic, describes the problem and research motivations. The aim of the thesis and how this aim is accomplished through research work is presented briefly. Furthermore, research contributions made to the science are outlined explicitly and an organisation of each chapter is given at the end of the chapter.

- Chapter 2 is divided into three parts: 2.1 Review of Existing Robotic Hands, 2.2 Review of Existing Robotic Arms and 2.3 System Architecture for the Robot Arm. It starts with an overview of the literature on the great robotic hand inventions. All these inventions are discussed from control, grasping, sensing and actuation point of view. The literature review is further extended to cover robotic arm designs in detail. Since no ambidextrous robot arm is

found in literature, a gap in the market is identified. Numbers of robotic arms are compared (from design to control point of view) to find out the efficiency of each system and how a future robotic arm (autonomous ambidextrous robot arm) can stand out in terms of design. A trend in improving existing designs of robot arm is noted, but none of them considered a novel structure such as the ambidextrous robot arm that is proposed in this thesis. Justification of equipment used in this project are given at the end of the chapter.

- Chapter 3 gives the reader detailed steps that are involved in designing the ambidextrous robot arm. It starts by defining a base for the ambidextrous robot hand and then moves to the ambidextrous robot arm.

- Chapter 4 presents the control element of the project. First, in regards to ambidextrous robot hand control, the number of conventional controllers such as PID, Bang-bang, BSC and NN is tested to find the most suitable one. PID combined with NN is found to be the best choice for the ambidextrous robot hand. Furthermore, in regards to ambidextrous robot arm control, inverse kinematics and forward kinematics problems are discussed in detail. Since the inverse kinematic problem is a complicated task to compute, artificial intelligence based methods are explored. An Artificial Intelligenc (AI) based controller such as modified MANFIS is found to be the best fit for the ambidextrous robot arm.

- Chapter 5 outlines the key findings of the project. Lessons learnt from various experiments, and key recommendations for further research are made.

1.6 Publications

INTERNATIONAL JOURNAL PUBLICATIONS

- Mukhtar, M., Akyürek, E., Kalganova, T., Nicolas, L., "Neural Network based Control Method Implemented on Ambidextrous Robot Hand". International Journal of Automation and Smart Technology, AUSMT, 7(1): pp.27-32, 2017. ISSN: 2223-9766 doi: 10.5875/ausmt.v7i1.1171

  This journal paper covers contribution of neural network based controller discussed in section 4.1.2 Implementation of Neural Network Based Controller of this thesis.

INTERNATIONAL CONFERENCE PUBLICATIONS

- Mukhtar, M., Akyürek, E., Kalganova, T., Nicolas, L., "Control of 3D printed ambidextrous robot hand actuated by PAMs". 2015 SAI Intelligent Systems Conference (IntelliSys), London, 2015, pp.290-300. DOI: 10.1109/IntelliSys.2015.7361158

  This conference paper covers control section presented in section 4.1.1 Comparison of Conventional Controller of this thesis

BOOK CHAPTER

- Mukhtar, M., Akyürek, E., Kalganova, T., Nicolas, L., "Implementation of PID, Bang–Bang and Backstepping Controllers on 3D Printed Ambidextrous Robot Hand". In: Bi Y., Kapoor S., Bhatia R. (eds) Intelligent Systems and Applications, Studies in Computational Intelligence 650, chapter 9, Springer International Publishing Switzerland, eBook ISBN: 978-3-319-333861; DOI: 10.1007/978-3-319-33386-1 (2016).

This book chapter covers the control section presented in 4.1.1 Comparison of Conventionl Controller.

CHAPTER 2

Literature Review

The aim of this literature review chapter is to summaries the notable triumphant robotic manipulators/arms and compile the references of existing work in the area of the robotics broadly related to the mechanical design and control strategies. Before, reviewing the challenges and futuristic implications of the development of these structures. A brief review of robotic hands is presented in section 2.1 and robotic arms is presented in section 2.2. This chapter helps to find gaps and discuss the possibility of contributions to science. Project requirements and choice of components used to build this project are also discussed in great detail in section 2.3

2.1 Review of Existing Robotic Hands

The Human Hand (HH) has a complicated structure, and it is the key part of the human body. Since mimicking HH involves a high level of complexity, previous attempts were mainly focused on meeting specific purposes [10]. For instance, a five-fingered robotic hand also known as Belgrade/USC Hand [11] was built to offer better-grasping ability and is capable of autonomous adaption. Similarly, a UMDH

hand [1] [12] is intended to function as a general-purpose research tool for the study of machine dexterity and teleportation systems. The term 'teleportation' in robotics means the possibility of being somewhere when you are physically not there. For instance Shadow Robot Company made the world's first haptic telerobot hand that allows users to feel and complete a task without being there. Similarly, Ava [2] Robotics has built a robot that allow users to interact in an environment where the user is not physically present. A five-finger Robonaut hand was developed by NASA [13] to meet the requirements of extravehicular activities. DLR Hand I and DLR hand II were designed with an aim to be used with a variety of arms. Many robotic hands and their key features are listed in Table 2.1.

In the late 1990s, some three-fingered hands and four-fingered hands [14–16] were introduced. Caffaz et al. developed four fingered with 12 degrees of freedom tendon driven named DIST hand in 1997 [17] and later MAC hand an upgrade of DIST that included tactile sensors [18]. A trend of five-fingered hands started in the last two decades, and now almost all robotic hands offer five fingers [19, 20]. Some of the key developments include novel solutions [21] for hand prostheses by a research group at the University of Pisa [22], ACT Hand developed at Carnegie Mellon University to study the behaviour of the hand and for surgical tests [23] and a unique design offered by Research Centre of Karlsruhe that follows exactly HH measurements in terms of link length and number of fingers and is well suited for grasping tasks [24]. A multi-finger hand system with quick finger motion of 180° per 0.1 s along with high-speed visual feedback at a rate of 1 kHz is proposed in [25] to catch falling balls. In [26], a bio-mechatronic approach to design an anthropomorphic artificial hand that is able to mimic the natural motion of the human fingers is proposed.

[1] UMDH is a dexterous hand deveoped by UTAH (The University of Utah) and MIT (Massachusetts Institute of Technology) institute.

[2] Ava is a telepresence robot that combines autonomous mobility with high-definition video conferencing devloped by Ava Robotics.

It is worth mentioning some of the most amazing prototypes built in recent years for instance the design concept of the ambidextrous robot hand [27] and a semi-autonomous anthropomorphic robotic hand developed by Computerized Tomography (CT) technologies that mimic the range of movements, flexibility and sensitivity just like HH [28]. A prototype of a multi-fingered robotic hand named GUH14 has been developed by the University of Calabria and the University of Girona that is to be used underwater for grasping and manipulation operations in a submarine environment [29]. A new mechanism named "twist drive" is introduced in [30] to drive joints of a prototype of the five-fingered robotic hand. A prototype of Three-dimensional (3D) printed open Bionic hand won a Dyson Award for super-fast manufacturing and presenting cost-effective solution [31]. Moley Robotics has created the World's first fully-automated and intelligent cooking robot hand/arm [32]. In the past two decades' several other hands have been proposed, for example the Sven hand, the MARCUS, the Soft hand and the KNU hand [33–35]. The mechanical design and manipulation aspect of the MANUS-HAND is discussed in [36]. A novel robot hand prototype designed with the purpose of being robust and easy to control as an industrial gripper called Pisa/IIT soft hand is introduced in [37]. A prototype called the FRH-4 hand was developed based on a new hybrid concept of an anthropomorphic five-fingered hand and a three jaw robotic gripper [38]. A prototype of a direct-driven optimised and light-mass hand exoskeleton named HEXOSYS II is presented in [39].

The review of existing hands reveals that the ambidextrous hand concept has already been introduced by Dr Emre [40]. Since, ambidextrous mechanical design already exists in the literature, the focus of the presented work was to improve the existing design (see section 3.1 for detailed steps followed to improve the existing pre-developed hand) and to find a better controller than what had already been tried [41].

2.1.1 Robot Hand Control

Research on multi-fingered robotic hands started in the 1960s. Thus, many survey papers [42–44] and books [45–47] on multi-fingered robotic hands can be found in literature. Detailed attention to the control aspect is paid by researchers and as a result many control algorithms have been proposed [48–54]. Although numerous control schemes have been developed for the control of robot hands, PID control remains one of the preferred approaches in different practical robotic systems [55]. The main reason is the intuitiveness in concept and simplicity in the design of the PID control structure. PID control offering the simplest and yet most efficient solution to many real-world robotic control problems. Nevertheless, the use of a classical PID control scheme has at least two key limitations for robotic systems. First, since the feedback gains of a classical PID controller are typically constant, the overall performance of the closed-loop system might be sub-optimal in case of dynamical uncertainties or external perturbations. To solve this issue, different approaches were developed to achieve the automatic tuning of PID gains, like genetic algorithm, fuzzy logic, NN or particle swarm optimisation [56–58]. Second, stability has always been a great concern with PID control in robotic systems, since un-modeled dynamics or disturbances are prone to drive the system out of its designed stability.

This section mainly focuses on finding a possible gap to control the ambidextrous robot hand. Number of conventional controllers have already been tested on the existing ambidextrous robot hand namely PPSC, Bang-bang, SMC, PID and BSC [40, 41]. It is difficult for the traditional controllers to control an ambidextrous hand because of the complexity parameters and nonlinear characteristics. In order to overcome this issue, conventional controller could be combined with Artificial intelligence based controller to achieve better results. Therefore, a Neural Network PID controller is proposed in order to improve the system performance and its robustness. The NN technique is applied to compensate for the effect of the uncertainties of the

robot model. Recently, neural network technology has attracted much attention in the design of robot controllers. It has been pointed out that multi-layered neural networks can be used for the approximation of any nonlinear function. Other advantages of neural networks often cited are parallel distributed structure, and learning ability. They make artificial intelligence technology attractive not only in application areas such as pattern recognition, information and graphics processing, but also in intelligent control of nonlinear and complicated systems such as robot manipulators [59].

It was noted that only four out of five fingers of the ambidextrous hand were used to provide sensory feedback. To obtain realistic results, sensors on all five fingers should be incorporated. Therefore, force sensors was chosen to be placed on each finger of the hand and data is collected from all the sensors to.

2.1.2 Applications of Robotic Hands

A wide variety of robots have been produced over the years, and a considerable amount of success has been recorded. Successive United Nations Economic Commission for Europe (UNECE)/International Federation of Robotics (IFR) reports, [60] have suggested that there is an important future market for robotic systems. Robots can be useful tools in many industries. For instance, using application robots to automate production lines is an easy way to save time and money. Industrial robots also reduce waste and produce high-quality products with continuous precision. An anthropomorphic robot hand aimed at practical use for broad service robot applications is proposed in [9].

Robotic hands along with robotic arms are widely employed in many industries. Each industrial robot application requires a unique end of arm tooling, specific reach, payload, and flexibility. They are being used in everyday tasks such as assembly, drilling, pick and place, sanding, appliance automation, milling, bomb disposal, and

working with hazardous chemicals. The HH is one of the universal tools in nature. It is no wonder that researchers are eager to apply the advantages of this evolutionary design to a new generation of robotic hands. The German Aerospace Centre (DLR hand), in cooperation with the Harbin Institute of Technology (HIT), has already developed a robotic hand similar to a HH with the aid of miniature actuators and high-performance bus technology [61].

The automotive industry is one of the very few industries that saw the opportunity to use robotic arms as these days production lines need to be more efficient, flexible and precise. The idea of collaborative robots has also been proven effective when in the Chinese automotive plant, Great Wall Motors (GWM), the welding lines became the most productive lines ever made with 27 ABB robots working at 30 different workstations, collaboration happening between handling robots and welding robots [62]. The applications and requirements of industrial robots in meat processing are widely discussed in [63]. It is readily apparent that a more dexterous and practical robot hand will be needed both for use in space and for commercial applications. Robotic hand development for both space missions on the International Space Station and commercial applications on the ground is reported in [64]. Key features of robotic hands driven by PAM found in the literature are listed in Table 2.1.

2.1.3 Challenges and Future Implications

Literature reveals many attempts made since the late 1970s to design robotic hands that can mimic the HH precisely or better than a HH either in range of movement or speed [27]. There is no argument on the progress and advances made since the introduction of the first robotic manipulator in 1960s, but still, there are issues that need to be addressed in almost all the areas being researched. Initially, robots were used as a gripper to lift heavy objects then its applications expanded from industrial use to interactions with humans. Almost all researchers used the HH hand as a standard to meet the goal of a perfect hand aiming to match properties namely

Table 2.1: Key features of robotic hands driven by PAM.

Name of Robot Hand	Year	No of actators	Type of actuators	Fingers	DOF	Range of Motion
Utah/MIT [12]	1985	16	Pneumatic muscles	4	16	< HH
Tokyo Hand [65]	1999	16	Pneumatic muscles	5	12	N/A
J. Sancho-Bru et al. [66]	2001	25	Pneumatic muscles	4	20	< HH
D. Wilkinson et al. [67]	2003	31	Pneumatic muscles	5	20	HH
The ExoHand [68]	2012	26	Pneumatic muscles	5	20	HH
Exisiting Ambidextrous hand [27]	2015	18	Pneumatic muscles	5	13	2*HH
Proposed Ambidextrous Hand	2018	20	Pneumatic muscles	5	14	2*HH

dexterity, anthropomorphic appearance, manipulability and control HH possesses. The journey of development passed through a phase of a three-fingered robots to four-fingered, and now almost all robotic hands developed these days are five-fingered. Since the number of fingers increased, the number of degrees of freedom (DOF) has also increased. It is noted from the literature review that the number of actuators in most cases stayed similar to the DOF offered by the system but there were notable attempts for designing underactuated hands [69]. For instance, the Barret hand that offered 8 DOF by using 4 actuators, the Tuat/ Karlsruhe hand that remarkably offered 20 DOF using only 1 actuator and G. Stellin et al. [70] offering 20 DOF with only 9 actuators. In the case of robotic hands driven by PAMs, the number of actuators has always stayed double the DOF except the ambidextrous robot hand developed at Brunel University London in 2015 that has 13 DOF and 18 PAMs.

2.2 Review of Existing Robotic Arms

The term robot comes from the Czech word robota. Mainly, there are two types of robots: industrial robots and service robots. Industrial robots are on the verge of revolutionising the manufacturing industry as they are relatively safer, reliable and incredibly cost-effective compared to a human workforce. Robots are currently being employed in various industrial roles. For instance, the use of robotic arms in the manufacturing industry to move heavy parts from point A to point B and attempting hazardous tasks in the chemical industry.

Numbers of robotic arms have been developed in the past few decades to offer solutions to industry and humankind [71]. In 1495, Da Vinci designed a 4 DOF wrist articulated robotic arm, Von Kemplen then presented an arm that plays chess. His work was focused on the industrial robot arm that was later evolved into the PUMA arm [72]. In 1963, the Rancho arm was presented. Minsky's Tentacle arm appeared in 1968, Stanford University developed a computer-controlled robot arm in 1973 and MIT's Silver arm appeared in 1974. The Edinburg Modular Arm system comprises powerful motors offering 2 DOF (flexion and extension of the elbow) and similar articulation for shoulder [73]. Other arms include the DLR lightweight robot III developed in 2003, KUKA robot arm LBR iiwa in 2013, Robonaut arm by NASA [74], Elu2-arm by ELumotion Ltd, Kinova 6 DOF robotic arm with unlimited rotation on each axis [75]. The Delft robot arm developed by TU Delft University of Technology is a low power and low mass safe manipulator offering 4 DOF. The Delft arm won the Amazon Picking challenge in 2016 [76]. The OpenArm v.2.0 is a low cost 7 DOF robotic arm that is actuated by servo motors. This arm is made keeping human safety in mind and comes with a teleoperation control scheme [77]. The WAM arm developed in 2010 by Barret Technology is highly dexterous. It is known as the most advanced robotic arm in the world by Guinness World Record Millennium Edition. It is available in two main configuration, 4 DOF and 7 DOF. Some of the highlighted

features the WAM arm offers include Teach and Play, Force Control and gravity compensation [78].

RE2 [3] offers innovative end effectors ranging from small to large arms. Their most famous product is a highly dexterous manipulation system (HDMS) capable of doing complicated manipulation tasks. The arm itself is highly dexterous, efficient and affordable [79]. More than two decades of experience make SCHUNK [4] one of the most important developers of manipulator and gripper systems. The SVH five-finger gripper hand is designed for higher productivity in service robot applications [80]. ST robotics developed an R12 collaborative robot arm and an R17 robot arm. Both arms are low cost five axis articulated using servos. The R12 arm offers fast performance for the price [81]. KUKA arm offers tailor-made automation solution for the industry. They have a wide range of products that suit industry needs. KUKA KR1000 titan is one of the powerful robots built for heavy loads. These six-axis robots move heavy parts safely and precisely [82]. Bionic arm developed by a Bristol startup company called open Bionics released a new range of "hero arms" that could be fitted to patients from nine years old to an adult of any age. It is the World's first medically certified 3D printed arm and costing around £10,000 is considered one of the cheapest on the market [83]. The Artificial Muscle Operated (AMO) arm developed by Ryerson University is controlled by brain signals. The AMO arm enables amputees to avoid invasive surgeries. It is controlled by the user's brain signals and powered by a pneumatic system [84].

Although, it was noted from the literature that ambidextrous concept has been picked up some interest in recent times as discussed in section 2.4 Chapter Summary but none of the robot arms discussed is capable of ambidextrous movement as proposed in this research. The aim was to propose an ambidextrous robot arm design that could

[3]RE2 Robotics empowers humans to do their job faster, safer, and better using autonomy of human-like robotic arms.

[4]SCHUNK With 2550 grippers, SCHUNK brand offers the most comprehensive range of standard gripping components on the market.

offer much greater range of movements and stability than a conventional arm. Main application of the proposed ambidextrous robot arm lies in industries those employ robotic arms to do various tasks. This is because the ambidextrous arm is expected to save cost in terms of power consumption when compared with conventional arm.

2.2.1 Mechanical Design of the Robot Arm

Robotic arms are composed of links that are interconnected by joints to form a kinematic chain. In robotics, mainly two types of joints are used: revolute and prismatic. There are three joints in a typical arm; shoulder joint offering 3 DOF (Pitch, Yaw and Roll). Usually, this joint has the broadest range of motion. The elbow with 2 DOF provide flexion and pronation/supination. The wrist joint offers 2 DOF (flexion/extension and radial/ulnar bend).

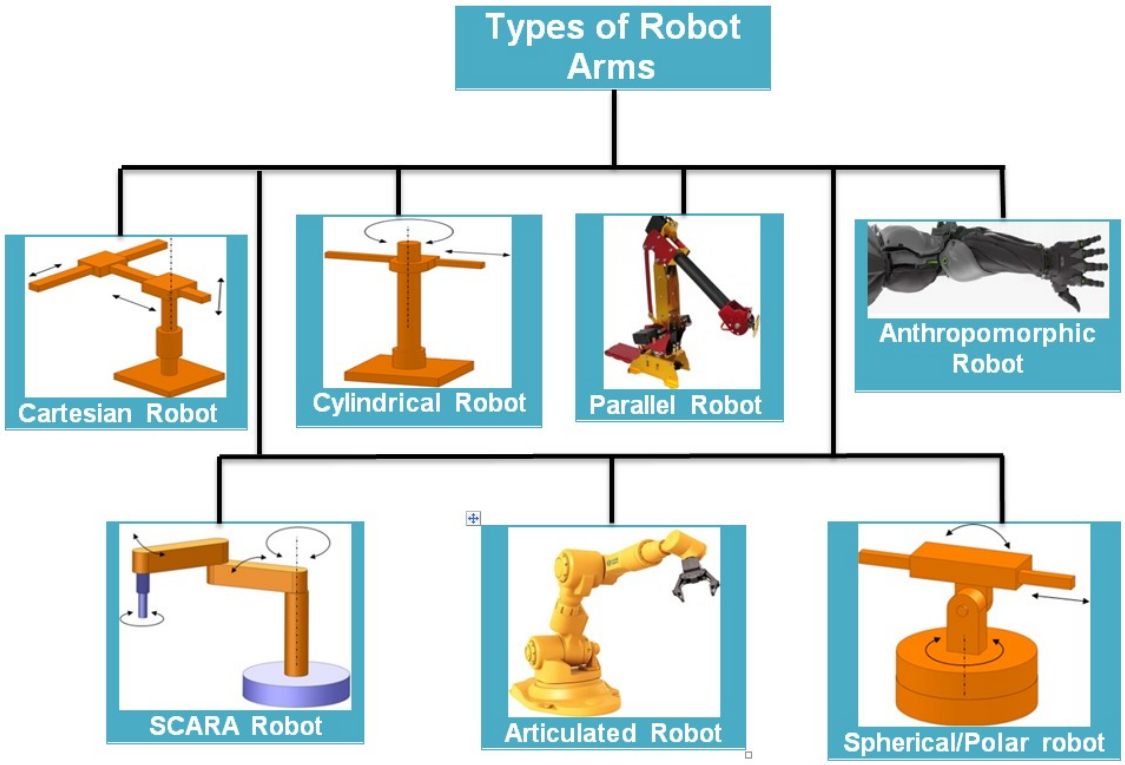

Figure 2.1: Types of robot arms.

From the literature, it is apparent that most of the researchers used one of the types of robot arm shown in Figure 2.1. Since none of the robot arm designs found in the literature challenged the breaking of human arm limits, this research will look into this aspect if an ambidextrous design could be feasible. The most popular types of robots with arms are cartesian robot, cylindrical robot, spherical robot, Selective Compliance Assembly Robot Arm (SCARA) robot, articulated robot and parallel robot.

- Cartesian robot / Gantry robot: Robot arms that have three prismatic joints and axes are coincident with Cartesian coordinates. These types of robots can be used for handling machine tools and arc welding.
- Cylindrical robot: This type of robot's axes form a cylindrical coordinate system. They are mainly used for assembly operations.
- Spherical robot / Polar robot: When axes form a polar coordinate system, then they are classified as polar or spherical robots.
- SCARA robot: This type of robot features two parallel rotary joints to provide compliance in a plane.
- Articulated robot: A robot whose arm has at least three rotary joints is called an articulated robot.
- Parallel robot: A robot that has concurrent prismatic or rotary joints in the arm is called a parallel robot.
- Anthropomorphic robot: If the robot arm resembles a human arm then it is classified as an anthropomorphic robot.

There are many different parameters used to compare robotic arms. Some of the key ones are speed, payload, bandwidth, compliance, human safety and cost. The nature of the tasks required from a robotic arm lay down the basis of its design.

Table 2.2: Advantages and disadvantages of using different robot arm as a base.

Type of Arms	**Joint Types**	**Advantages**	**Disadvantages**
Cartesian X: base travel Y: height Z: reach	• Prismatic Waist • Prismatic Shoulder • Prismatic Elbow	• Easy to visualise • Rigid structure • Easy off-line programming • Easy mechanical stops	• Reach only to front and back • Requires a large floor space • Axes are hard to seal • Expensive
Cylindrical Θ: base rotation Φ: height Z: reach	• Revolute Waist • Prismatic Shoulder • Prismatic elbow	• Can reach all around • Rigid Y, Z-axes • θ- axis easy to seal	• Cannot reach above itself • Less rigid θ-axis • y-z-axes hard to seal • Will not reach around obstacles • Horizontal motion is circular
Spherical Θ: base rotation Φ: elevation angle Z: reach	• Revolute waist • Revolute shoulder • Prismatic elbow	• Can reach all around • Can reach above or below obstacles • Large work volume	• Cannot reach above itself • Short vertical reach
Articulated Θ: base rotation Φ: elevation angle Ψ: reach angle	• Revolute waist • Revolute shoulder • Revolute elbow	• Can reach above or below obstacles • Largest work area for least floor space	• Difficult to program off-line Two of more ways to reach a point • Most complex robot

For instance for grasping and manipulation, high repeatability, maximum payload requirement (the maximum mass a robot arm can lift) and a low backlash are important. A factor of human safety is only considered if the robot has to interact in an environment where humans work too. Table 2.2 lists the advantages and disadvantage of using different types of robot arms in research.

Table 2.3: Low cost educational robotic arms.

Name	**DOF**	**Payload (g)**	**Height (mm)**	**Control System**	**Approx. Price (£)**
Arm trainer	5	130	510	Motor board	70
AL5D	6	110	482.6	RIOS	305
Edubot100	5	100	350	Robotica	1285
RCS-6 kit	6	50	609.6	C++	455
SG6-UT	6	403	495.3	PBASIC	455

Table 2.4: Low cost industrial robotic arms.

Company Name	**DOF**	**Payload (kg)**	**Height (mm)**	**Control System**	**Approx. Price (£)**
ABB	6	3	580	IRB120	17000
KUKA	6	5	680	KR 5 SIXX R650	20000
Mitsubishi	6	1.5	418	RV-1-A-S11	17000
Adept	6	5	653	Viper S650	27000
Motoman	6	185	15015	SP 185R	20000
Epson	6	1	600	C3-A601S	25000
Staubli	6	2.3	515	TX40	20000
Kawasaki	4 arm	2 kg/arm	495.3	Dual arm SCARA	20000

Table 2.5: Research orientated robotic arms.

Name	**DOF**	**Payload (kg)**	**Height (mm)**	**Mass (kg)**	**Controller**
Nero Arm 3.1	6	0.75	600	5	PID Controller
Katana 450	6	0.4	517	4.8	RT Linux
UR-6-85	6	5	850	18	C based controller
Ambidextrous Arm (Proposed)	5	1.12	609.6	2.3	Modified MANFIS Controller

Table 2.6: Modular light weight arms.

Name	**DOF**	**Payload (kg)**	**Height (mm)**	**Weight (kg)**	**Controller**
Robotnik Modular	5-7	9	400-1300	19	C++
Kuka Light Weight	7	7	868	15	KRC 2 lr Controller

Robotic arms found in the literature can be categorised in one of four classes: Low-cost educational arms (suitable to test simple joint control and manipulation tasks), Low cost industrial arms (offering high precision and robustness but controllers

are generally not open source making it a poor choice to investigate different configurations), Research oriented arms (suitable for research purposes and may not able to simulate real-world industrial applications), and Modular light-weight arms (suitable for industrial and domestic use but the price is significantly higher [85]. Tables 2.3, 2.4, 2.5 and 2.6 compare the key features of the arms available in each class. Therefore, from a researcher's point of view selecting an appropriate arm design and controller is an important decision. It is apparent from the literature that most advanced robotic arms were developed either by big companies or their collaborative labs based at different universities. These advanced robotic arms are currently being used in various robotics labs to investigate novel applications and intelligent control designs. None of these arms considered the ambidextrous design and modified MANFIS controller as proposed in this thesis.

2.2.2 Comparison of Ambidextrous Robot Arm with Similar Arms

A set of requirements was chosen as shown in Tables 2.7, 2.8 and 2.9. to ensure the proposed arm meet the set criteria. There were various factors kept in mind while designing the arm such as making sure the ambidextrous robot arm was fully compliant in terms of human safety, a maximum speed of at least 1.0 m/s and payload of at least 1.12 kg. Tables 2.7, 2.8 and 2.9 list some of the robot arms that were used as a basic guideline to design the ambidextrous arm. In the next coming tables term 5th percentile and 95th percentile means 95 percent of the time data points are below that value and 5 percent of the time they are above that specific value.

Table 2.7: Comparison of shoulder movements.

Movement	Shoulder rotation		Shoulder flexion		Shoulder abduction	
	5^{th}%	95^{th}%	5^{th}%	95^{th}%	5^{th}%	95^{th}%
Human Arm	360°	222°	204°	294°	173°	188°
Requirements to be ambidextrous	360°		270°		270°	
Robotic arm by Onur Bas [86]	0°		360°		180°	
Robotic arm by Luis Orejel [87]	0°		0°		250°	
Simple robotic arm-Airbrush [88]	0°		360°		120°	
Robot Arm for Airbrushing [89]	0°		360°		180°	

Table 2.7 shows none of the arms offers 360° shoulder rotation so there is a gap that could be filled by designing the ambidextrous arm in such a way that it offers complete shoulder rotation. The ambidextrous robot arm should also be able to make 360° shoulder abduction by coupling the other two joints. Table 2.8 clearly shows that improvement can be made at forearm pronation/supination as other arms usually do not offer this movement. It is possible for the ambidextrous robot arm to make wrist radial/ulnar bend just like other arms listed in Table 2.9, the ambidextrous arm can also make a 360° rotation and by coupling two other joints can offer wrist radial/ulnar bend.

Table 2.8: Comparison of elbow movements.

Movement	Elbow Flexion		Forearm Pronation	
	5^{th}%	95^{th}%	5^{th}%	95^{th}%
Human Arm	110°	129°	162°	242°
Requirements to be ambidextrous	270°		360°	
Robotic arm by Onur Bas [86]	270°		0°	
Robotic arm by Luis Orejel [87]	230°		0°	
Simple robotic arm-Airbrush [88]	280°		0°	
Robot Arm for Airbrushing [89]	340°		0°	

The range of motion of a human arm presented in Tables 2.7, 2.8 and 2.9 is extracted from [90].

Table 2.9: Comparison of wrist movements.

Movement	Wrist Flexion		Wrist Abduction	
	5^{th}%	95^{th}%	5^{th}%	95^{th}%
Human Arm	102°	173°	35°	85°
Requirements to be ambidextrous	270°		360°	
Robotic arm by Onur Bas [86]	270°		0°	
Robotic arm by Luis Orejel [87]	250°		0°	
Simple robotic arm-Airbrush [88]	300°		0°	
Robot Arm for Airbrushing [89]	180°		0°	

2.2.3 Control of the Robot Arm

Precision control of a robotic arm is a challenging task especially when the design of the arm does not meet conventional parameters. Different mechanical designs naturally lead to different control solutions. As a result, many control solutions have been proposed over the last few decades. For instance, in [91] the author proposed to determine the joint motion of the end effector by evaluating the feasibility of the joint motion. The determined joint motion is called an inverse kinematic solution with singularity robustness because it denotes a feasible solution even at or in the neighbourhood of singular points. The robust singularity inverse (SR-inverse) is introduced as an alternative to the pseudoinverse of the Jacobian matrix. Several simulation results are also shown to illustrate the singularity problem and the effectiveness of the inverse kinematic solution with singularity robustness.

In [92] a novel algorithm for the adaptive control of a robot manipulator containing kinematic loops is presented. The algorithm identifies the mass properties of each link and the viscous friction coefficients for each joint of the manipulator. It is similar to the Newton-Euler inverse dynamics algorithm and, hence, obtains its computational efficiency through the recursive nature of the algorithm. Simulation results presented show the effectiveness of the controller. Similarly, in (165), the author considered the adaptive control of robotic manipulators in task space or Cartesian space. A general Lyapunov-like concept is used to design an adaptive control law. From the results, it is verified that global stability and convergence can be achieved for the adaptive control algorithm. The algorithm has the advantage that the inverse of the Jacobian matrix is not required. A robust control method using a switching-sliding algorithm for a planar dual-arm manipulator system is developed in [93]. The proposed controller is useful for modelling imprecision and disturbances, inertial-based problems, as well as space-based free-floating platforms.

Most of the research on robot trajectory control has assumed that the kinematics of the robot are known precisely. However, when a robot picks up tools of uncertain lengths, orientations, or gripping points, the overall kinematics becomes uncertain and changes according to different tasks. To overcome this problem, a new adaptive Jacobian tracking controller for robots with uncertain kinematics and dynamics is presented, and experimental results justify the performance of the proposed controller in [94].

Mainly, two types of actuator are used to drive robotic arms in the literature: PAMs or Electric Motors. Robots are exoskeletons with actuators that provide the motion through torque and forces on the joints. Usually, higher power applications require electric or hydraulic power to move, but pneumatics still have the potential to deliver high power with a compact design. The evolution of robot arms actuated by PAMs has its origin in the 1950s with physicist Joseph L. McKibben [95], who designed and developed the first prototype of an artificial muscle for the pneumatic control of an orthosis that would expand and contract like an actual human arm; this artificial device is a close emulation of biological muscles [96]. In [97], the neural map algorithm has been employed to control a five joint pneumatic arm and gripper through feedback from two video cameras. Similarly, in [98] the author developed a pneumatic robot arm driven by pneumatic actuators as a versatile end effector for material handling systems.

PAMs have advantages over other actuators as they offer great initial force, high acceleration capacity, steady movement, are lightweight and sturdy, and can be positioned at different angles without losing properties, which make them appropriate for hazardous environments such as space environment. In [99], the author developed McKibben pneumatic artificial muscles that behave like human arms. The author states the drawback of using a PAM as an actuator is non-linearity of the muscle due to hysteresis and friction between fibres inside the woven shell. Pneumatic systems require a complex controller to achieve high accuracy, and they are not

robust to load variance. Caballero et al. [100] studied the nonlinearity aspect of a PAM, and their results concluded that the woven shell-inherent distortions result in nonlinear contraction repetitiveness as claimed in [99]. PID control offers a solution to the nonlinearity issue; therefore, learning-oriented alternatives like artificial neural networks and sliding mode controllers are also being considered. Artificial neural networks have the main advantage of incorporating nonlinear effects during the training stages allowing for the construction of a network to develop an intelligent control system that improves response times and PID control stabilisation. Sliding mode controllers can overcome the model uncertainties and external disturbances. A sliding mode controller is shown to offer excellent control of a robotic arm in following the desired trajectory in [101].

A neural network controller for a mobile manipulator to track the given trajectories is introduced in [102]. The dynamics of the mobile manipulator are assumed to be unknown and learned online by the Radial Basis Function Network (RBFN) with weight adaptation rule derived from the Lyapunov function. Generally, an RBFN can be used to approximate a non-linear function accurately. However, there remains some approximation error inevitably in a real application. An additional control input to suppress this kind of error source is also used. Simulation results confirmed the effectiveness of the system in an unknown workspace.

In [103], the authors investigated the implementation of inverse kinematics and a servo controller for a robot manipulator using an Field Programmer Gate Array (FPGA). They have evaluated the performance of the proposed circuit design through an experimental system that consisted of the FPGA-based motion controller and a Mitsubishi RV-M1 micro-robot and collected the experimental results to evaluate correctness and effectiveness. Similarly, in [104] an inverse kinematics method to control the servo angles of 5 DOF arm joints to get the desired tip position controlled by teleoperation is proposed. A strategy for solving the inverse kinatics equations of a 6 DOF robot arm system, using the robot arm assembled by seven AI servos is

proposed in [105]. A 5 DOF robotic arm driven by servo motors is controlled using an SSC-32 control board in [106]. The author added another servo to rotate the gripper and proved the concept of controlling all actuators using a single board. Controlling a robotic arm with stereo vision is presented in [107]. It is rare to find a robot arm controlled with a camera and even more challenging to find a controller that employs multiple cameras. The authors have made a vision recognition application which can recognise certain key points on the robotic arm. These points are placed at the joints, over each motor. The authors have used stereo distance calculation to know how much movement the robotic arm needs at the base joint. The concept of a soft robot arm with new series Pneumatic Artificial Muscles (sPAM) and their application as an actuators is introduced in [108]. Unlike a traditional tendon that has driven continuum robot (Continuously curving manipulator), the robot is entirely soft and contains no hard components, making it safer for human interaction. Models of both the sPAM and soft continuum robot kinematics are presented and experimentally verified.

From the survey of robot arm control, it is apparent that none of the researchers employ two complete sets of separate actuators in such a setting as to control the whole system and none of the projects found in the literature use a modified MANFIS controller to drive an ambidextrous arm. Therefore, the gaps identified in the literature could be filled by experimenting with a different actuator (for instance, PAMs and Electric Motors synced together) to drive the system and investigating the use of modified MANFIS controller to drive the arm.

2.3 System Architecture for the Robot Arm

In this section, the choice of components is discussed. Since a large number of components are used to build the project, only the key components are presented.

2.3.1 Microcontroller

A Microcontroller Unit (MCU) is a mini computer on a chip and designed to control operations in an embedded system. It is vital to choose the most suitable MCU as actuators are controlled by the MCU and if the number of input/output ports is not enough, it could become a challenging task to accommodate at a later stage. By keeping the requirements of the project in mind and for the ease of simplicity, an Arduino Mega 2560 MCU board was chosen. The Arduino is an open-source prototyping platform developed to be easy to use. To control an Arduino board, the user needs to send a group of instructions to the MCU. The most common method to control the Arduino board is using the Arduino programming language that is based on Wiring, and the Arduino Software IDE, based on Processing [109].

The Arduino board can also be controlled through other software such as MATLAB and LAB Windows. To do so, the user will need to install support packages that will enable the connection between the Arduino board and this software. The Arduino Mega 2560 was used in this project; this board has 54 digital outputs of which 15 can be used as Pulse Width Modulation (PWM) outputs. It is a MCU board based on the chip ATmega2560, which is a low-power CMOS 8-bit MCU based on the AVR enhanced RISC architecture [110].

Key technical specifications of the Arduino Mega 2560 board are listed in Table 2.10. The output voltage of the Mega 2560 board is 5 V; this means that the maximum amplitude that can be achieved by the output voltage of the PWM signal is 5 V.

Table 2.10: Technical specifications of the Arduino Mega 2560.

Operating Voltage	0-5 V
Input Voltage (recommended)	7-12 V
Input Voltage (limit)	6-20 V
Digital I/O Pins	54 (of which 15 provide PWM output)
Analog Input Pins	16
DC Current per I/O Pin	20 mA
DC Current for 3.3 V Pin	50 mA

2.3.2 Valves and Pneumatic Artificial Muscles

Solenoid valves are used to control the air flow in systems. Since PAMs are chosen to actuate the ambidextrous robot hand, there is a need for air valves. Mainly, there are five types of air valves; direct acting valves, pilot operated valves, two-way valves, three-way valves and four-way valves. Each air valve functions differently; for instance, a coil magnetically opens direct acting valves by lifting the shaft. The plunger opens the pilot operated valve while built up pressure causes the valve to open and close. Similarly, two-way, three-way and four-way valves comes with two, three and four ports respectively. A two-way valve is found to be the best fit for the ambidextrous robot hand project.

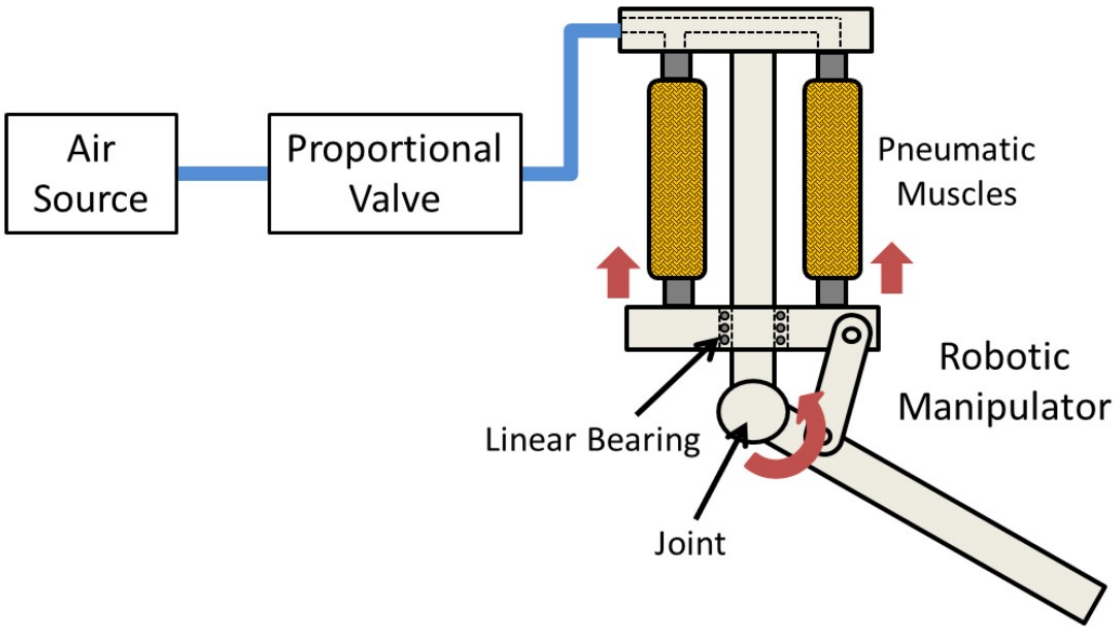

Figure 2.2: The working principle of PAM is demonstrated.

McKibben air muscles were first invented in the 1950s for orthotics [111]. They have several advantages over other types of actuators, for example they are easy to fabricate, lightweight, and have load-length curves similar to human muscles. PAMs are pneumatic structures that inflate and deflate according to the pressure of air. The working principle of PAMs is shown in Figure 2.2. Air is pumped into the PAM that makes the PAM inflate and as a result a tendon pulls the object connected with that PAM.

Similarly, releasing compressed air from the PAM deflates the PAM and the object goes back to its original position. When inflated, they bulge, shorten and thereby generate a contraction force. This contraction force depends on the applied pressure and on the muscle's length. Two big players in the market of PAM manufacture are Festo and Shadow Robot. Each PAM has a maximum pressure limit, for instance in Shadow Robot PAMs it is 4 bars. Actuation of a robotic hand is only possible if the number of actuators is connected in such a fashion to provide multiple movements.

For this purpose Y, or tee tube-to-tube, adapters are used as shown in Figure 2.3b. The adapter helps to divide air flow efficiently between the valves. Solenoid valves manufactured by Mead Fluid Dynamics were used in the ambidextrous robot hand project. A user can control these valves electronically, and their operating voltage is 24 V DC.

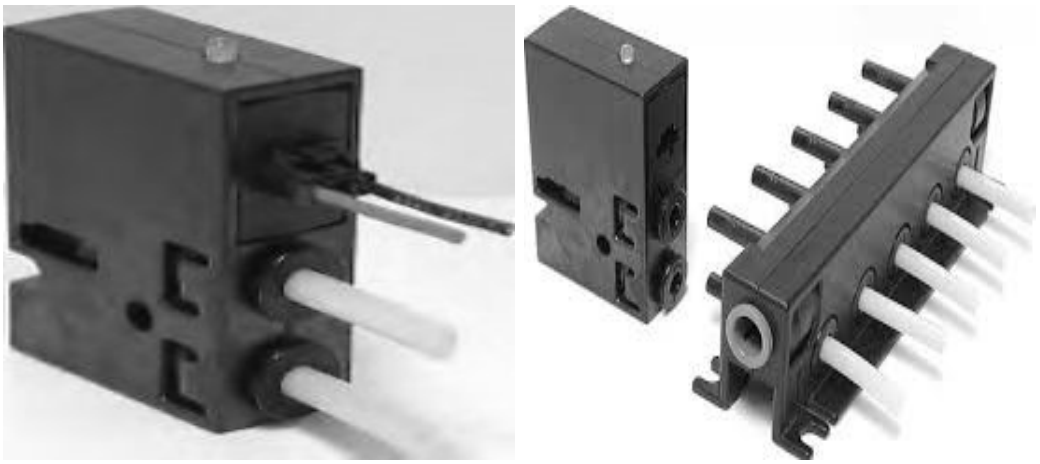

(a) (b)

Figure 2.3: Tee tube-to-tube adapter.

These valves are marke 'IN' and 'OUT', so a tube is inserted in both places accordingly. When these valves receive an electronic signal to turn on, the valves open like a gate and let air enter into the PAM. Similarly, when they are turned off, air cannot pass through the valves.

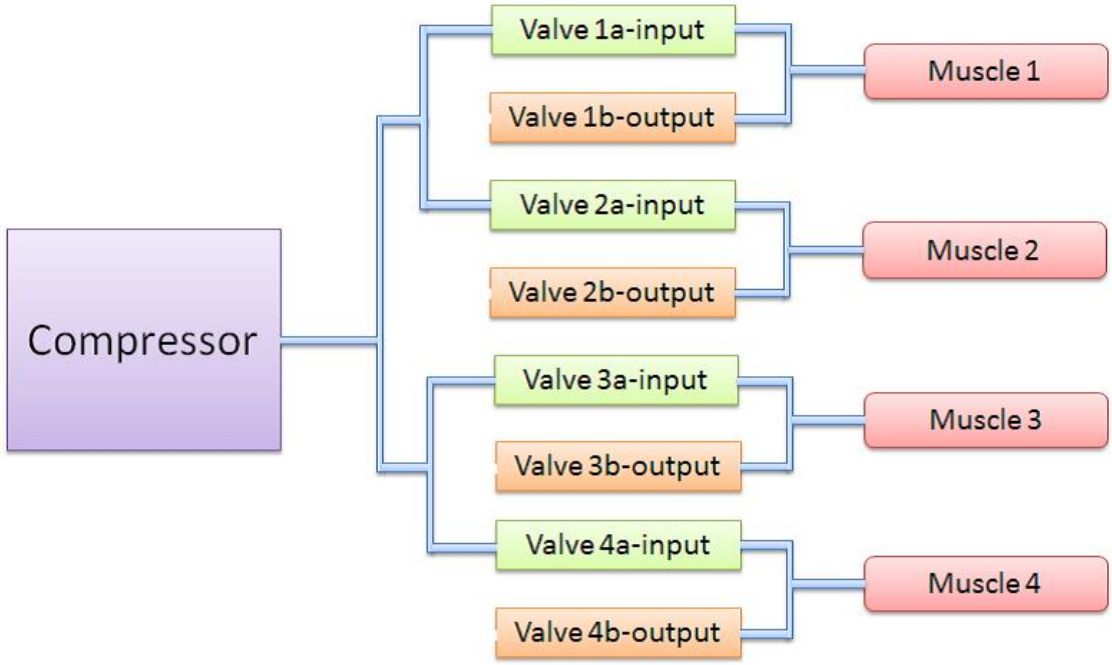

Figure 2.4: The configuration of PAMs and solenoid valves.

The configuration of how the muscles (only 4 muscles considered here as an example) are connected with solenoid valves is presented in Figure 2.4. Each muscle is connected with two valves. One valve lets air pass in, and the other let air out of the PAM. So for instance, if there is a need to contract muscle 3 and extend muscle 4, valve 3a needs to be open, and 3b should be closed. On the other hand, to extend muscle 4, valve 4a should be closed, and 4b should be open. Figure 2.5 shows the real-time configuration of solenoid valves attached to adapters for efficient distribution of air flow.

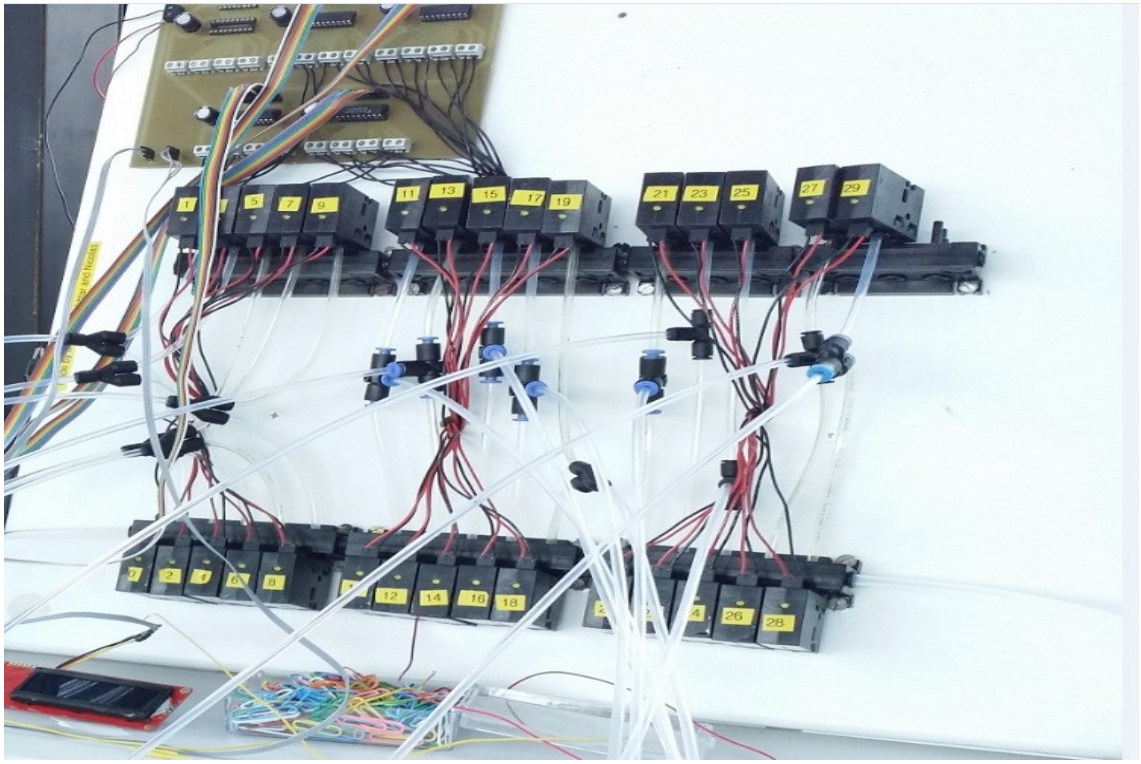

Figure 2.5: Solenoid valves attached to an adapter.

2.3.3 Air Compressor

An air compressor as shown in Figure 2.6 is an extremely powerful device that produces compressed air. The Euro-Tec compressor was considered for the robot hand project solely on the basis that it is very quiet and it meets the suction capacity of the project. The Euro-Tec 20 A is capable of supplying 6 bar of maximum pressure and has a tank capacity of 1.5 L. It can supply a maximum air flow of 20 L/min and has an auto turnoff feature. The re-designed version of ambidextrous robot hand alone offers 14 DOF by employing twenty PAMs. Therefore, a total of forty valves were used. Through an experiment, it was established that maximum air pressure never exceeded 3.5 bar.

(a) (b)

Figure 2.6: Air compressor connected with a switch where (a) is a connecting valve and (b) shows overall connection with air compressor.

2.3.4 Material

In terms of printing material, there were not lots of options available as the hardware was 3D printed at Brunel University 3D Printing lab. Two options to choose from were ABS and the PLA plastic. ABS is an obvious choice for engineers as it offers higher strength compared to PLA plastic [112]. ABS and PLA are both thermoplastic. PLA is stronger and stiffer than ABS but poor heat resistance. ABS is weaker and less rigid but tougher and lighter making it better plastic for prototyping applications. Every material is different in terms of properties as shown in Table 2.11.

Table 2.11: Comparison of different ABS meterial's flexural strength.

Mechanical propertiees	**Test methods**	**English**	**Metric**
ABS Plus Flexural Strength (Method 1, 0.05"/min)	ASTM D790	1,160 psi	8 Mpa
ABS ESD7 Flexural Strength (Method 1, 0.05"/min)	ASTM D790	8,800 psi	61 Mpa
PC ABS Flexural Strength (Method 1, 0.05"/min)	ASTM D790	8,500 psi	59 Mpa
PC ISO Flexural Strength (Method 1, 0.05"/min)	ASTM D790	13,100 psi	90 MPa

From Table 2.11, it is apparent that the PC ISO had the biggest flexural strength but P430 ABS Plus was chosen to print the ambidextrous robot arm due to limited options available. 3D printing is a process of adding multiple layers of material to form an identical shape as instructed by 3D Computer Aided Design (CAD) software. 3D printing technology was first patented more than three decades ago and since then the technology has evolved to offer many applications in mechanical and aerospace.

2.3.5 Motors

There are there main types of motors widely available in the market; DC motors, stepper motors and servo motors. Servo motors are considered the best option where precision control is required whereas DC motors are used to save cost as they are relatively cheaper than servos. Since precision control is an important factor in the ambidextrous robot arm project, it was decided to choose a servo motor that offers the highest torque possible. Servo motors that offer the highest torque are manufactured by GearWurx, but the most appropriate to be used in ambidextrous robot arm project is i01855 (PWM signal) or i04050. They both offer 11.3 Nm at normal rate and 22.6 Nm at peak and 270° degree of rotation. These servo motors require a power supply of 12 V DC and 3 A.

Servo motors are composed of four parts: a motor, a potentiometer, gears and a control circuit. The gears are linked to the motor, increasing the torque, and to the potentiometer. A user sends a command to the control unit which is then compared with the current position of the motor and any difference found in current position is adjusted by making a move. Servo motors have three inputs (as shown in Figure 2.7); the positive power supply, the negative power supply and the command signal. A servo can be driven by an analog signal or a PWM signal. When driven using an analog signal, the position is directly linked to the voltage. With a PWM signal, the position of the motor is determined by the width of the pulse. The technical specification of motor used in the project is presented in Table 2.12.

Table 2.12: Technical specifications of the motors used in the project.

Technical specification	Motor (i04050)	Motor (HS-805BB)
Travel (deg)	990	280
Control	Position	Position
Time for 90 deg	1.5 Sec	0.14-0.19 Sec
Power Input Voltage	10-14 V	4.8-6 V
Power Input Current	Up to 3 A depending on load	Up to 830 mA/No load running
Control Input Voltage	0-5 V, analog or PWM	0-5 V

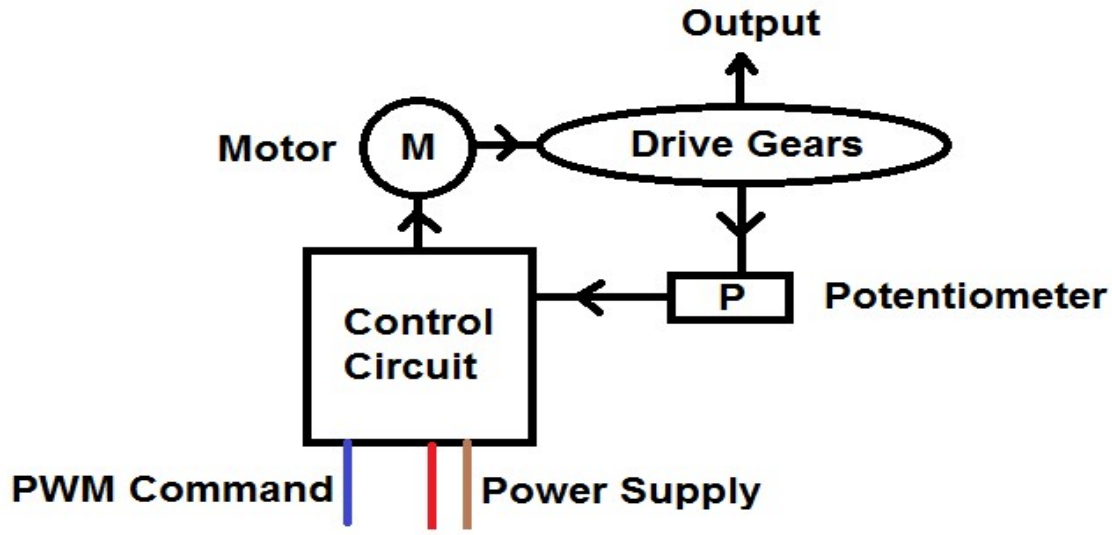

Figure 2.7: Working diagram of a servo motor.

In order to drive shoulder and elbow joints more than one motor should be used in the same direction at the same time to meet the torque requirements. So both motors need to be synchronised at the same rate and the same direction otherwise it will damage the motor gear (see Figure 2.8). To avoid this damage, either the motor needs to be opened to adjust the potentiometer placed at each junction or the software programme (shown in Figure 2.9) provided by the manufacturer can be used to make changes in response, rotation and offset.

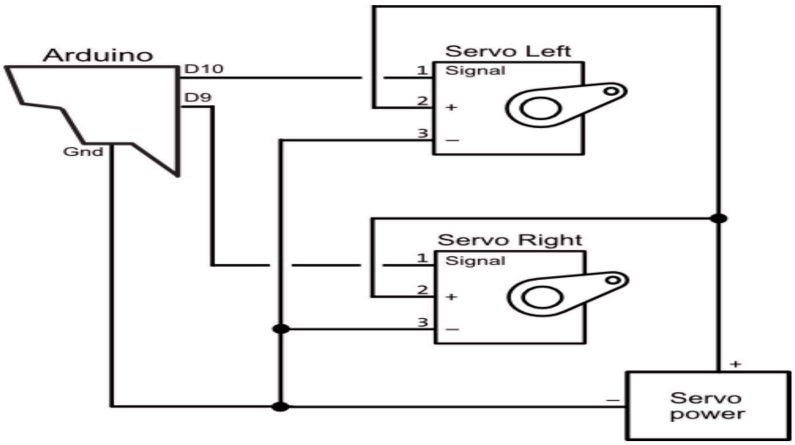

Figure 2.8: Servos are working against each other.

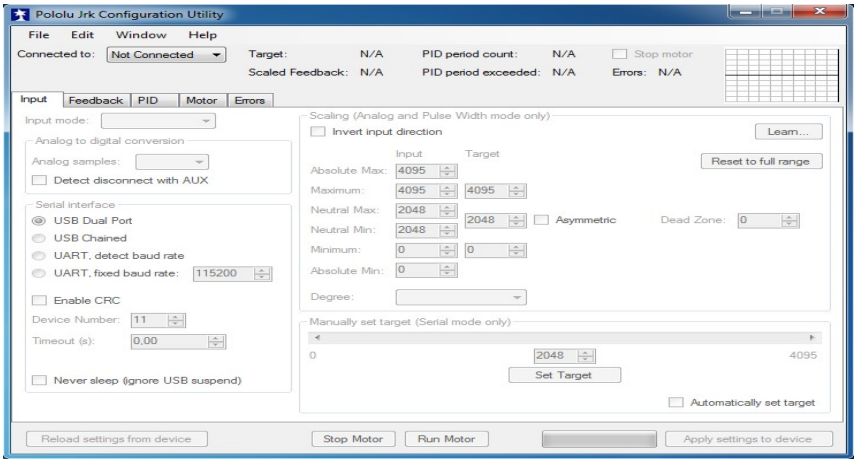

Figure 2.9: Servo configuration software.

Figure 2.10 shows the possible link that can be made between servo motors connected in parallel and the elbow using a spring.

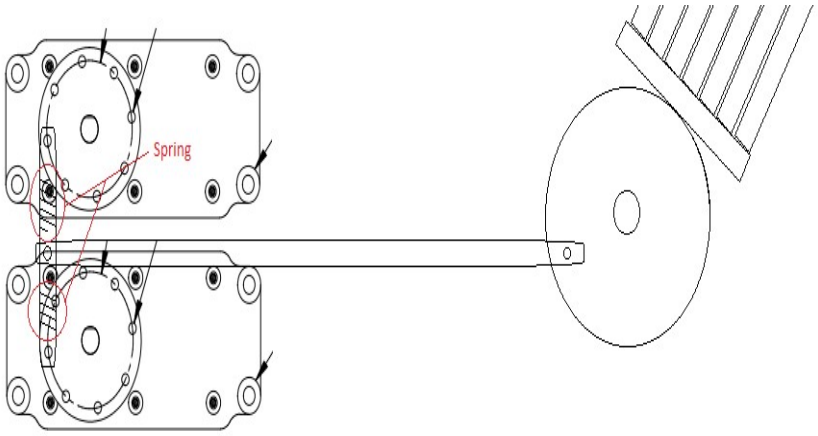

Figure 2.10: A link between servos and the elbow with a spring.

The power input voltage of servo i04050 is between 0-5 V, and same applies for the Arduino Mega 2560 PWM output. This means the Arduino board can be used directly to control the servo i04050. The HS-805BB servo motor is manufactured by HITEC. Like the i04050, the HS-805BB has a control input voltage range between 0-5 V, so an Arduino Mega 2560 can be used to control it without any modification.

The servo i04050 is chosen to perform the flexion and extension movement in the elbow (see Figure 2.11). The torix servo is capable of offering up to 990° rotation. This should be more than enough to make an ambidextrous move.

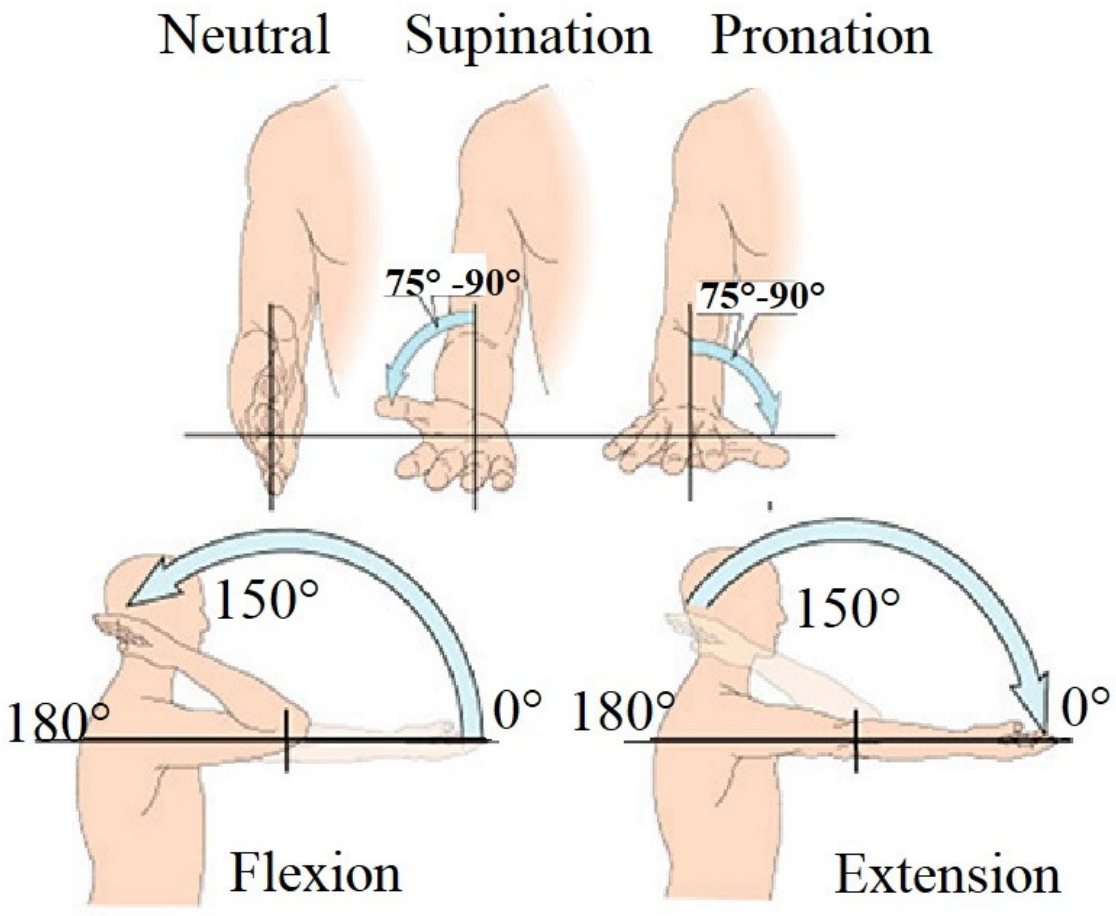

Figure 2.11: Elbow movements.

The HS-805BB Mega Power servo is chosen to make the pronation and supination of the forearm (see Figure 2.11). It is capable of making a 280° turn, and this should easily meet the requirement of the ambidextrous robot arm elbow movement.

The Industrial Torxis Servo i04050 is chosen to perform the vertical shoulder flexion and vertical extension movements as shown in Figure 2.12.

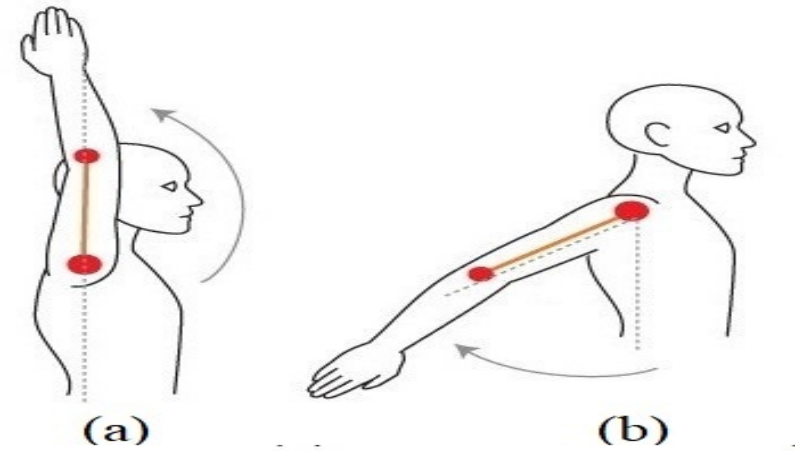

Figure 2.12: Vertical flexion (a) and vertical extension (b) of the shoulder.

Two Industrial Torxis Servo i04050 motors need to work together to perform the shoulder abduction and adduction movements as shown in Figure 2.13. Both motors are interconnected to produce enough torque to work together.

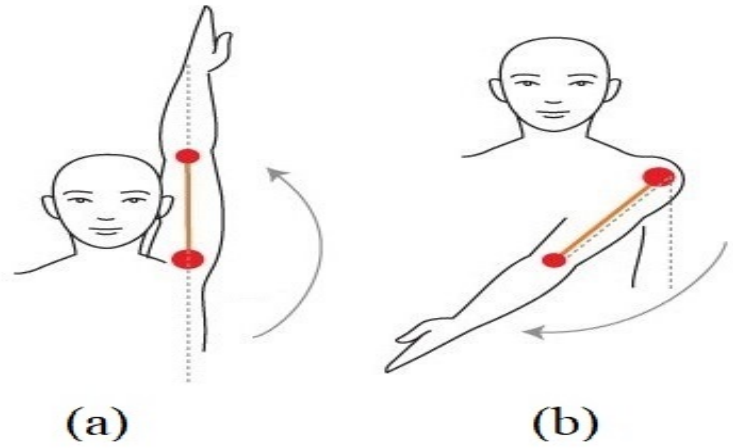

Figure 2.13: Abduction (a) and adduction (b) of the shoulder.

Similarly, the Servo i04050 was chosen to make the horizontal shoulder flexion and horizontal extension movements as shown in Figure 2.14.

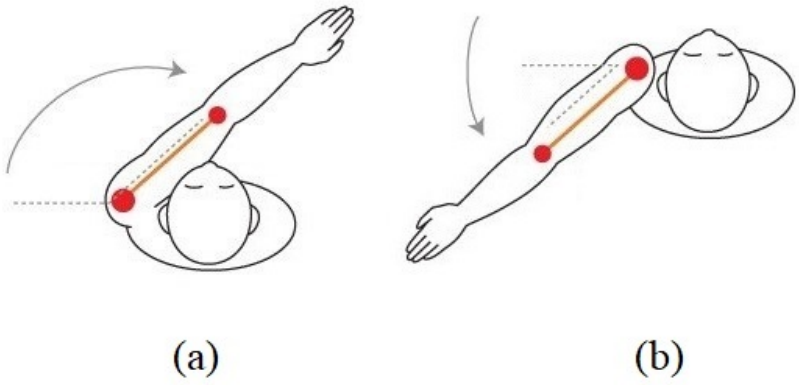

Figure 2.14: Horizontal flexion (a) and horizontal extension (b) of the shoulder.

2.3.6 Software

Choice of software plays a key role in completing the task within the required timeframe. There are many softwares that could be considered for this project. Some of the most popular ones are MATLAB, GNU Octave, Scilab, Julia and Sage. Others are Freeman, Genius Mathematics Tool, Maxima, NumPy, Wolfram Mathematics, Maple and SymPy. Comparison of the most popular packages is given below in Table 2.13.

After careful analysis, it was decided to use MATLAB due to the widely available toolboxes and open source libraries. Some of the most important ones required are Neural Network Toolbox, Fuzzy Logic Toolbox, Robotic System Toolbox, Optimization Toolbox, Control Toolbox and Simulink. It was important to select a software package that can define a robot model, perform inverse kinematics and dynamic calculations and be able to import files from Solidworks using Simulink B. MATLAB software met all the requirements of the project. Hence, it was chosen to be used in the ambidextrous robot arm project.

Table 2.13: Comparison of software available.

Software Name	Price	Platform compatibility	Key Features
Maple	Starts at £70 Per year	Windows, Mac OS X, Linux	Multiple languages interface, Equation editor, variable manager, Control design, Statistical data analysis and Live data Plot
Wolfram Mathematics	Starts at £118 per year	Windows, Mac OS X, Linux	Multiple function libraries, Geo visualisation/animation tools, 2D/3D image processing, automated machine learning, graphical computations and Multiple languages interface
GNU Octave	Free	Windows, Mac OS X, Linux	Free and open-source, Data manipulation and visualisation, interactive command line interface, a wide variety of packages and Multiple languages interface
Scilab	Free	Windows, Mac OS X, Linux	Free and open-source, Free "Xcos" package, 2D/3D visualisation, control system analysis, network computations and GPU computing.
SageMath	Free	Windows, Mac OS X, Linux	A browser-based notebook that lets you review and reuse previous inputs/outputs.
MATLAB	£60	Windows, Mac OS X, Linux	MATLAB is one of the easiest software to learn and use due to its toolboxes and widespread use.

2.4 Chapter Summary

The literature review chapter was divided into three main sections and the key points made in each section are as follows:

- Notable robotic hand inventions and the control strategies tried so far on robotic hands were discussed in 2.1. After careful consideration, it was apparent that many mechanical designs and controllers have already been proposed in the literature for dexterous robotic hand structures but use of a hybrid controller (use of conventional controllers with artificial intelligence based controllers) on ambidextrous robot hand is difficult to find in literature. Therefore, the combined use of PID with NN is proposed to drive the ambidextrous robot hand.

- In section 2.2, notable robotic arms are presented. Most of the robot arms aim to offer a range of motion close to the human arm, but none of the research focused on extending dexterous robot arm capability to ambidextrous design in a way that it can replicate right and left arm movements and offer a greater range of motion than the conventional human arm. However, literature does suggest recent interest of scientists in the ambidextrous concept to speed up the tasks of manipulation [113, 114], a novel ambidextrous approach for self-learning robot [115] and the ambidextrous robotic master controller [116] but none of these are able to replicate both left and right arm movements as proposed in this research. They rather use two arms in parallel to complete the task. The ambidextrous arm design proposed in this research is appreciable from design point of view since it is a single arm offering ambidextrous movements. Comparison of robotic arms available in the market with the proposed ambidextrous robot arm was presented in Tables 2.3, 2.4 and 2.5. Furthermore, since none of the arms found in literature offer ambidextrous feature, an ambidextrous robot

arm design is proposed.

- Since the proposed ambidextrous robot arm design is unique, it naturally requires a unique controller too. From the literature review, it was confirmed that none of the controllers that exist in literature are suitable to drive the ambidextrous arm. A modified version that suits the need is required. Hence, artificial intelligence based methods were chosen to be explored to find the most appropriate one to use as a base.

- In section 2.3, choice of key components was justified. The literature review gave the direction of future research. It was deduced that improvement in mechanical design of the ambidextrous hand is required to interlink with the arm. The NN combined with PID control is appropriate to drive hand than simply using conventional controllers. Furthermore, the proposed novel design of the ambidextrous arm seems like a best fit with current market trends given the fact many dexterous arms already exist and does not offer ambidextrous feature.

CHAPTER 3

Design of the Ambidextrous Robot Arm

This chapter is divided into two main parts: re-design of existing ambidextrous robot hand and the design concept of the ambidextrous robot arm. Before designing an ambidextrous robot arm and interlinking with the hand, it was imperative to understand how the ambidextrous robot hand could be redesigned. The ambidextrous robot hand concept was originally proposed by Dr Emre Akyürek in 2013 [40]. The existing design was good enough to prove the basic ambidextrous design concept of hand, but it was not possible to interlink the ambidextrous robot hand with ambidextrous robot arm without improving the existing robot hand design. Therefore, it was important to go back for a closer look to see if the existing robot hand could be improved. After careful consideration, some issues were identified in the existing robot hand design. Key changes such as the addition of wrist movement offering another degree of freedom, re-routing of the tendons (for greater strength), complete replacement of tendon string material (polyethene material string is used to avoid breaking issues), replacement of 4 mm hose tail barb to 8 mm for better speed of the system, and exchanging all metal parts to newly designed 3D printed parts in a bid to reduce weight and improve the design have been carried out. By making these changes, the new design met the requirements of being a fully 3D printed

ambidextrous robot hand offering 14 DOF with improved control.

3.1 Redesign of Existing Ambidextrous Robot Hand

In order to accurately re-design an anthropomorphic ambidextrous robotic hand, numbers of changes are made to the existing ambidextrous hand design [27]. For instance, addition of wrist movements, re-routing of the tendon with better quality material (use of polyethene strings), force and vision sensors incorporated, complete 3D printed solution by replacing all metal parts used in the existing design, and implementation of a three tendons routing scheme with the use of offset pulleys.

Since the heavy mass of the structure makes control difficult, all the metal elements used in the existing ambidextrous robot hand project were exchanged with 3D printed parts in a bid to reduce the mass of the whole structure from 3.2 kg to 2.3 kg (see Figure 3.1 for visuals of the existing and the proposed forearm design) E.

(a) Existing. (b) Proposed.

Figure 3.1: Visuals of existing and proposed design.

Tendons kept breaking during experiments, so there was a clear need to re-run the tendon routing to address a problem where the wrong routing led to strings getting stuck and eventually breaking into small pieces as shown in Figure 3.2.

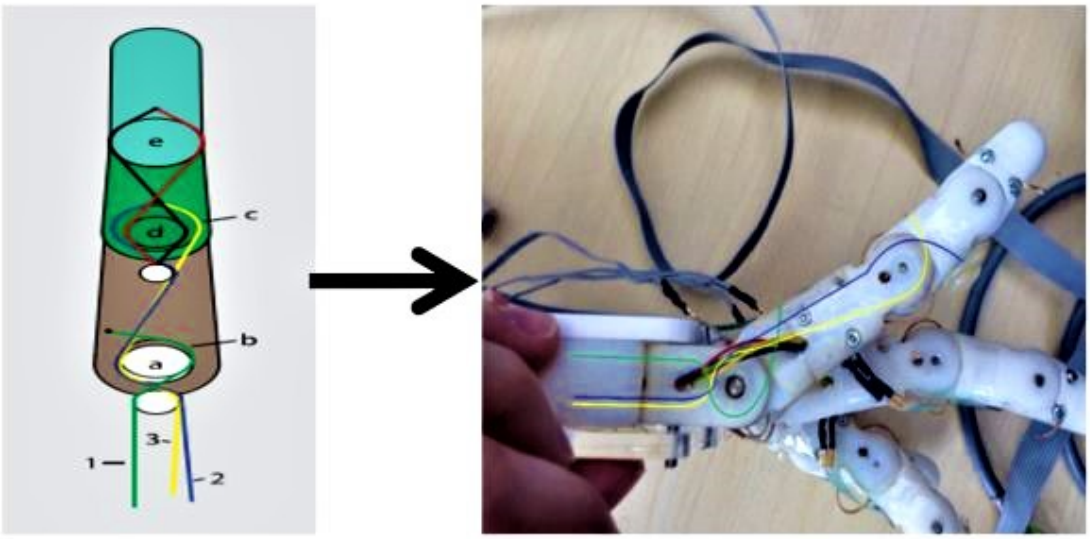

(a) Existing tendon routing (b) Proposed tendon routing

Figure 3.2: Path of the replaced tendons through a finger.

The design aims to mimic HH movements; it is important to replicate the degree of freedom to ensure more fluidity in the motion. The ambidextrous robot hand is already bigger in terms of length when compared with a human counterpart. To save some space, the solution to actuate the hand without using motors was proposed. Two of the existing extra un-used PAMs were also employed to add wrist movements.

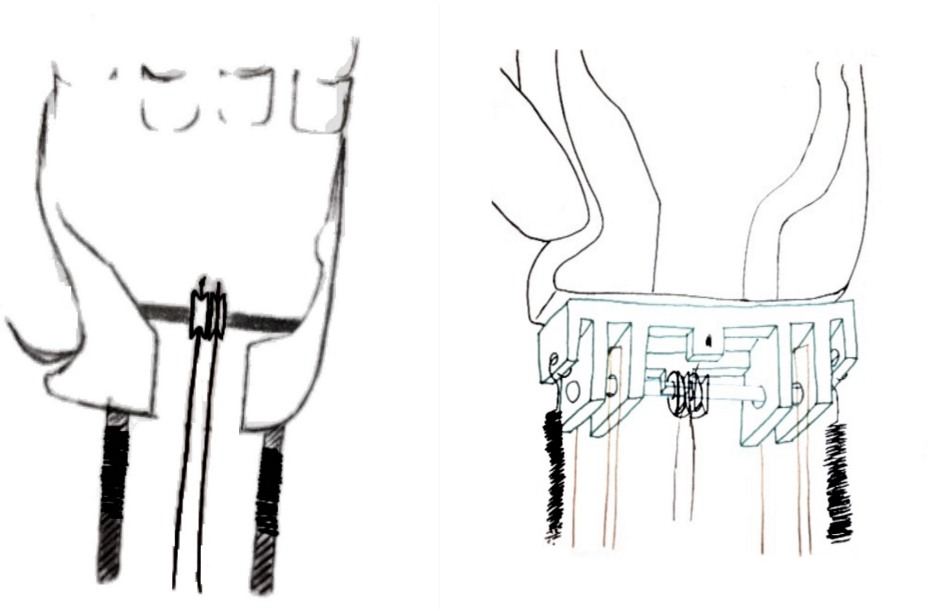

(a) The First Solution. (b) The Second Solution.

Figure 3.3: Wrist design solutions.

One idea was to simply add a spring in the middle of the screws so the hand can offer flexion and the spring would hold the hand in default vertical position (as shown in Figure 3.3a). The idea would have worked if a spring that is strong enough to hold the hand structure could be found. After some research, it was concluded that the simple addition of a spring will not work. Then, 3D parts are designed to try another idea (see Figure 3.3b and Figure 3.4).

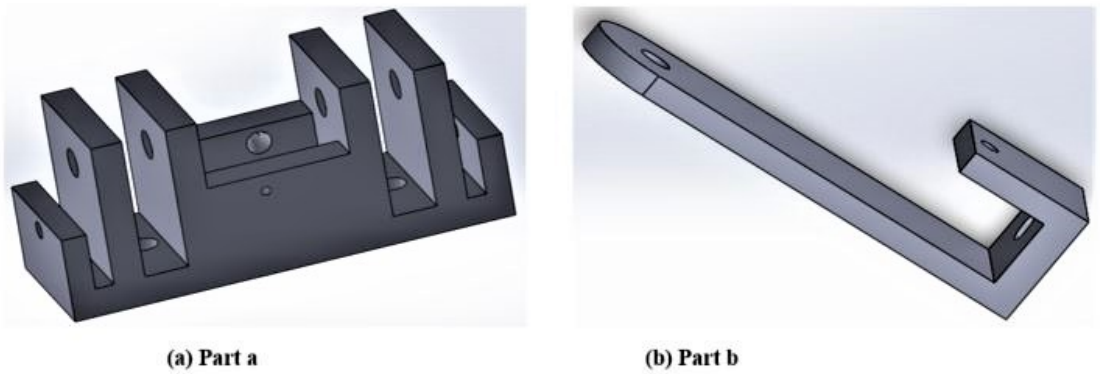

Figure 3.4: Solidworks design of the wrist first solution.

A few issues were found in the first wrist design solution: the spring holder on the hand is under the rotation axis. This implies that the spring stretches the most during flexion movement. Also, the spring holder was square, which is not acceptable when the hand rotates over 45°.

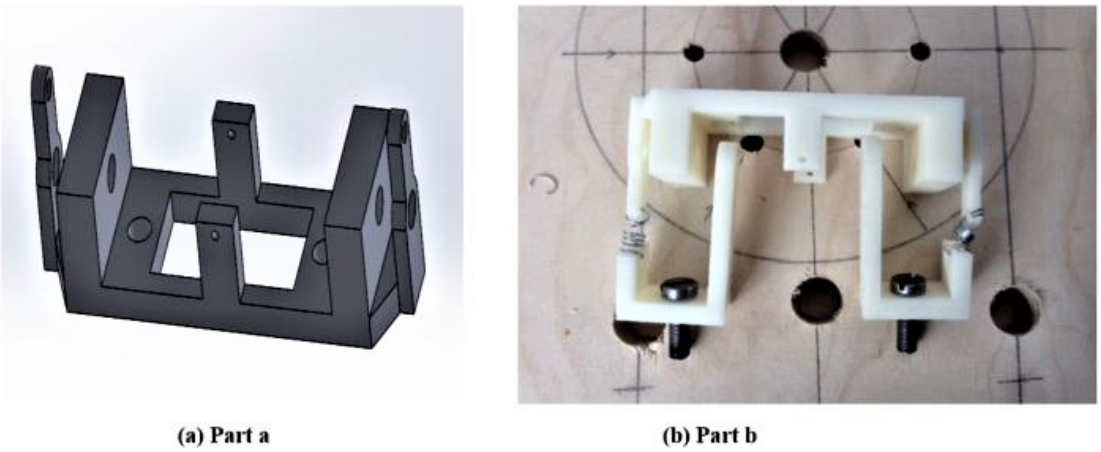

Figure 3.5: Solidworks design of the wrist second solution.

Problems found in the first design of wrist lead to thinking about a new solution. The second solution is presented in Figure 3.5.

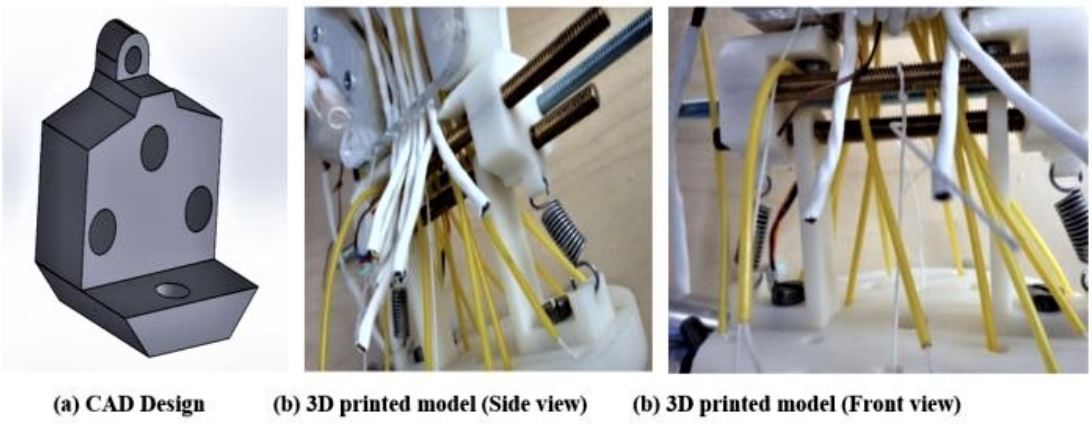

Figure 3.6: A CAD model of the third design shown in (a) and printed model in (b) and (c).

Even after passing the simulation test when the solution is used in reality, the spring holder broke after a few experiments. This led to believe the thickness of design is not enough to hold the mass. Then, new idea coming up (as shown in Figure 3.6). With the key improvements made to this final design of the ambidextrous hand [117], it can now imitate the movements of both left and right hands including a wrist that is capable of moving 270°.

The human fingers can make two kinds of antagonist movements: flexion and extension, or abduction and adduction. Flexion and extension control the angular displacement of the three phalanges of a finger. Abduction and adduction imply lateral rotations of a whole finger and constitute another DOF, which makes a total of four distinct DOFs per finger. As abduction and adduction are not essential for many applications, robot hand can be built without taking them into account. It allows easing the control of the structure and reduces the number of needed actuators. Robot fingers are usually built as a succession of three phalanges, with sockets preventing them from reaching non-natural angles. These sockets were adapted to reach the range necessary to ambidextrous fingers. The ambidextrous hand design is shown in Figure 3.7.

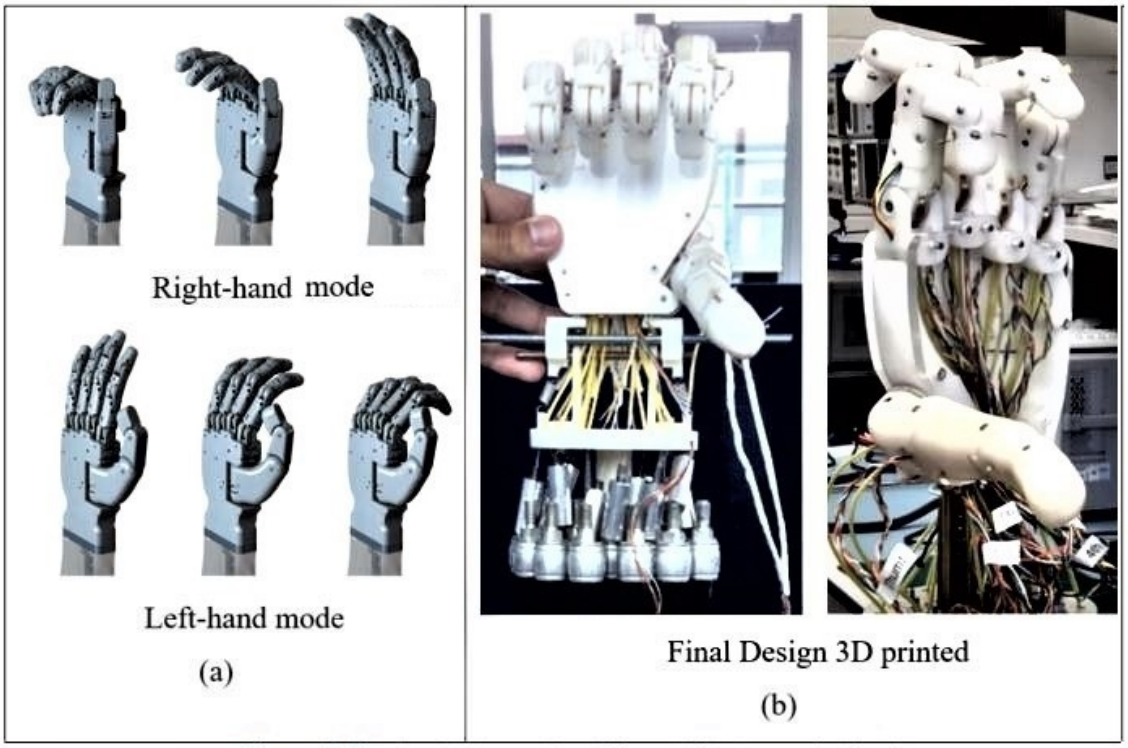

Figure 3.7: Final re-design version of the ambidextrous robot hand.

3.2 Design of the Ambidextrous Robot Arm

The human arm has always been considered the perfect model to start designing robotic arms. An arm is mainly divided into two parts; upper limb that connects shoulder joint and the elbow joint and forearm refers to a part between hand and elbow. The most common feature of the arm is to act as an extender for the hand and help in effective completion of various tasks. A human arm offers a total of 7 DOF; three in the shoulder (Pitch, Yaw and Roll), two in the elbow (Pitch and Roll) and two in wrists (Pitch and Yaw).

As part of re-designing the ambidextrous hand, it was decided to re-design the elbow too. The forearm design itself is not complicated except for the printing part. At Brunel University's 3D printing lab, printing options were limited to a maximum of

400 mm in the length of each part. So in order to print a 700 mm length part, it was necessary to break it up into two parts and later glue those parts together (see Figure 3.1b).

The human elbow can make two movements (Flexion-Extension and Supination-Pronation). It was decided to follow the human model and the design solutions outlined in Table 3.1 were proposed.

Table 3.1: Comparison of three different elbow design options.

Design 1	Design 2	Design 3
Design 1 is the most straightforward design, but the orientation of motors, in this case, increases the width of the arm.	This design is composed of two belts which transfer the movement of the two motors changing its direction. The size of the elbow is the best size possible. The problem with this design is the lousy performance of the belt. A chain was also tried, but it did not work.	Design 3 is very similar to Design 2, but the only difference is the transmission method of torque. A system similar to the one used in trains is employed to save the torque lose. All the torque of the two servo motors is transmitted to the rotation axis so that it can lift the forearm weight.

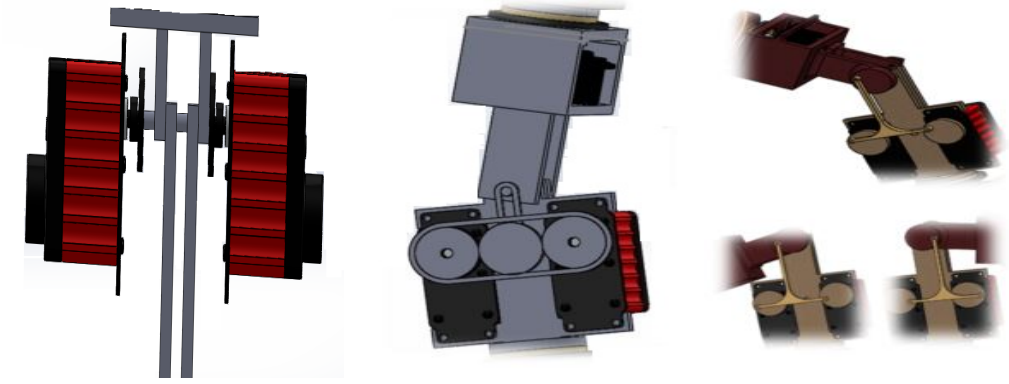

(a) Design 1 (b) Design 2 (c) Design 3.

Figure 3.8: Three different elbow design options.

Design 3 in Figure 3.8c, met the elbow movement requirements, but in turn, it created another problem in shoulder design. Since, this design is based on using

two large servo motors, each servo motor having a mass of 1 kg, it increased the overall mass of the forearm. With this mass increase, the design of the shoulder became very bulky; indeed the torque was more than 30 Nm to move the shoulder. Servomotors that could meet the torque requirements were available on the market but were too expensive and bulky. So, it was decided to re-design the elbow using one servo motor. Figure 3.9 shows the final design of the elbow CAD model.

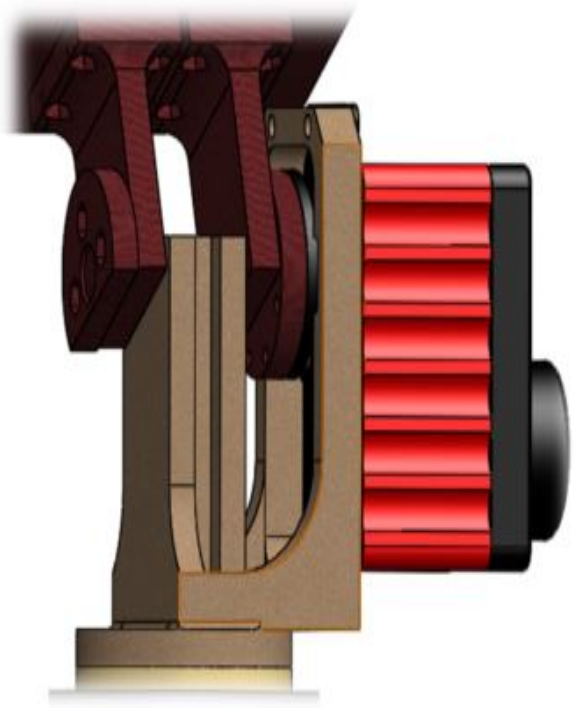

Figure 3.9: Elbow design.

After some testing, it was apparent that the final design met the requirement (see Figure 3.10). It provided not only a simple but also the least heavy solution.

(a) Elbow side view.

(b) Elbow front view.

Figure 3.10: Design of elbow with one motor.

The pronation and supination movement was made possible by using a bearing and driving it with small servo motor as shown in Figure 3.11.

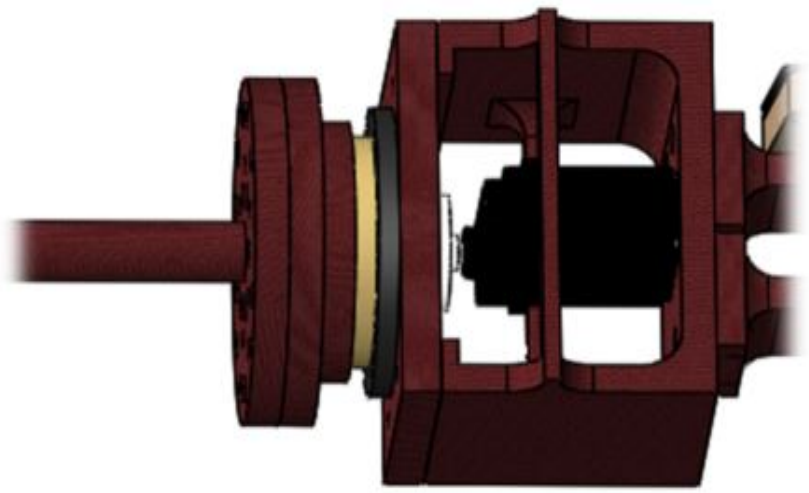

Figure 3.11: Elbow rotation using a bearing.

The shoulder is composed of three joints (rotation, flexion and abduction). The rotation movement in the shoulder was a replica of what was achieved in the elbow except for this requiring relatively higher torque. Servo motors were used for rotation movements in the elbow and the shoulder, and bearings were inserted allowing the unlimited free rotation. For the abduction and flexion movement, a unique idea of using the same joint to make two movements was tested. The concept was very similar to the elbow flexion, but this joint required much higher torque, so it was not possible to drive it with only one servo motor. Two servo motors were used as shown in Figure 3.12b to generate required torques.

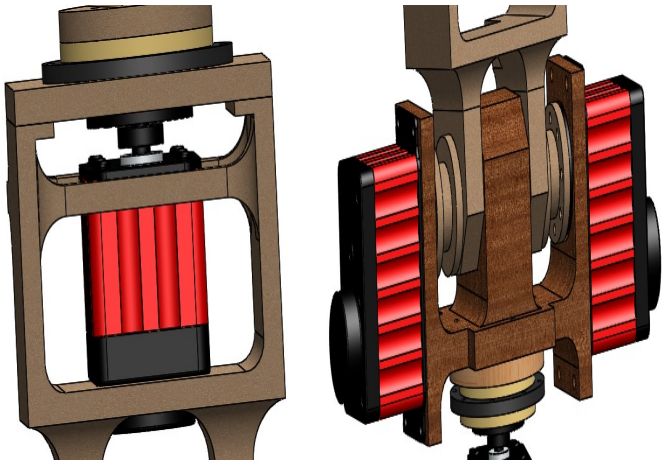

(a) abduction/adduction (b) flexion/extension

Figure 3.12: Shoulder rotation joint angle.

The ambidextrous robot arm is capable of making most of the movements a human arm can. Figure 3.13 shows some of the most important angles that make this arm unique. For instance, a human arm offers 70° rotation at the shoulder whereas the ambidextrous arm offers 360°.

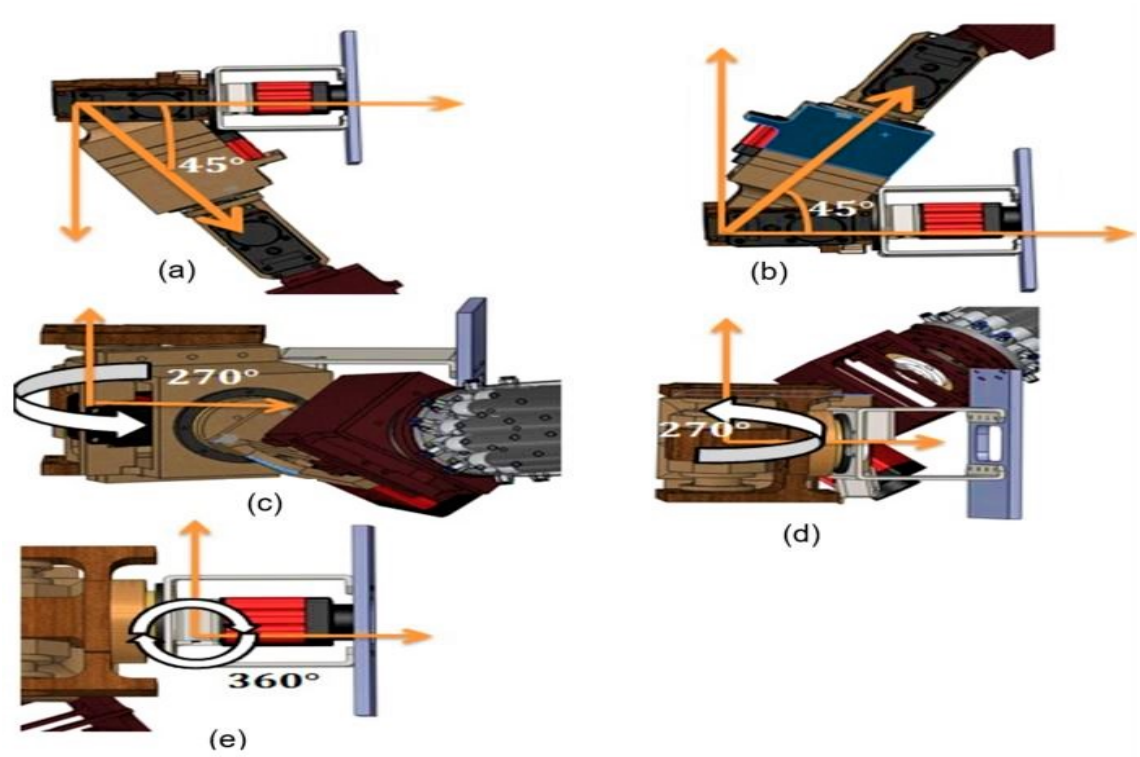

Figure 3.13: Possible shoulder movements in the ambidextrous robot arm.

Similarly, a human shoulder offers 200° and 180° in flexion/extension and abduction/adduction respectively whereas the ambidextrous arm offers 270° for each as shown in Figure 3.13.

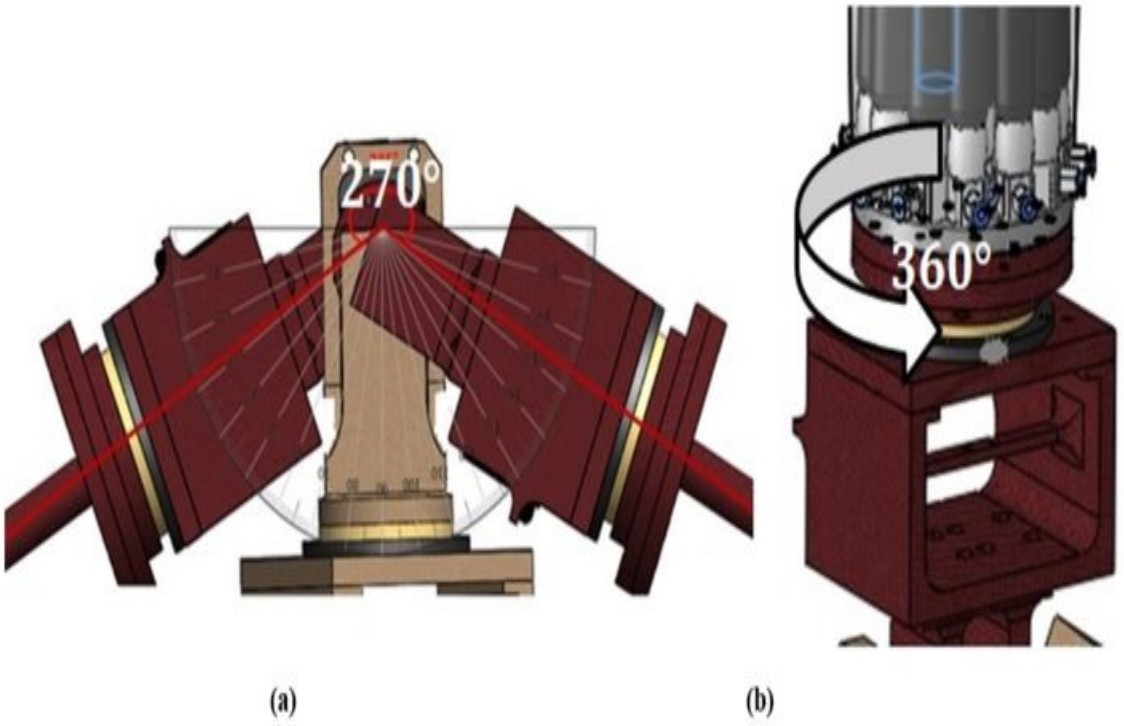

Figure 3.14: Elbow movements in the ambidextrous robotic arm.

The ambidextrous arm offers a much higher range of movement in the elbow than the shoulder. By offering flexion/extension of 270°, forearm pronation of 360° and end effector rotation of 360°, the ambidextrous arm is capable of making almost any movement within a range of an elbow as shown in Figure 3.14. The length of a human arm is proportional to the length of the entire human body. Many factors determine the length of a person's arm. Therefore this ratio is used to evaluate correctly. The data presented in Table 3.2 is extracted from [118].

Comparison of ratios in Table 3.2 and 3.3 confirm that the forearm is a little bigger than the upper arm and the hand. The ratio between the hand and the upper arm of the ambidextrous robot arm is close to the ratio of the human arm (0.632 instead of 0.826). However, there is a more significant difference between the forearm and upper arm ratio for the robot arm and the human arm.

Table 3.2: The ratio between part of the human arm and the size of the person.

	Length (cm)		
Forearm arm	28.98		
Upper arm	23.76		
Hand	19.62		
The ratio for the human arm	Upper arm	Forearm	Hand
Upper arm	1.000	1.220	0.826
Forearm	0.820	1.000	0.677
Hand	1.211	1.477	1.000

So to be more realistic the forearm should be smaller. However, due to the size of the muscles, it was not possible to reduce the size. Figure 3.15 shows the final design of the ambidextrous robot arm. After the designing process, the 3D printing process needed to be followed. However, before printing, there was a final check on each component to see if it met the strength analysis (full stress analysis is presented in the appendix D).

Table 3.3: The dimension of the ambidextrous arm.

		Length (cm)	
Forearm		62.8	
Upper arm		34.8	
Hand		22.0	
The ratio for the ambidextrous robot arm	Upper arm	Forearm	Hand
Upper arm	1.000	1.804	0.632
Forearm	0.554	1.000	0.350
Hand	1.582	2.854	1.000

Ashby's material diagram of material strength vs material density is shown in Figure 3.16. It indicates the best choice of material against density. As the P430 ABS plus thermoplastic is located inside the blue area of the graph, it offers a good ratio between density and strength. So using this material can not only help to improve design reliability factor but also reduce mass on the servo motors.

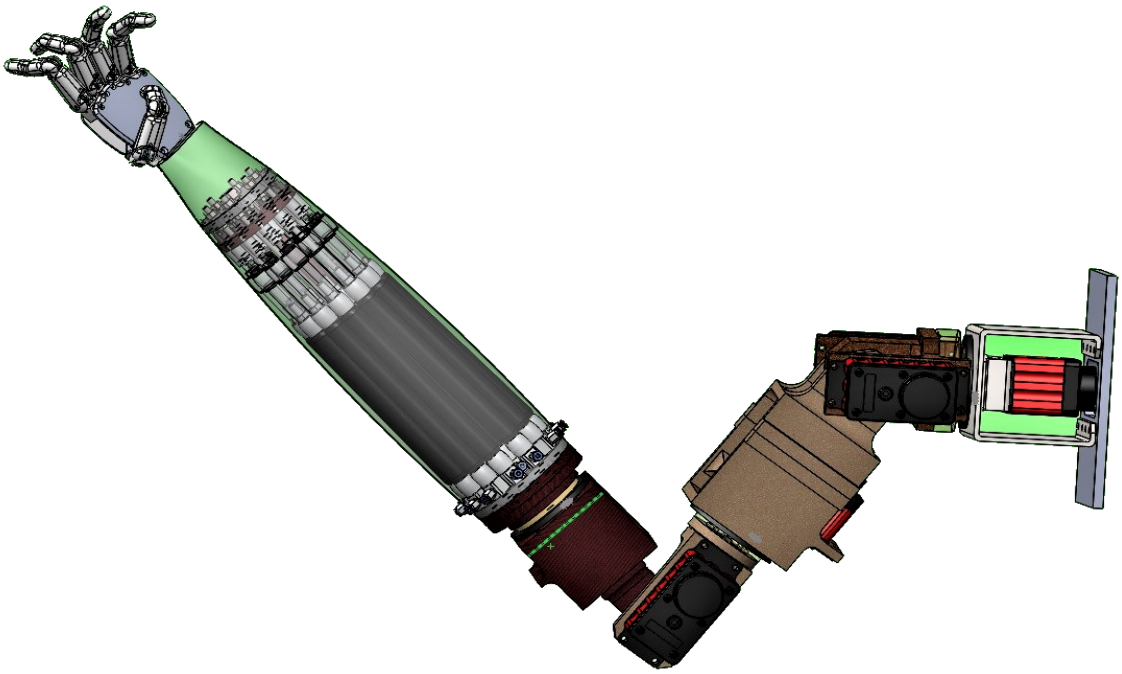

Figure 3.15: The ambidextrous robot arm design.

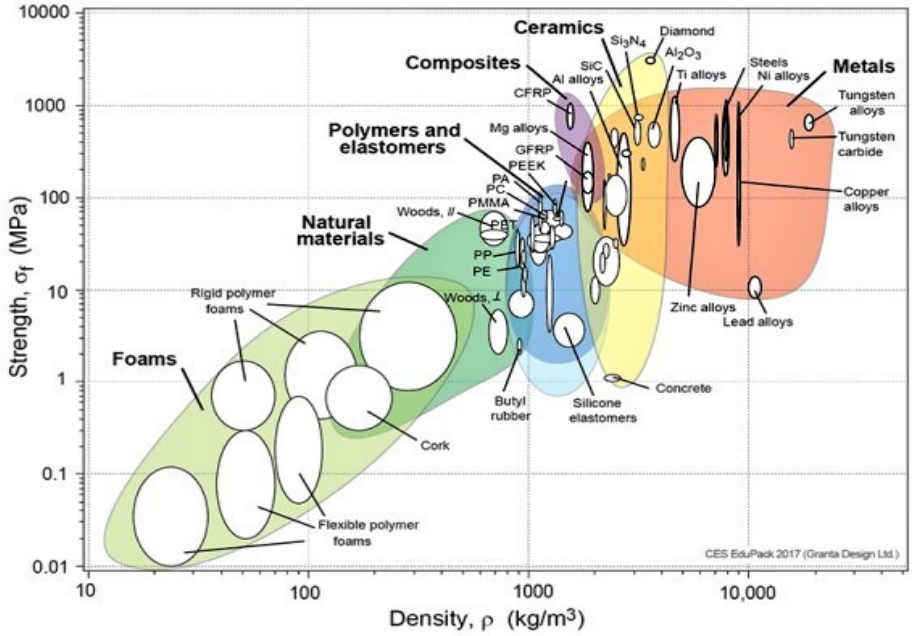

Figure 3.16: Ashby's diagram of materials strength versus density.

When it comes to stress analysis, not all the area needs to be strong. Usually, the stress force covers a specific area on the printed 3D part. The concept of stress concentration factor is introduced in [119] by Young, Budynas and Sadegh. In their published book, a standard guideline is given to minimise the stress concentration and hence maximum active stress. Stress analysis was performed on each part in Solidworks (see appendix D for detailed stress analysis) and the final design was then sent to the 3D printing lab.

All 3D printed parts were assembled to make the ambidextrous robotic arm. Figure 3.17 shows the assembled version of the ambidextrous robot arm. The assembly process took place in the Sustainable Electric Power (SEP) lab at Brunel University London.

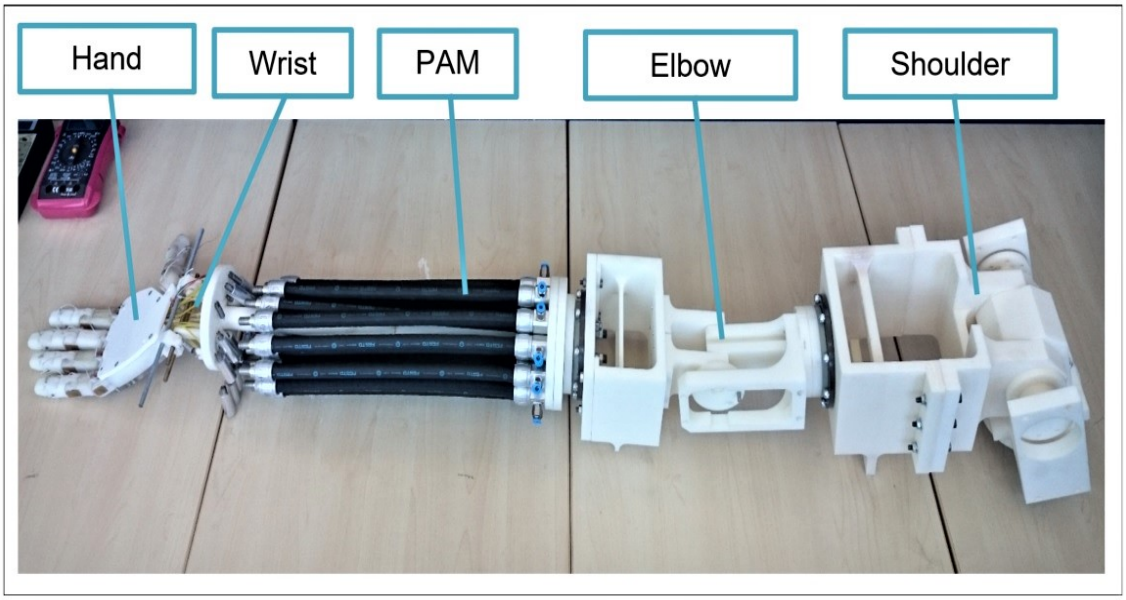

Figure 3.17: The assembled version of the ambidextrous robot arm.

Finally, the ambidextrous robot arm was attached to a metal part that is fixed on a surface as shown in Figure 3.18.

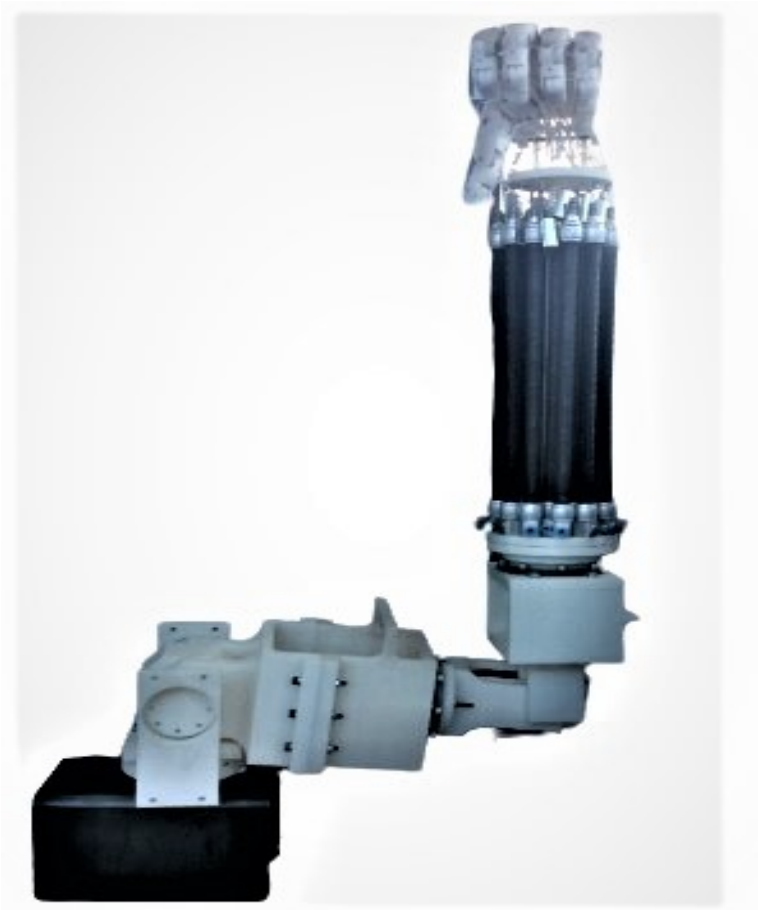

Figure 3.18: The ambidextrous robot arm in its default position.

3.3 Chapter Summary

This chapter has summarised the steps followed in re-designing an existing ambidextrous robot hand and developing a new ambidextrous robot arm design. It gave an overview of how each part was designed to meet the ambidexterity requirement of this project. A brief introduction to 3D printing and ambidextrous robot arm assembly were presented. All the movements aimed for were achieved and manually tested to confirm the range of motion.

Chapter 4

Control of the Ambidextrous Arm

A customised version of neural network controller is introduced in this chapter, and an effort is made to choose the most appropriate controller to drive the ambidextrous robot arm by comparing it with existing controllers. To begin with, forward and inverse kinematics problems are presented. With the help of Denavit-Hartenberg notation, the inverse kinematics of the robot is solved to find a set of feasible joint configurations required to perform the task. Solving the inverse kinematics is usually a challenging step which requires in-depth analyses of the robot. The module then solves the inverse dynamics of the robot to analyze the forces and torques applied on each joint and link in the robot. Furthermore, a calculation for the energy consumption is performed for each configuration. Since solving the inverse kinematic problem for the ambidextrous robot arm model became complicated due to the nature of the design, an ANFIS based solution is explored. To further improve the results, a modified MANFIS controller is used and results are presented.

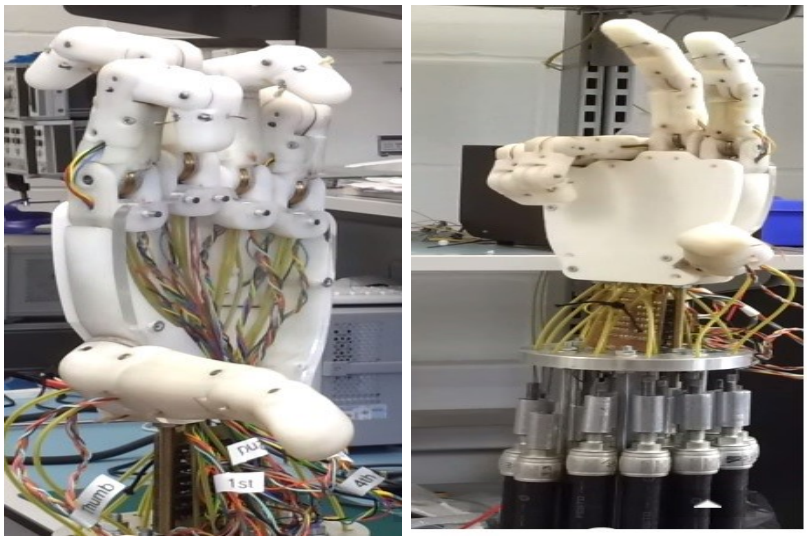

(a) (b)

Figure 4.1: The ambidextrous robot hand, where (a) is the ambidextrous mode and (b) is the left mode.

Ambidextrous nature of hand can be seen in Figure 4.1 and the working principle of the ambidextrous robot arm operation is simplified in Figure 4.2. The ambidextrous arm is composed of key units such as mechanical unit (rigid links and joints and supporting structures i.e. forearm, wrist, end-effector), sensor unit (position sensors, force sensors and vision sensors), actuation unit (PAMs and servo motors) and a supervision unit (task planning and control, artificial intelligence and reasoning).

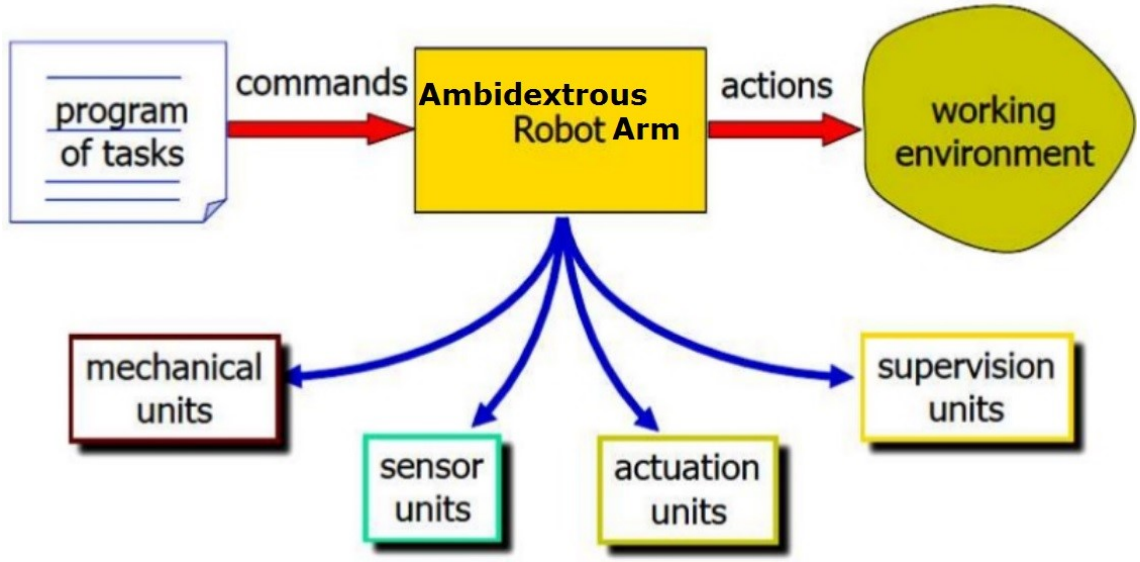

Figure 4.2: The working principle of the ambidextrous arm in a simplified version.

4.1 Control of the Ambidextrous Robot Hand

The ambidextrous robot hand is a robotic device for which the specificity is to imitate either the movements of a right hand or a left hand as shown in Figure 4.1. The modified version of ambidextrous robot hand offers a total of 14 DOF and is actuated by 20 PAMs. Comparison of existing and modified version is shown in Table E.1. The possibility of controlling a uniquely designed ambidextrous robot hand using PID controller combined with neural network controller is validated.

4.1.1 Comparison of Conventionl Controller

In this section, a comparison of the conventional controllers (PID, Bang-bang and Backstepping) is presented. Figure 4.3 shows a snapshot of the ambidextrous robot hand holding a can of coke when each controller is applied.

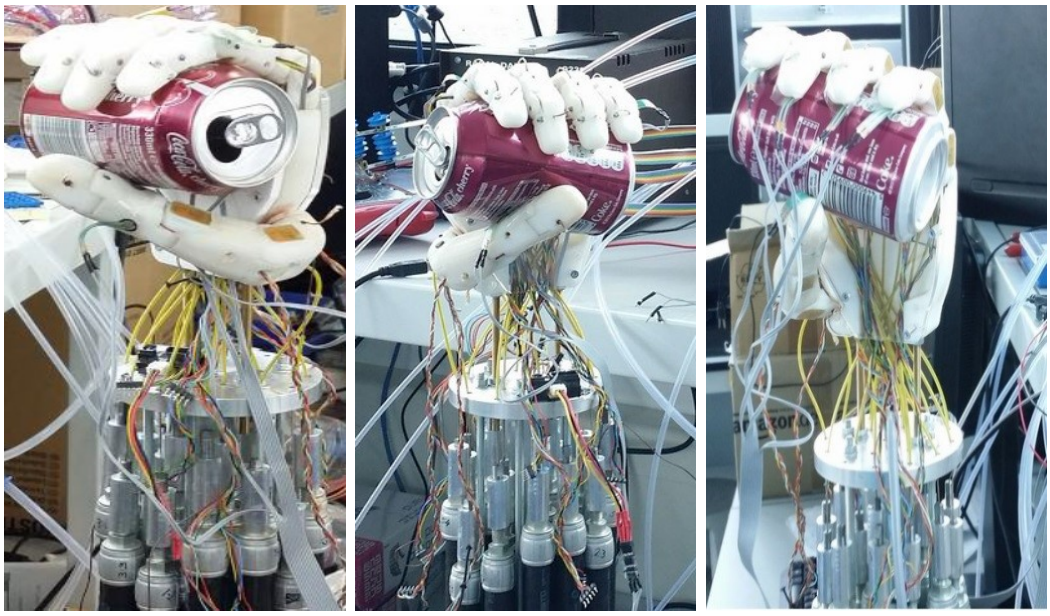

(a) (b) (c)

Figure 4.3: The ambidextrous robot hand is holding a can with a grasping movement implemented with PID controllers (a), with bang-bang controller (b) and with backstepping controller (c).

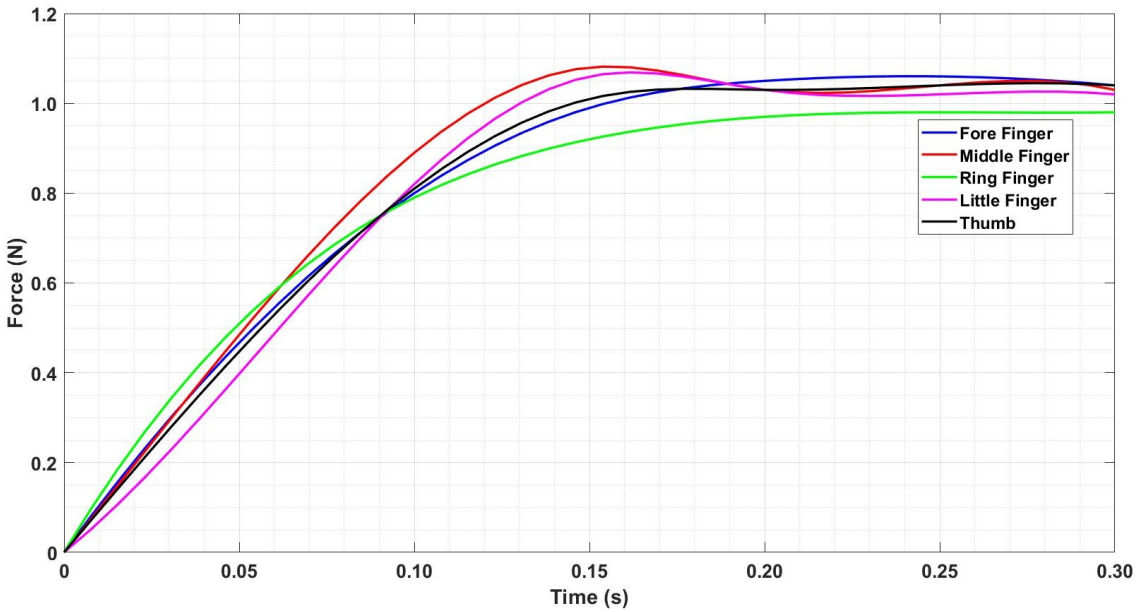

Figure 4.4: The graph shows force against time of the five fingers while grasping a drink can with PID controllers.

From Figure 4.4, it can be seen that grasping of an empty can of soft drink began at 0.10 seconds approximately and it became more stable after 0.20 seconds. An overshoot of 10% occurred on all fingers but stayed in a limit of 0.1 N where the system automatically adjusted at the next data collection. These small overshoots occurred because different parts of the fingers get into contact with the object before the object gets into contact with the force sensor. This results in the bending of fingers slower when phalanges touch the object. Since the can of soft drink does not deform itself, it can be deduced that the grasping control is both fast and accurate when PID loops drive the ambidextrous hand.

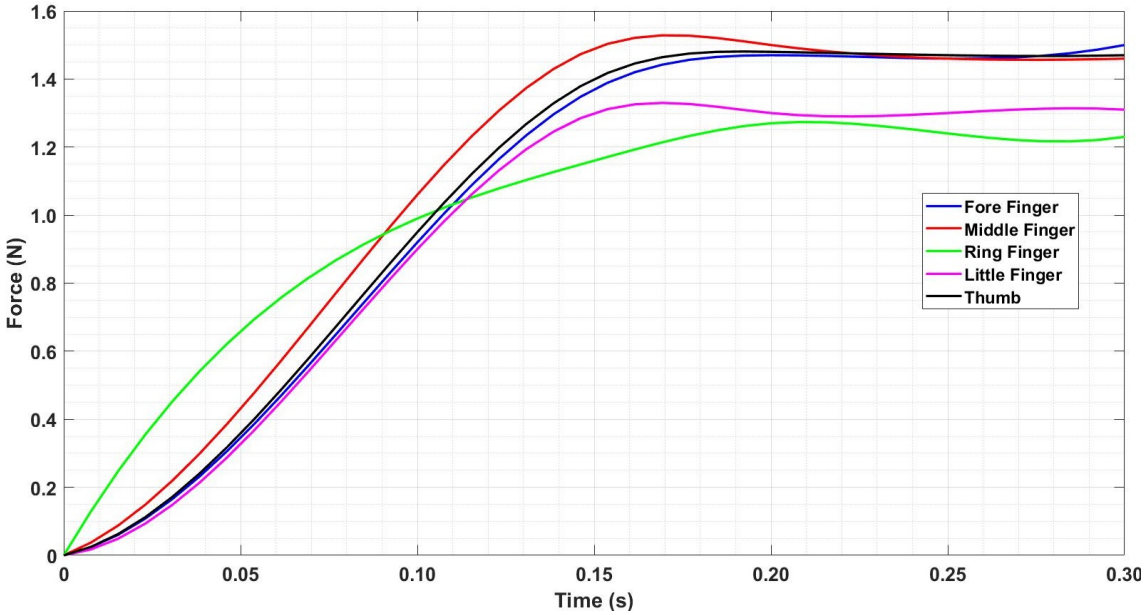

Figure 4.5: The graph shows force against time of the five fingers while grasping a drink can with bang-bang controllers.

The phalanges must close with appropriate speed ratios to tighten around objects when interacting with an object. By repeating the experiments realised earlier, the graph is obtained from the data collection of the left mode. It is noticeable from Figure 4.3b that the can of soft drink deforms itself when it is grasped on the left-hand side. Also, the speed of fingers does not change when it touches the objects. That explains why the graph has higher curves than previously obtained in Figure

4.4. This makes the bang-bang controller faster than PID loops. The bang-bang controllers also stop when the value of 1 N is overreached but, without predicting the approach to the set point, the process variables have huge overshoots (see Figure 4.5). The overshoot is mainly visible for the middle finger, which overreaches the set-point by more than 50%. Even though backward control is not implemented in the bang-bang controller, it is seen that the force applied by some fingers decreases after 0.15 seconds. This is due to the deformation of the can, which reduces the force applied on the fingers. Contrary to PID loops, it is seen that the force applied by some fingers may not change between 0.18 seconds and 0.25 seconds, which indicates the grasping stability is reached faster with bang-bang controllers. The bang-bang controllers can consequently be applied for heavy objects.

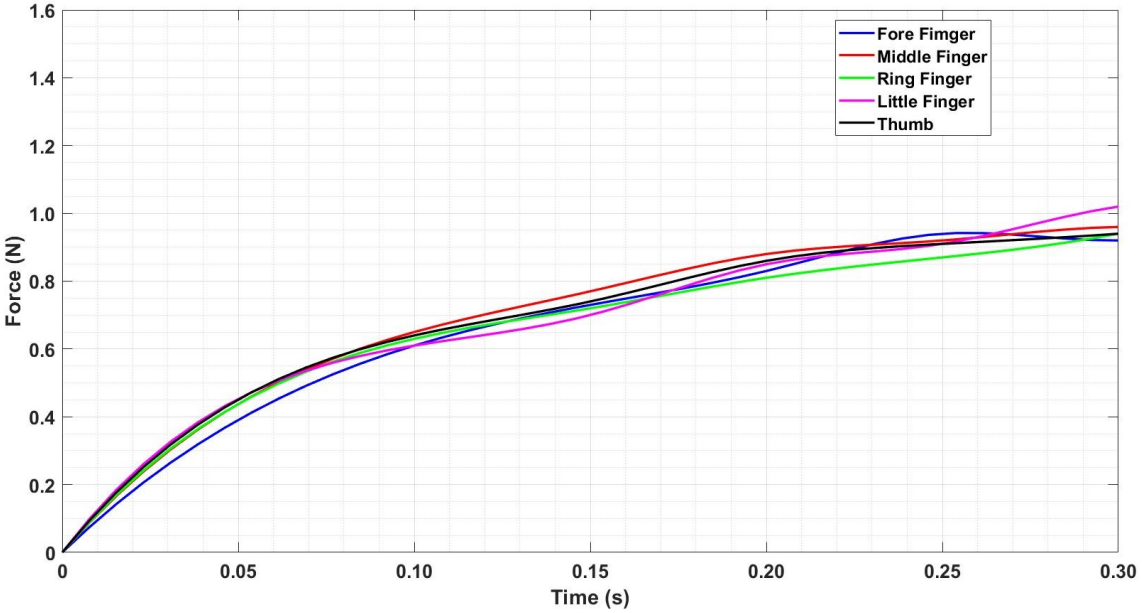

Figure 4.6: The graph shows force against time of the five fingers while grasping a drink can with backstepping controllers.

The grasping features obtained with the BSC are illustrated in Figure 4.3c. The force against time graph obtained from the data collection is shown in Figure 4.6. During the experiment, it was noticed that the speed of finger tightening using backstepping control was much slower compared to the PID controller and bang-bang

controller. Since the backstepping controller's target is based on force feedback and speed stability, it offers greater flexibility than PID and bang-bang but takes longer to stabilise. The fingers provided enough force to grab the can of soft drink at 0.15 seconds, but it is seen the system carries on moving until 0.30 seconds.

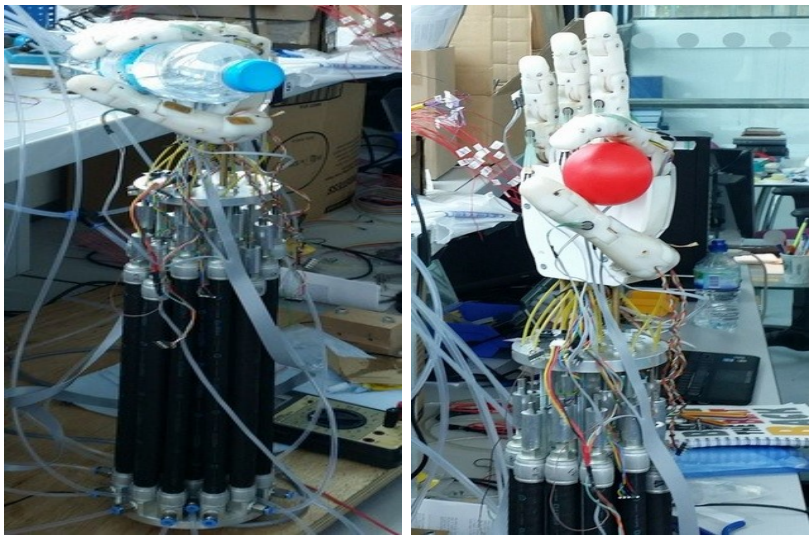

(a) (b)

Figure 4.7: The ambidextrous robot hand is holding a water bottle in (a) and ball in (b).

Therefore it is deduced that BSC takes longer to stabilise. It can also be noted that the hand speed is slower using BSC, as none of the sensors reads more than 1.2 N. The higher speeds of the PID and bang-bang controllers are respectively explained because of the integrative term and the lack of derivative control. The ambidextrous robot hand is capable of grasping various objects of different sizes and shapes as shown in Figure 4.7.

It can be seen from previous experiments that the best performances are reached with PID and BSC controllers, as both of them are accurate and permit the fingers to adapt to the shape of objects with backward movements. However, PID loops proved faster than any other controller, which could be one of the main reasons for finding a high number of resources in the literature review. Despite its accurate

implementation, the BSC did not reveal as robust results. The fingers stabilise themselves after 0.30 seconds with BSC, against 0.20 seconds for PID and bang-bang controls. The main advantage of BSC is its ability to regulate nonlinear actuators. This is the reason why these two algorithms receive feedbacks from pressure or position sensors [120, 121].

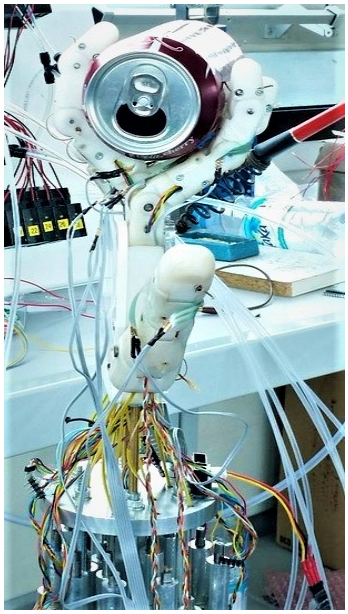

Figure 4.8: The ambidextrous robot hand is grabbing a can in ambidextrous fashion.

Nevertheless, in the case considered here, the feedback is received from force sensors directly implemented on the mechanical structure instead of the actuators themselves. Even though bang-bang control is the fastest of the three compared algorithms, it is not smooth enough to adapt itself to the shape of the objects and can crush them. The shooting function of the bang-bang controller is too sudden without additional controllers, which is why it is cascaded [122]. However, bang-bang control can be used to grab a heavy object. The higher is the PAMs' pressure, the slower the PAMs contract, which is why their elasticity automatically opposes itself to the shooting function effect in that case. By implementing force sensors both on the right and left sides of the fingers, the ambidextrous hand can also grab objects in atypical

positions, as shown in Figure 4.8.

4.1.2 Implementation of Neural Network Based Controller

Key performance differences when conventional robotic hand controllers (PID, bang-bang and Backstepping) are combined with neural networks (NN) is subject of invetigation in this section. Tests were performed on the ambidextrous robot hand. The ambidextrous hand is actuated using PAMs and can bend its fingers both left and right, offering full ambidextrous functionality. Force sensors are placed on the fingertips. In this NN based control method, the grasping trajectory of each finger combines its data with that of the neighboring fingers to obtain accurate results. Robotic manipulators have become increasingly important in the field of flexible automation. NNs can flexibly map nonlinear functions and can be trained and applied both on and off-line. Of the many NN types, two of the most widely used are the Multi-Layer Perception (MLP) and radial basis function (RBF) [123]. Back-propagation is the most popular method of implementing MLP. There are three dominant learning paradigms: supervised learning, unsupervised learning and reinforcement learning. Each learning paradigm is suitable for solving a specific set of problems. A 3-layer NN with full interconnections is shown in Figure 4.9.

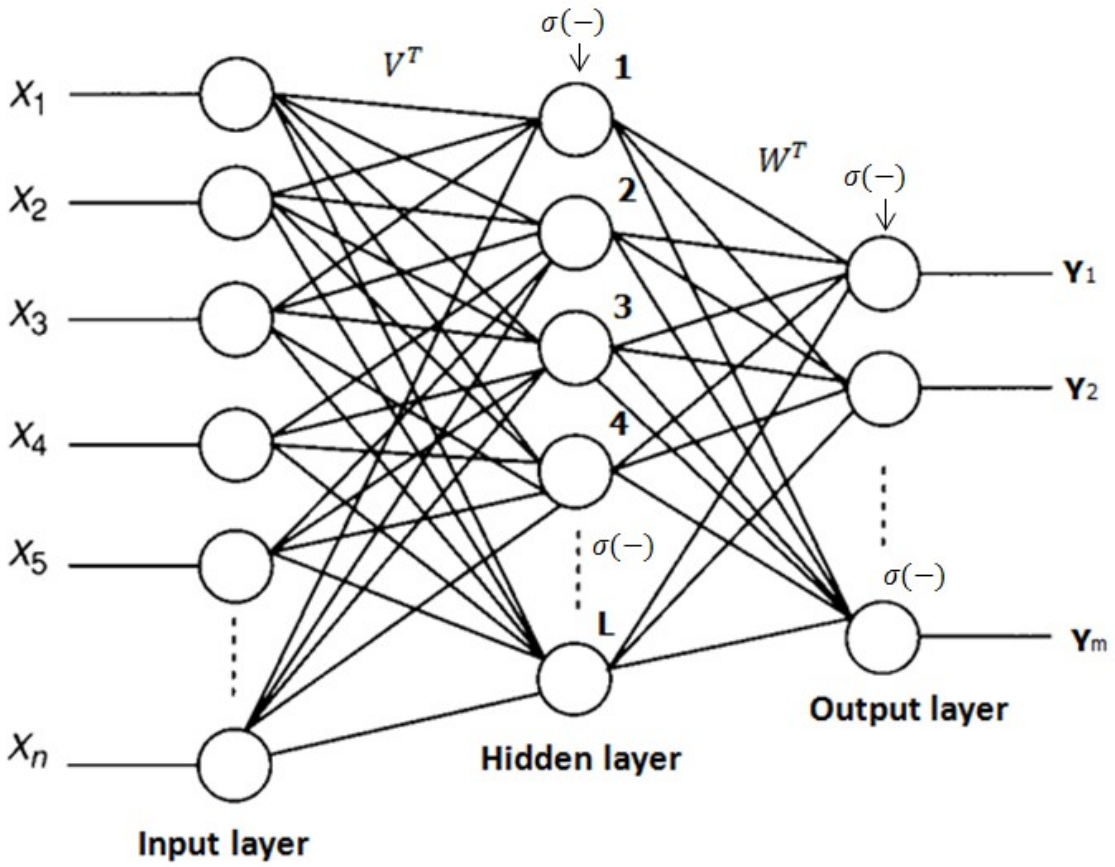

Figure 4.9: Three-layer Neural Network (NN).

Neural networks have been widely applied in robot control and motion planning [124, 125]. They have been used to achieve motion control of manipulators [126], to help robots follow predetermined trajectories on city streets [127] and to achieve visual control of robotic arms [128]. A real-time learning neural robot controller was used to solve the inverse kinematics problem [129] and an artificial neural network was used to help a robotic arm system with 6 DOF to track and grasp a moving object [130]. Neural networks can be implemented into robotic structures in several ways and with different controllers to provide improved solutions. For instance, in [131], a learning process is designed for the two-links PAM manipulator to have an adaptive and dynamic self-organising structure using NN and fuzzy logic. The NN was connected to PID loops in [132], to create an intelligent Phasing Plane Switch

Control (PPSC) to overcome nonlinearities in PAM pressure feedback. NNs have also been integrated into particle swarm optimisation to increase system accuracy [133].

Unlike pressure sensors that are connected to the PAMs and always detect variations when a robot hand is interacting with objects, force sensors only cover some strategic points of the fingers. Therefore, when an object gets into contact with robotic fingers at a place not covered by force sensors, the fingers carry on closing without any variations in the grasping algorithms. This is the reason why grasping algorithms are combined with an NN, used as a security system. In the following, F_f refers to the force F applied by each of the four other fingers (where F is a notation), F_t to the force defined as target and $F_f(t)$ the force received from each finger. For the force feedback of each finger $F_f(t)$, the values of the closest fingers $F_{(f-1)}(t)$ and $F_{(f+1)}(t)$ are also considered. In case $F_f(t) = 0$ but $F_{f-1}(t)$ or $F_{f+1}(t)$ receives a high force feedback, two different outcomes are possible. Either the object is not in contact with the sensor F_f or the object is not in contact with the finger at all. In the first case, the grasping controller must stop running as the finger actually touches the object. In the second case, the shape of the object does not cover the whole hand and that all the fingers are not necessary for the grasping. The detection of this case is translated as follows (constant 0.9 is the ratio experimentally defined to react at the object's presence):

$$\begin{aligned} & F_{cf} \geq 0.9 * F_f \\ \textit{where} \quad & F_{cf} = [F_{f-1}(t) \cup F_{f+1}(t)] \\ \textit{and} \quad & F_f(t) \simeq 0 \end{aligned} \tag{4.1}$$

If Equation (4.1) is true, then at least one of the fingers close to the finger f is close enough to grab the object. If Equation (4.1) is true and $F_f(t) \simeq 0$, then the object is either not in contact with the sensor or not in contact with the finger. So the

grasping controller must either stop at that point or make the finger return back to a vertical position accordingly. In a case where the finger f is in contact with the object, the process must react in a different way by reading the angular angle. Thus angular feedback is read, taking the angle of the vertical position as a reference. In Equation (4.1) F_{cf} refers to neighboring fingers on both sides of the concerned finger. In Equation (4.2), θ_f(t) refers to the angle of each finger and a constant of 0.8 is the ratio experimentally defined to determine whether there is an abnormal increase of grasping angles

$$\theta_{f-1}(t) < 0.8 * \theta_f \tag{4.2}$$

and

$$\theta_{f+1}(t) < 0.8 * \theta_f \tag{4.3}$$

If both (4.2) and (4.3) are true, then the finger f has an angle much lower than the ones of its adjacent fingers f_{-1} and f_{+1}. Consequently, the more the finger f closes itself, the bigger $\theta_f(t)$ becomes. Thus, a constant lower than value 1 is used to check if $\theta_{f-1}(t)$ or $\theta_{f+1}(t)$ have stopped increasing at a smaller angle. If the finger f does not touch any objects, then it is brought back to its vertical position. $\theta_f(t)$ is then compared to a value close to $\pi/2$ to know if the finger f is perpendicular with the palm. In that case, the finger f goes back to the vertical position without getting into contact with any objects. These algorithms are summarised in Figure 4.10. F_0 is the thumb, for which the angle is not taken into account.

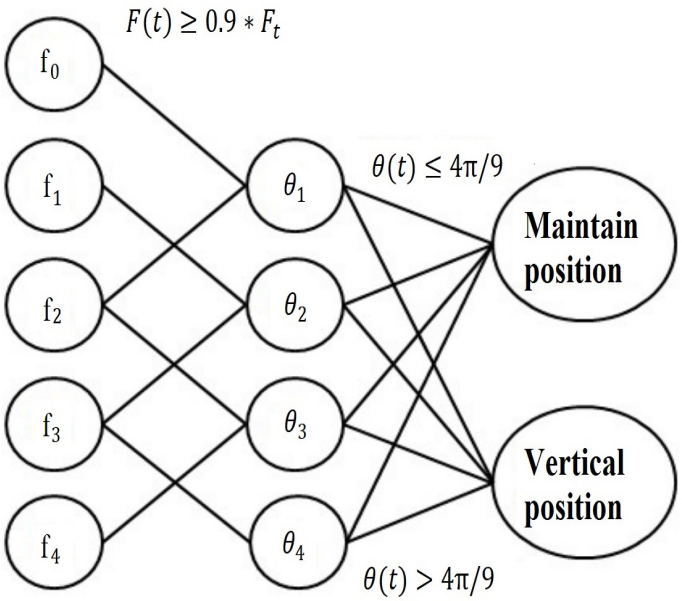

Figure 4.10: Neural network mapping (from the thumb f_0 to the little finger f_4).

Figure 4.11 and Figure 4.12 show the hand grasping a ball and a water bottle respectively. The position of the fingers changes depending on the shape of the object being grasped. The force target is 2.25 N ± 10% for the bottle and 1 N ± 5% for the ball. The indicated angles are those of the proximal phalanges. When the hand grasps the bottle, the fingers come into contact with the object within 0.2 seconds, but the angles continue to increase until 0.45 seconds because the fingers continue closing until the bottle is pressed up against the thumb on the far side.

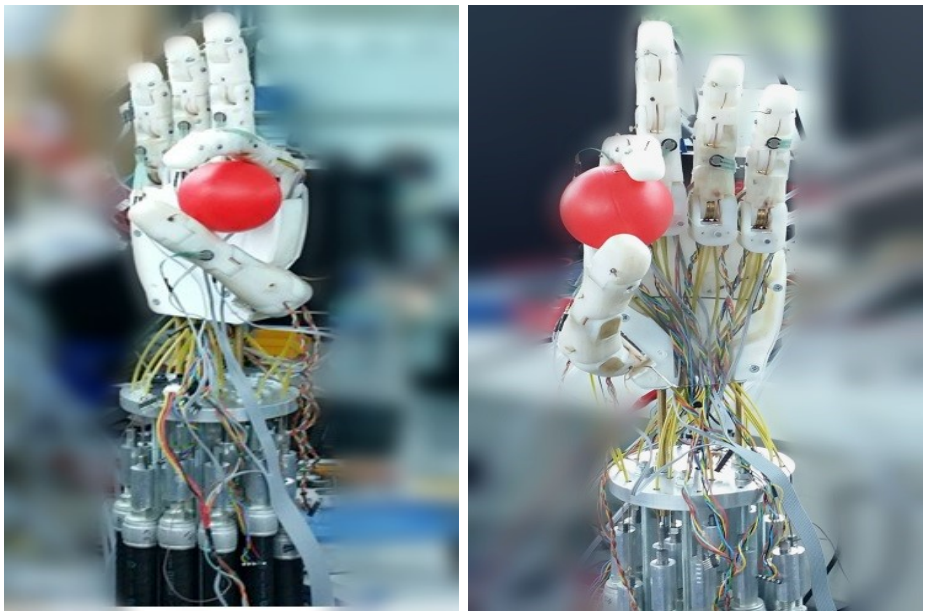

(a) (b)

Figure 4.11: The ambidextrous robot hand holding a ball in both (a) and (b).

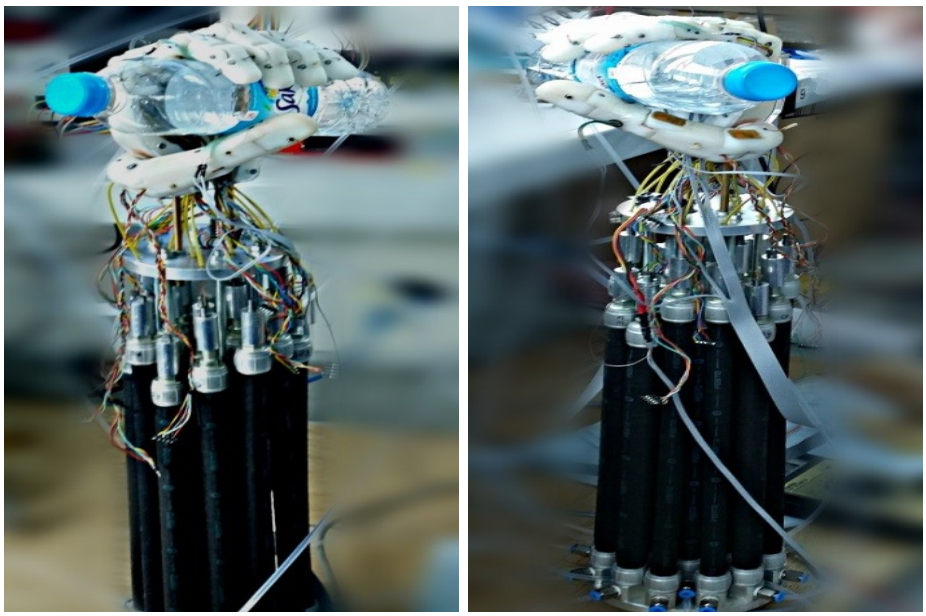

(a) (b)

Figure 4.12: The ambidextrous robot hand is holding a water bottle in both (a) and (b).

The middle finger is longer than the others; thus the force sensor on the tip of the middle finger does not come into contact with the object. However, because of the implemented NN, the force data collected from the adjacent fingers also plays a key part in the grabbing process as shown by the angle reached. The fingers react differently when grabbing a ball. The forefinger comes into contact with the object at 0.1 seconds, and its movement stops at 0.3 seconds (as opposed to 0.4 seconds for the bottle), as the object is bigger and the target force is smaller. Also, this grabbing action only involves the thumb and forefinger. As seen in Figure 4.13 and Figure 4.14, the different finger shape results in the middle finger having the slowest movement, whereas the little finger is the fastest.

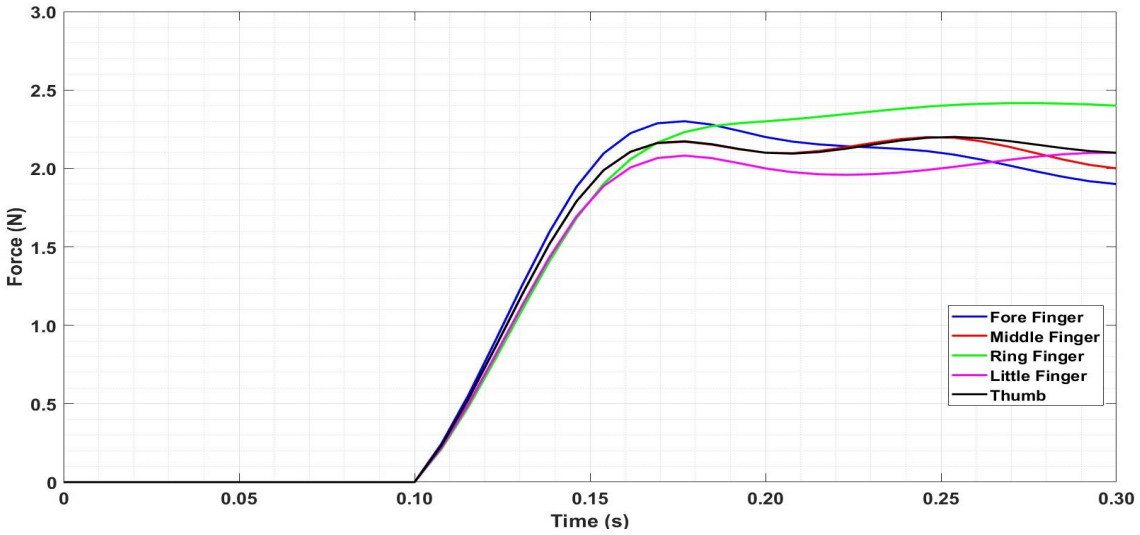

(a)

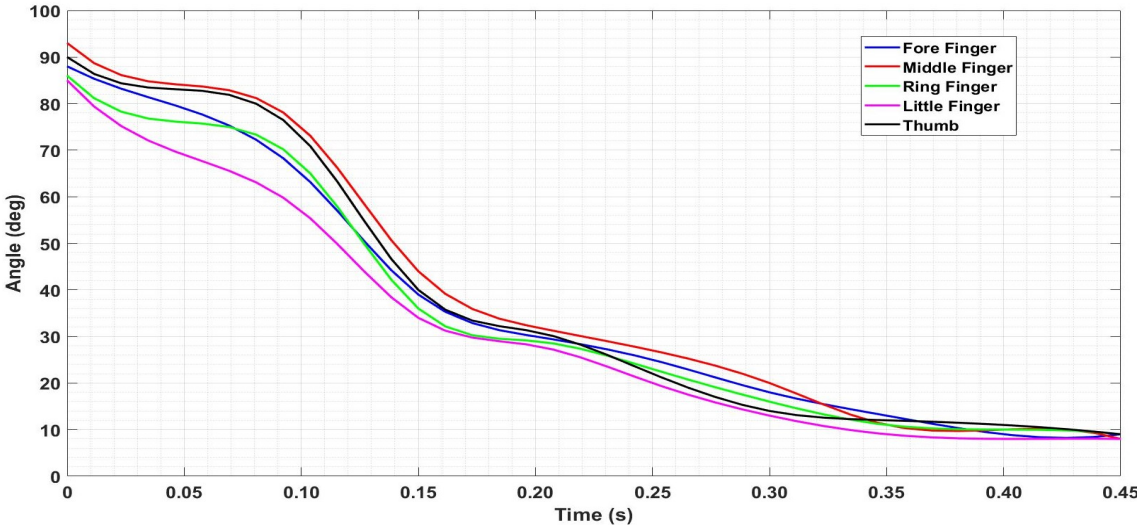

(b)

Figure 4.13: Forces against time are plotted in (a) and angle against time in (b) when the hand grabs a bottle.

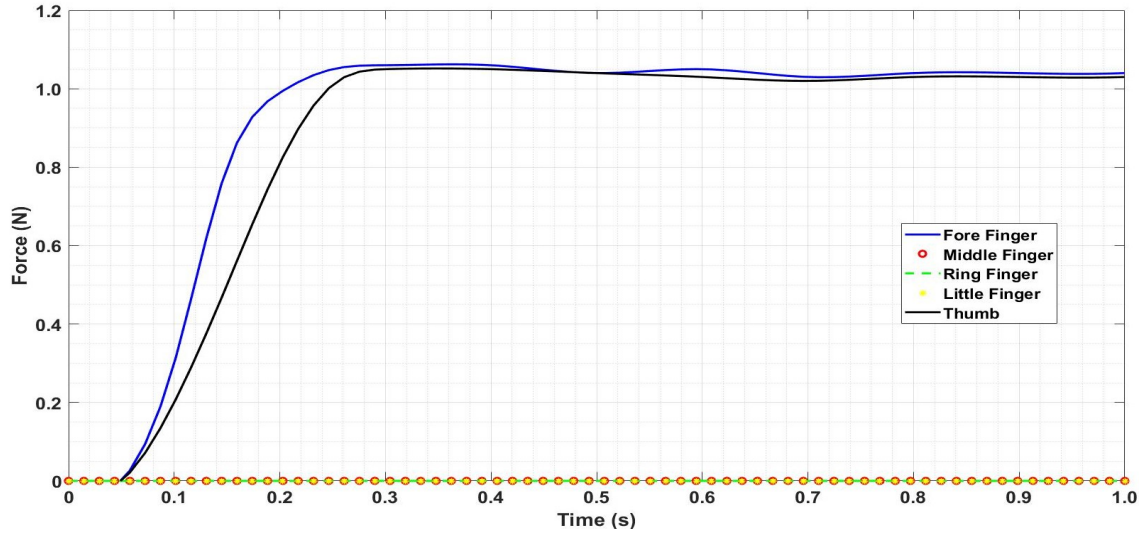

(a)

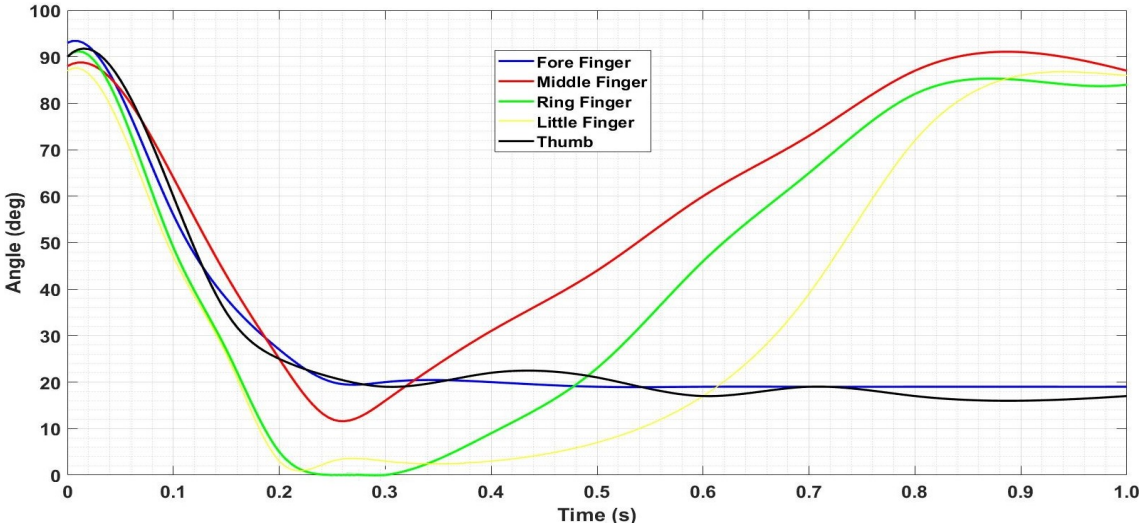

(b)

Figure 4.14: Fingers' forces against time are plotted in (a) and angle against time in (b) when the hand grabs a ball.

As it applies no force and its angle becomes much smaller than that of the forefinger, it is deduced that middle finger is not in contact with the object. Therefore the finger starts rising before 0.25 seconds. Next the NN is applied in the same way to the ring finger at 0.30 seconds, and finally, the little finger starts returning to its vertical position at 0.40 seconds. The little finger moves more slowly than the middle and ring fingers because compressed air is already being used to drive their movement.

The speed of the middle and ring fingers barely varies, as the PAM is in the middle of their contraction. Thus, a small increase of pressure still implies an important variation of the PAM's lengths. The movement speed of the little finger increases at 0.65 seconds when the middle finger approaches the vertical position and has its speed reduced. The compressed air is therefore only involved in the movements of the ring and little fingers. Finally, only the forefinger maintains its closing position, whereas the middle, ring and little finger return to their vertical positions. The grabbing movement for the bottle was completed in 0.35 seconds, which for the ball took 1 second because it comprised both closing and opening movements.

Table 4.1: Performance comparison of conventional controllers when combined with NN.

Grasping algorithms	**Algorithms to which it is combined**	**Averaged rising time (s)**	**Averaged % of overshoot**	**Averaged grasping time (s)**	**Averaged settling time (s)**
PID (Proposed)	NN	0.16	10%	0.20	0.20
Bang-bang	NN	0.10	52%	0.15	0.20
BSC	NN	0.29	2.30%	0.37	0.30

Bang-bang control is the fastest algorithm but also the least efficient one. It is not smooth enough to adapt itself to the shape of the objects and can crush them. As explained in [134] and, the shooting function of the bang-bang controller is usually regularised by employing additional controllers. However, bang-bang control can be used to grab a heavy object. The higher the PAMs pressure, the slower the PAMs contract, which is why their elasticity automatically opposes itself to the shooting function effect in that case. BSC may be the most accurate algorithm, but also the

slowest one. As for PID control, BSC permits the fingers to adapt to the shape of objects with backward movements.

Nevertheless, because of proportional and integral controls, PID loops have the advantage of making the fingers move faster. As for conventional PID, BSC depends on derivative and double derivative controls. This is the reason why the grasping time is much higher with the BSC, as it is not combined with proportional or integral controls. Therefore, it takes 0.30 seconds for the fingers to stabilise themselves with BSC against 0.20 seconds for PID control and 0.20 seconds for bang-bang control. Indeed, the main advantage of BSC is its ability to regulate nonlinear actuators. This is the reason why these two algorithms receive feedback from pressure or position sensors, as in [121]. Nevertheless, in the case discussed here, the feedback is received from force sensors directly implemented on the mechanical structure instead of the actuators themselves, as in previous research [27, 135].

4.2 Control of the Ambidextrous Robot Arm

Forward and inverse kinematics of robotic manipulators are two of the most common problems in robotics addressed in almost all major textbooks on this subject. In the forward kinematics problem the end-effector's location in Cartesian space, that is, its position and orientation, is determined based on the joint variables. The joint variables are the angles between the links, in the case of rotational joints, or the link extension, in the case of prismatic joints. Conversely, given a desired end-effector position and orientation, the inverse kinematics problem refers to finding the values of the joint variables that allow the manipulator to reach the given location. While forward kinematic is rather straightforward, solving the inverse kinematics problem for robotic manipulators is a difficult and also quite challenging task. The complexity of this problem is given by the robot's geometry and the nonlinear trigonometric equations that describe the mapping between the Cartesian

space and the joint space [136–139]. Although a closed form solution to this problem is preferable in many applications, most of the time this is impossible to find. Therefore, various other ways to determine the solution to the inverse kinematics problem were proposed. These include, among others, listed in [140], geometrical solutions (where possible), numerical algorithms based on optimisation techniques [141–143], evolutionary computing [139, 144–147] or neural networks [148–150].

The forward and inverse kinematics of the ambidextrous robot arm are discussed in this section. The use of ANFIS to produce the solution to the inverse kinematic problem for the ambidextrous robot arm is presented. The ANFIS is trained using the data provided by the forward kinematics to learn the inverse forward mapping of the configuration space. This means, the end-effector's position, as well as its orientation are given as inputs and the ANFIS identifies which joint configuration corresponds to the given localization of the end-effector. The modified MANFIS controller is found to be the best control to drive the ambidextrous arm. Efficiency of the arm is proved through experiments by comparing its performance with a traditional robot arm.

4.2.1 Forward Kinematics of the Ambidextrous Robot Arm

Robotic arms are composed of links that are interconnected by joints to form a kinematic chain as shown in Figure 4.15. First of all, geometric parameters are used to define the ambidextrous robot arm as shown in Figure 4.16. The arm has five joints as shown in Figure 4.17. It consists of one fixed link and five movable links that are fixed with the ambidextrous robot hand [151]. It is connected with the 14 DOF hand that also possess ambidextrous features; hence, it can bend its fingers in both ways left side and right side [152]. In robotics, mainly two types of joints are used: revolute and prismatic. In our case, revolute joints connect all the links

through a serial link mechanism.

The length of each link is defined to be the distance between adjacent joint axes. The servo motor that is driving link one is permanently fixed to the base of an ambidextrous arm, $\theta_1$represents the angle between the x-axis and link 1. θ_2 is the angle between link 1 and link 2, θ_3 between link 2 and link 3. An actuator driving link 4 generating θ_4 and θ_5 is generated by actuator driving link 5. Robotic manipulators are designed to perform various tasks mostly using end effectors. So in order to perform such tasks, the position and orientation of the end effector must be known. Then, the position and orientation of the end effector in terms of a joint variable are calculated. This technique is called forward kinematics. Calculating forward kinematics of a robot is often considered the very first step in robotic research. The Denavit Hardenberg (DH) approach has been used to determine the forward kinematics and to assign the axis to movable joints. There are various approaches to model the robot arm such as Screw Theory representation; Hayati Roberts and geometric modelling DH approach are suitable for the ambidextrous robotic arm structure. Other approaches may be beneficial only in the case where the DH approach does not handle parallel $z - axis$.

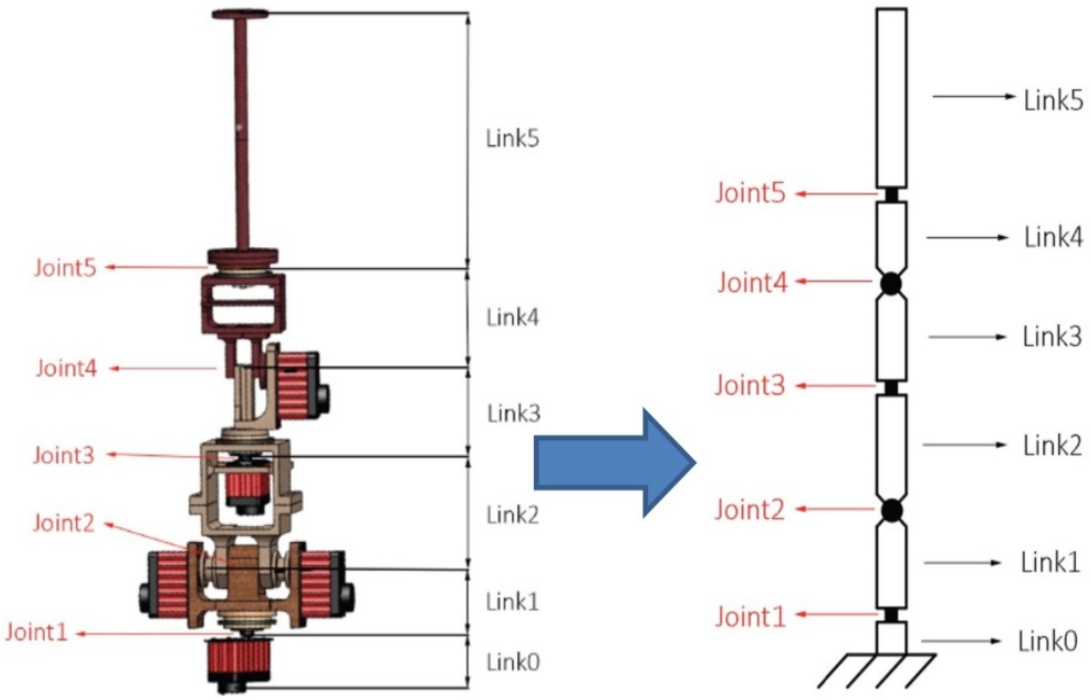

Figure 4.15: Mechanical structure of the ambidextrous robot arm translated into links and joints.

The DH convention describes a systematic way to develop the forward kinematics of any robot. The kinematic analysis allows the designer to obtain key information on the position and orientation of each joint and link within the mechanical structure. This information is necessary for subsequent dynamic analysis along with control paths. The transformation set given below can be used to locate $i-1$ axes of a point x_i (revolute joint) placed on the i^{th} link:

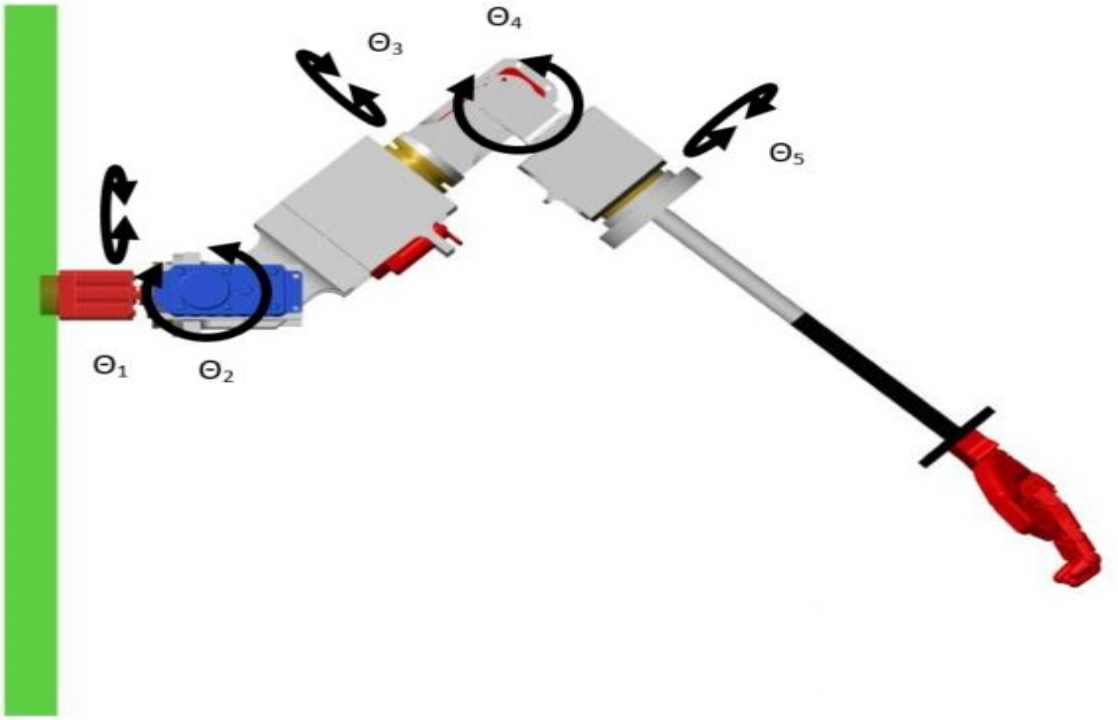

Figure 4.16: Kinematic configuration and joint model of the five-joint ambidextrous robotic arm.

$$\boldsymbol{A_i} = \mathbf{H}(d, z_{i-1})\mathbf{H}(\theta, z_{i-1})\mathbf{H}(a, x_i)\mathbf{H}(\alpha, x_i) \qquad (i = 1, ...n) \tag{4.4}$$

where H is a 4 x 4 matrix. It is used to represent a homogeneous transformation.

$$where \qquad \boldsymbol{H}(\alpha, x_i) = \begin{bmatrix} 1 & 0 & 0 & 0 \\ 0 & \cos(\alpha_i) & -\sin(\alpha_i) & 0 \\ 0 & \sin(\alpha_i) & \cos(\alpha_i) & 0 \\ 0 & 0 & 0 & 1 \end{bmatrix} \tag{4.5}$$

$$\boldsymbol{H}(a, x_i) = \begin{bmatrix} 1 & 0 & 0 & a_i \\ 0 & 1 & 0 & 0 \\ 0 & 0 & 1 & 0 \\ 0 & 0 & 0 & 1 \end{bmatrix} \tag{4.6}$$

$$\boldsymbol{H}(\theta, z_{i-1}) = \begin{bmatrix} \cos(\theta_i) & -\sin(\theta_i) & 0 & 0 \\ \sin(\theta_i) & \cos(\theta_i) & 0 & 0 \\ 0 & 0 & 1 & 0 \\ 0 & 0 & 0 & 1 \end{bmatrix} \tag{4.7}$$

$$\boldsymbol{H}(d, z_{i-1}) = \begin{bmatrix} 1 & 0 & 0 & 0 \\ 0 & 1 & 0 & 0 \\ 0 & 0 & 1 & d_i \\ 0 & 0 & 0 & 1 \end{bmatrix} \tag{4.8}$$

Applying the matrix multiplication

$$\boldsymbol{A_i} = \begin{bmatrix} \cos(\theta_i) & -\cos(\alpha_i)\sin(\theta_i) & \sin(\alpha_i)\sin(\alpha_i) & a_i\cos(\theta_i) \\ \sin(\theta_i) & \cos(\theta_i)\cos(\alpha_i) & -\sin(\alpha_i)\cos(\theta_i) & a_i\cos(\theta_i) \\ 0 & \sin(\alpha_i) & \cos(\alpha_i) & d_i \\ 0 & 0 & 0 & 1 \end{bmatrix} \tag{4.9}$$

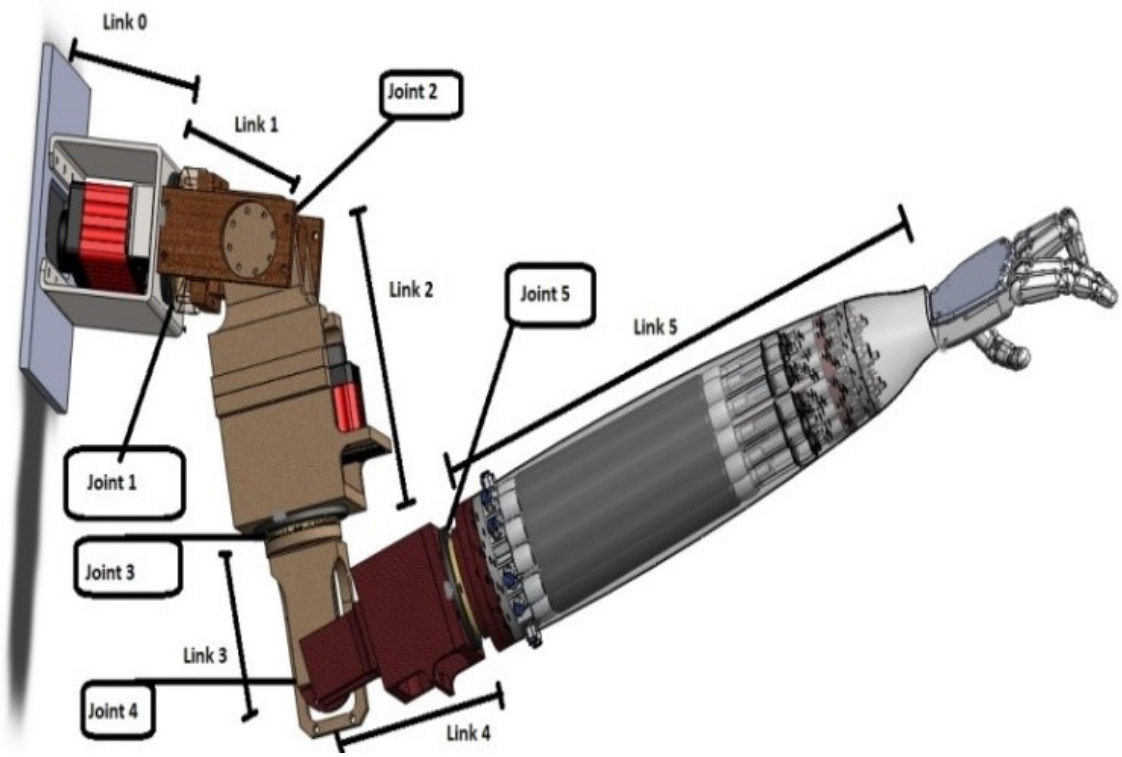

Figure 4.17: 3D model of the ambidextrous robot arm.

Table 4.2: DH parameter of the ambidextrous robot arm.

Link	d_i	a_i	α_i	θ_i
1	l_1	0	90	θ_1
2	0	0	-90	θ_2
3	$l_2 + l_3$	0	90	θ_3
4	0	0	-90	θ_4
5	$l_4 + l_5$	0	0	θ_5

Using the DH convention, θ_i describes joint angle of x_i axis relative to x_{i-1} axis defined according to the right-hand rule about z_{i-1} axis, distance from the origin is denoted by d_i of the $i-1$ axes to the intersection of the z_{i-1} axis with the x_i axis and measured along the z_{i-1} axis, a_i is minimum distance between z_{i-1} and z_i and α_i describes an offset angle of z_i axis relative to z_{i-1} axis measured about the x_i axis using right-hand rule. To obtain the forward kinematics transformation matrix T_n^0 based on homogenous transformations and DH convention. All the reference systems

are located that are required in making sure the DH coordinate frame assumptions are satisfied. Then the table of link parametera is created as shown in Table 4.2. A homogeneous transformation matrix A_i is formed that was later used to compute the position and orientation of the end effector. Since all the parameters are known that are required to form the homogeneous transformation matrices A_i, it is time to enter these parameters into Equation (4.9) to find A_1, A_2, A_3, A_4, A_5 and T_1^0, T_2^1, T_3^2 , T_4^3 and T_5^4.

Position and orientation of the tool frame expressed in the base coordinates can be located easily from T_5^0.

$$T_1^0 = A_1 = \begin{bmatrix} \cos(\theta_1) & 0 & \sin(\theta_1) & 0 \\ \sin(\theta_1) & 0 & -\cos(\theta_1) & 0 \\ 0 & 1 & 0 & l_1 \\ 0 & 0 & 0 & 1 \end{bmatrix} \tag{4.10}$$

$$T_2^1 = A_2 = \begin{bmatrix} \cos(\theta_2) & 0 & \sin(\theta_2) & 0 \\ \sin(\theta_2) & 0 & -\cos(\theta_2) & 0 \\ 0 & -1 & 0 & 0 \\ 0 & 0 & 0 & 1 \end{bmatrix} \tag{4.11}$$

$$T_3^2 = A_3 = \begin{bmatrix} \cos(\theta_3) & 0 & \sin(\theta_3) & 0 \\ \sin(\theta_3) & 0 & -\cos(\theta_3) & 0 \\ 0 & 1 & 0 & l_2 + l_3 \\ 0 & 0 & 0 & 1 \end{bmatrix} \tag{4.12}$$

$$T_4^3 = A_4 = \begin{bmatrix} \cos(\theta_4) & 0 & \sin(\theta_4) & 0 \\ \sin(\theta_4) & 0 & -\cos(\theta_4) & 0 \\ 0 & -1 & 0 & 0 \\ 0 & 0 & 0 & 1 \end{bmatrix} \tag{4.13}$$

$$T_5^4 = A_5 = \begin{bmatrix} \cos(\theta_5) & 0 & \sin(\theta_5) & 0 \\ \sin(\theta_5) & 0 & -\cos(\theta_5) & 0 \\ 0 & 1 & 0 & l_4 + l_5 \\ 0 & 0 & 0 & 1 \end{bmatrix} \tag{4.14}$$

$$T_5^0 = \begin{bmatrix} r_{11} & r_{12} & r_{13} & d_x \\ r_{21} & r_{22} & r_{23} & d_y \\ r_{31} & r_{32} & r_{33} & d_z \\ 0 & 0 & 0 & 1 \end{bmatrix} \tag{4.15}$$

$$T_5^0 = A_1 A_2 A_3 A_4 A_5 = T_1^0 T_2^1 T_3^2 T_4^3 T_5^4 \tag{4.16}$$

Where the values of the transformation matrix elements have been listed in appendix A.

The forward kinematics matrix computed above has been implemented and verified in MATLAB that is a computer programming language. MATLAB is a multi-paradigm numerical computing environment and proprietary programming language developed by MathWorks. A maximum range of motion (full-extension, when all joints are stretched to cover maximum area where an arm can reach) in the xyz plane of the ambidextrous robot arm is shown in Figure 4.18.

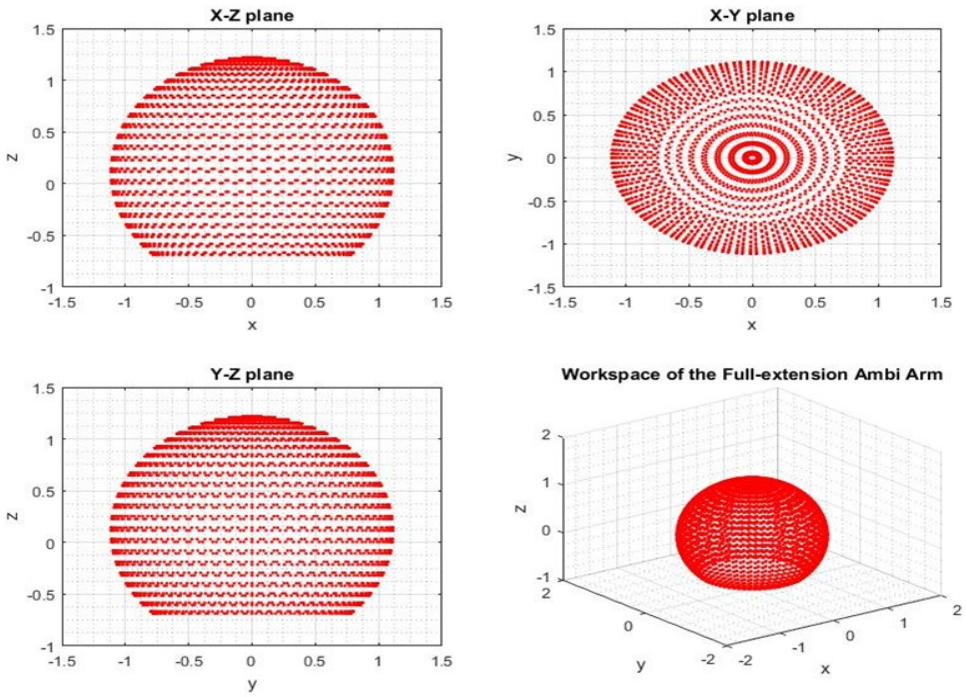

Figure 4.18: Workspace of the ambidextrous arm in full-extension mode.

The full extension represents the total area covered by the end effector while manipulator executes all possible motions. In MATLAB program, all joint variables were given specific DOF and simulation was run to evaluate the area. The derived equation using the forward kinematic approach is verified using MATLAB program. Theta values and position of end-effector for each plot is given in Table 4.3 and snapshot of different angles an ambidextrous arm is capable of making is shown in Figure 4.19.

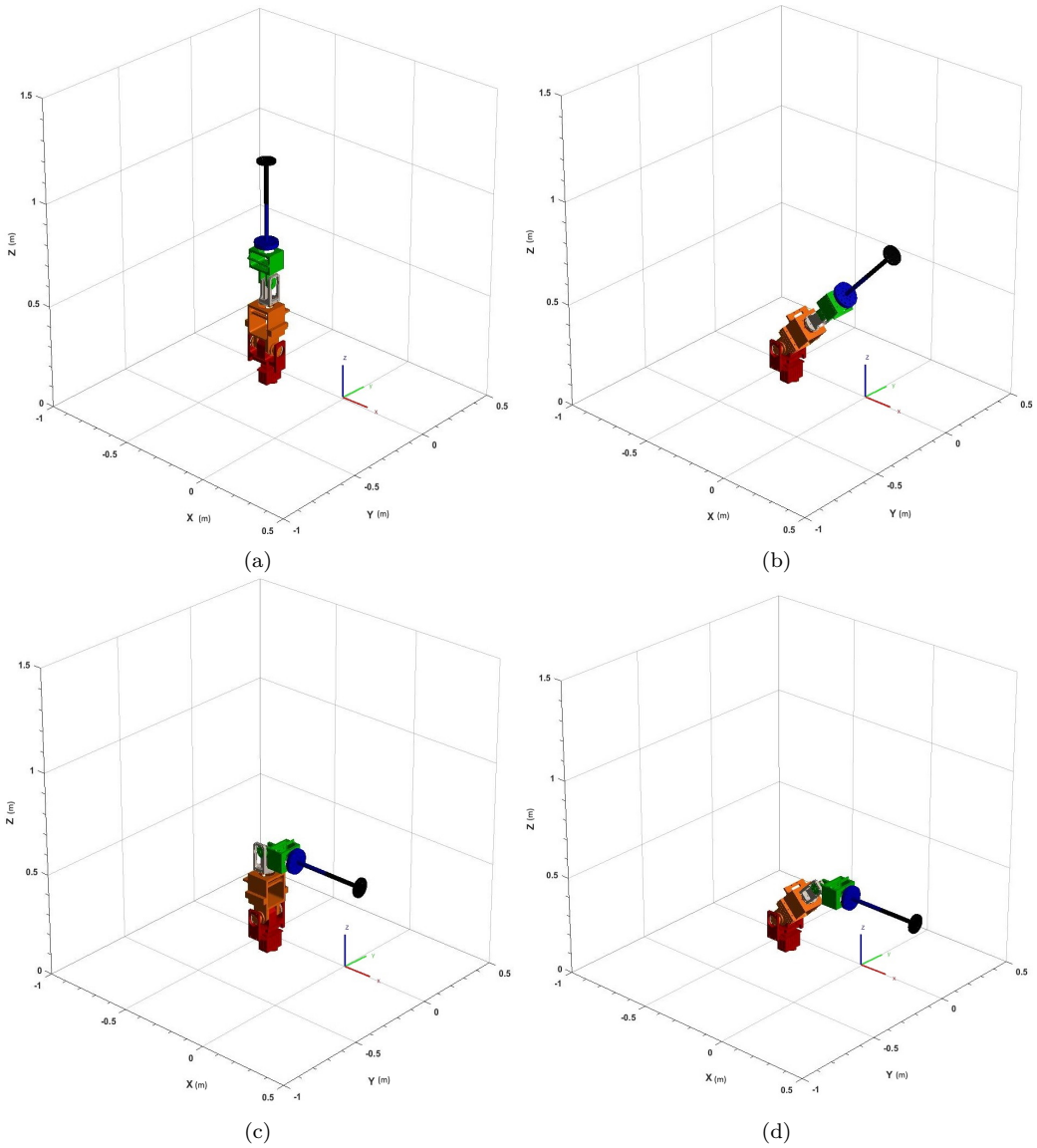

Figure 4.19: Forward kinematic equation verified at various angles listed in Table 4.3.

There are many software available in the market to calculate the forward dynamics of the robot arm. Robo-Analyzer is employed in this research to design a 5 DOF robot arm and assigned the input parameters such as joint type, joint offset, link lengths, and twist angles, initial and final values to replicate the ambidextrous robot arm movements.

Table 4.3: Theta values and position of end-effector for each plot.

Position	Theta values (deg)					The position of End Effector (m)		
	J1	J2	J3	J4	J5	X-axis	Y-axis	Z-axis
a	0	0	0	0	0	-0.40	-0.10	1.20
b	90	45	0	0	0	0.37	-0.17	0.90
c	90	0	180	90	0	0.25	-0.17	0.50
d	90	45	180	45	0	0.45	-0.17	0.40

4.2.2 Inverse Kinematics of the Ambidextrous Robot Arm

Unlike forward kinematics, finding an inverse kinematic solution is relatively hard in particular when dealing with multiple DOF robots. Usually, there is always more than one inverse solution and choosing the best solution by specifying the type of configuration the user prefers is key to moving the robot arm to the desired position. For instance, a one revolving joint robot arm will have only one possible inverse solution to define the position of the end effector while a six revolving joint robot may have 16 different solutions to define the same position of the end effector. The relationship between Joint Space and Cartesian Space as well as forward kinematics and inverse kinematics is shown in Figure 4.20.

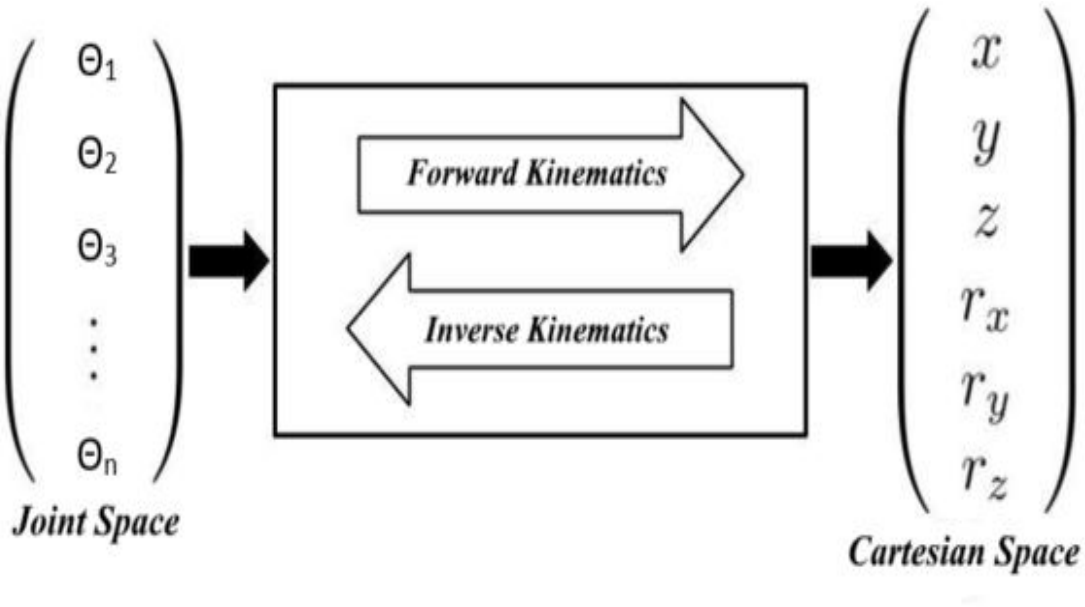

Figure 4.20: Forward and inverse kinematics relationship.

In inverse kinematics the most challenging task is to solve the complicated equations and to deal with multiple possible solutions. The complexity of this problem and possible alternative approaches are discussed in [153, 154]. Some simulation based platforms exist that do all the calculations but sometimes selecting the best one is difficult. In order to explain the difficulty of solving the inverse kinematics problem, the position of the hand (d_x, d_y, d_z) will be formulated with respect to arm base frame as Equation (4.17):

$$\begin{bmatrix} d_x \\ d_y \\ d_z \end{bmatrix} = \begin{bmatrix} C\theta_1 C\theta_2 C\theta_3 + S\theta_1 S\theta_3)S\theta_4 - (C\theta_1 S\theta_2 C\theta_4)](l_4 + l_5) - (l_2 + l_3) - (C\theta_1 S\theta_2) \\ -(S\theta_1 C\theta_2 C\theta_3 + C\theta_1 S\theta_3)S\theta_4 (S\theta_1 S\theta_2 C\theta_4)](l_4 + l_5) - (l_2 + l_3) - (C\theta_1 S\theta_2) \\ -(S\theta_2 C\theta_3 S\theta_4 + C\theta_2 C\theta_4)(l_4 + l_5) - (l_2 + l_3)(C\theta_2) + l_1 \end{bmatrix} \tag{4.17}$$

By differentiating both sides of Equation (4.17) with respect to θ, the velocity in the

task space of the hand will result as Equation (4.18).

$$\dot{x} = J\dot{\theta} \tag{4.18}$$

where $\dot{x}$ is the velocity at task-space, J is the robot arm Jacobian matrix that map the position and the orientation of the hand to the joint-space, and $\dot{\theta}$ is the joint velocity. The Jacobian matrix is represented in Equation (4.19).

$$J = \begin{bmatrix} \frac{\partial P_x}{\partial P_{\theta_1}} & \frac{\partial P_x}{\partial P_{\theta_2}} & \frac{\partial P_x}{\partial P_{\theta_3}} & \frac{\partial P_x}{\partial P_{\theta_4}} & \frac{\partial P_x}{\partial P_{\theta_5}} \\ \frac{\partial P_y}{\partial P_{\theta_1}} & \frac{\partial P_y}{\partial P_{\theta_2}} & \frac{\partial P_y}{\partial P_{\theta_3}} & \frac{\partial P_y}{\partial P_{\theta_4}} & \frac{\partial P_y}{\partial P_{\theta_5}} \\ \frac{\partial P_z}{\partial P_{\theta_1}} & \frac{\partial P_z}{\partial P_{\theta_2}} & \frac{\partial P_z}{\partial P_{\theta_3}} & \frac{\partial P_z}{\partial P_{\theta_4}} & \frac{\partial P_z}{\partial P_{\theta_5}} \end{bmatrix} \tag{4.19}$$

The problem of the inverse kinematic is to get the velocity in configuration space ($\dot{\theta}$) by giving the velocity in task space ($\dot{x}$). Therefore, Equation (4.18) should be inverted to get a linear form as Equation (4.20).

$$\dot{\theta} = J^{-1}\dot{x} \tag{4.20}$$

It is clear from Equation (4.20) that the matrix of Jacobian is not square. So, the inversion process is not straightforward. Many methods in literature have dealt with this problem either analytically or numerically. One of the most commonly used methods is an ANFIS.

4.2.3 Adaptive Network Fuzzy Inference System (ANFIS)

Fuzzy interference system (FIS) is commonly used in robotics field where complex systems (n-joint robotic arms operating in three-dimensional input spaces) are employed. In simple terms, if an arm is required to move from point A to point B, a microcontroller runs inverse kinematics calculations from initial configuration

of the arm to the desired configuration. The higher the DOF, the higher the complexity of the calculations required to complete the task. This complexity increases the time it takes to make all the necessary calculations and slows down the productivity of the whole system. FIS is employed to address this problem by creating a simple mathematical function having all the parameters of an arm. Then all the microcontroller has to do is extract the value of given input depending on an algorithm instructed by the user.

Adaptive Network (AN) is a network structure consisting of nodes and directional links, and in practice, AN is considered a superset of multilayered feed forward NNs with supervised learning capabilities. The basic rule of AN is based on gradient descent and the chain rule. ANFIS utilises network topology to reduce the optimisation search space. The design objective of the fuzzy controller is to learn and improve in terms of performance despite the system facing disturbances. An ANFIS is similar to a NN that is based on Takagi-Sugeno fuzzy interference system. The objective of ANFIS is to integrate both fuzzy logic and NN principles. Fuzzy logic (FL) and artificial neural networks (ANNs), despite their successful use in many challenging control situations, still have drawbacks that limit them to only some applications. Their combined advantages have thus become the subject of much research into ways of overcoming their disadvantages. Neuro-fuzziness is one resulting rapidly emerging field. ANFIS network, proposed by Jang, is one popular neuro-fuzzy system [140, 155–157]. It could offer the benefit of both in a single framework and be considered as a universal estimator. ANFIS is best option to choose between neural network and fuzzy systems, providing smoothness (due to fuzzy control) and adaptability (due to neural network back propagation). For example in [158], ANFIS is applied to solve the IK of the SCARA robot, in [159] it is applied to a redundant planar 4 DOF manipulator with rotational joints and in [160] for a 6 DOF human upper limb.

However, in all these papers which report the ANFIS based solution to the IK only the position of the end-effector is taken into account. Its orientation is not used to compute the angular position of joints. As far control of the ambidextrous robot arm is concerned both position and orientation problem is considered. ANFIS corresponds to a set of fuzzy if-then rules that have learning capability to approximate nonlinear functions. Fuzzy if-then rules express conditions IF A THEN B, where A and B are fuzzy set labels characterised by appropriate Membership Function (MF). If-then rules help the user make decisions in an uncertain and imprecise environment. Thus, a hypothesis is created from the parameterised mathematical model and data is generated using forward kinematics (due to quick and straightforward outcomes). The NN is used to tune the MF of Sugeno type fuzzy interference system.

There are two types of fuzzy systems: Mamdani and Sugeno models. Fuzzy interference system is shown in Figure 4.21.

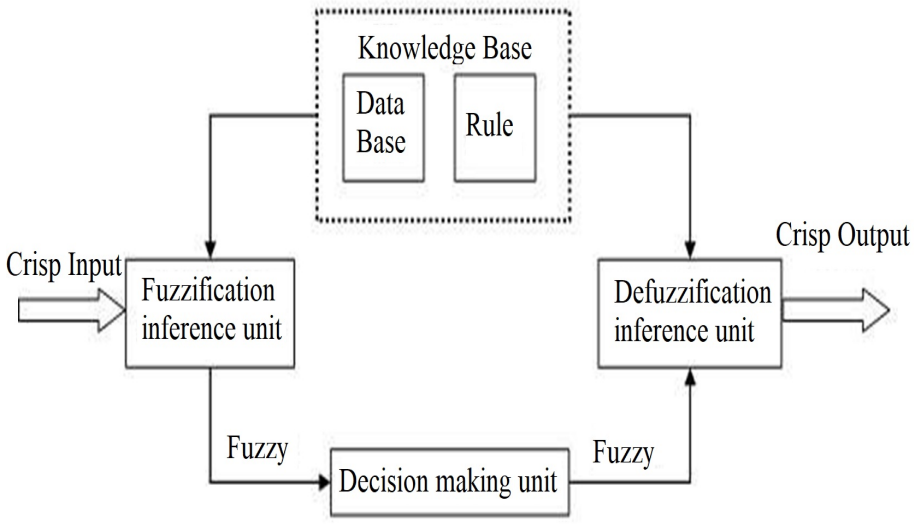

Figure 4.21: Schematic diagram of a fuzzy inference system.

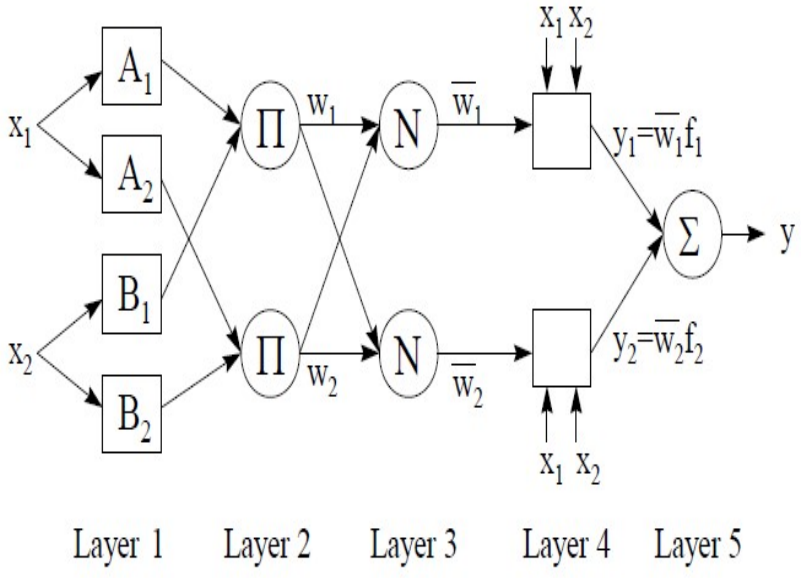

Figure 4.22: ANFIS architecture

There are three main blocks of FIS as listed below:

1. A fuzzification interference unit which transforms the input into degrees of a match with linguistic values works by comparing the input variables with the MFs to obtain membership values of the linguistic label.

2. A knowledge-based composed of the database (define MFs of the fuzzy set) and rule-based (contain If-Then rule).

3. A defuzzification interference unit which transforms the fuzzy results into an output.

ANFIS is a multi-layered feed forward network in which each node performs a particular node function as shown in Figure 4.22. To represent different adaptive networks both circle nodes (fixed node) and square nodes (adaptive node) are used. The formula of function may vary node to node as it depends on the overall input-output function. For simplicity, consider a first order Sugeno fuzzy model with two

inputs, x and y and one output z. Imagine rule base contains two if-then rules of Takagi and Sugeno:

$$Rule1 : IF(x \quad is \quad A_1) \quad and \quad (y \quad is \quad B_1) \quad then \quad (f_1 = P_1x + Q_1y + R_1)$$

$$Rule2 : IF(x \quad is \quad A_2) \quad and \quad (y \quad is \quad B_2) \quad then \quad (f_2 = P_2x + Q_2y + R_2)$$

Where x and y are the inputs, A_i and B_i are the fuzzy sets, f_i are the outputs within the fuzzy region specified by fuzzy rules: P_i, Q_i and R_i are the design parameters that are determined during the training process.

Layer 1: Every node is a square node (adaptive nodes) in layer 1. Parameters in the layers are called premise parameters. The output of layer 1 is a fuzzy membership grade of the inputs, which are given by

$$O_i^1 = \mu_{A_i}(x) \quad i = 1, 2 \tag{4.21}$$

or

$$O_i^1 = \mu_{B_i}(y) \quad i = 1, 2 \tag{4.22}$$

Where x (or y) is the input node i and A_i or B_i is a linguistic label associated with this node and μ_{A_i} (x), μ_{B_i} (y) can adopt any fuzzy MF.

Layer 2: Every node is a circle node in layer 2.

$$O_i^2 = W_i = \mu_{A_i}(x) \quad \mu_{B_i}(y) \tag{4.23}$$

Where $i = 1 : 2$, W is weight and O is the output of the layer. The output of this layer can be represented as a firing strength of the rules.

Layer 3: Every node is a circle node in layer 3.

$$O_i^3 = \overline{W_i} = \frac{W_i}{(W_1 + W_2)} \tag{4.24}$$

Where $i = 1 : 2$ the i^{th} node calculates the ratio of i^{th} rule's firing strength to the sum of all firing outputs are called normalized firing strengths.

Layer 4: Every node is a square node in layer 4. The output of each node in this layer is a product of the normalised firing strength and a first-order polynomial.

$$O_i^4 = \overline{W}_i f_i = \overline{W_i}(P_i x + Q_i y + R_i) \tag{4.25}$$

Where $i = 1 : 2$, $\overline{W_i}$ is the normalized firing strength from layer 3 and $(P_i x + Q_i y + R_i)$ is the parameter set of this node.

Layer 5: This layer has only one node that sums all incoming signals and represents the overall output of the model. This node performs the summation of all incoming nodes.

$$O_i^5 = \sum_{i=1}^{2} \overline{W}_i f_i = \frac{\sum_{i=1}^{2} W_i f_i}{W_1 + W_2} \quad i = 1, 2 \tag{4.26}$$

After this phase, the optimal values of these membership function parameters and consequential parameters are set by a hybrid learning algorithm that combines the method of least squares with the backpropagation learning algorithm. Finally, the ANFIS output is calculated by means of consequential parameters and Least Square Error (LSE) [161].

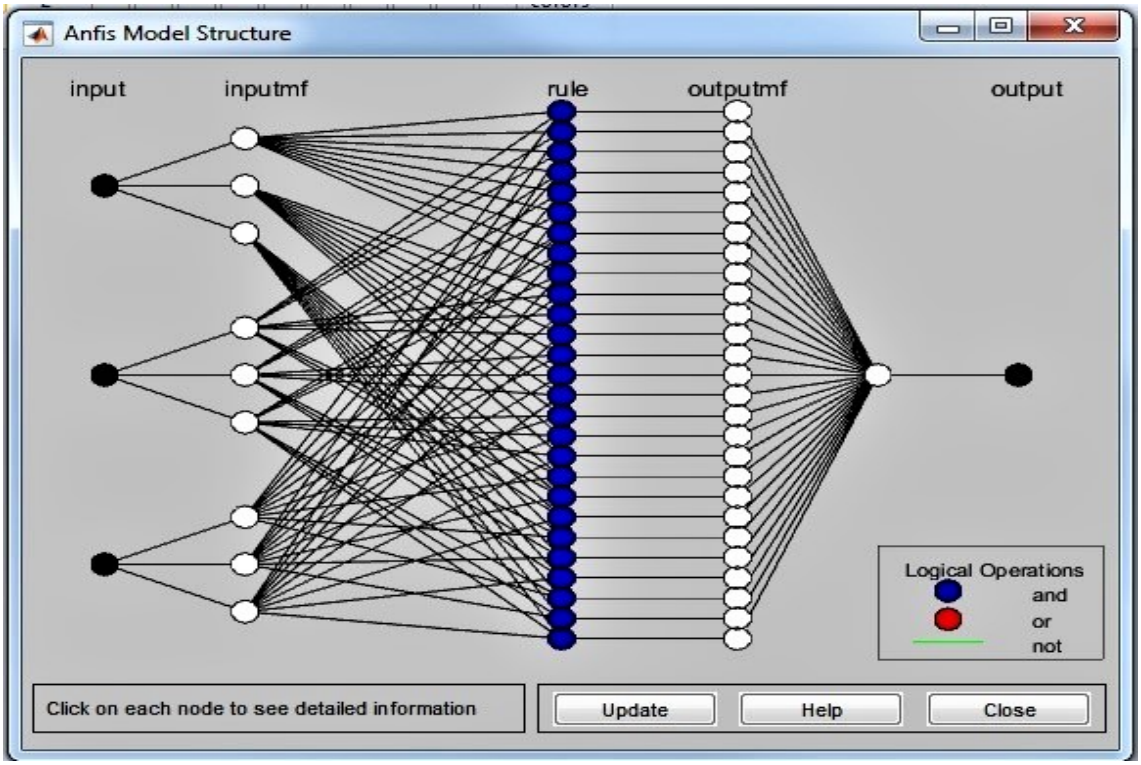

Figure 4.23: ANFIS Model Structure.

The Neuro-Fuzzy Designer app (as shown in Figure 4.23) is used to design, train, and test adaptive ANFIS using input/output training data. It is useful in modifying interference system before tuning MF of Sugeno type FIS, based on training data generate an initial inference system, prevent over fitting to the training data, using testing data test the generalisation ability of tuned system and export tuned data to MATLAB workspace. A basic flow diagram of computation in ANFIS is presented in Figure 4.24.

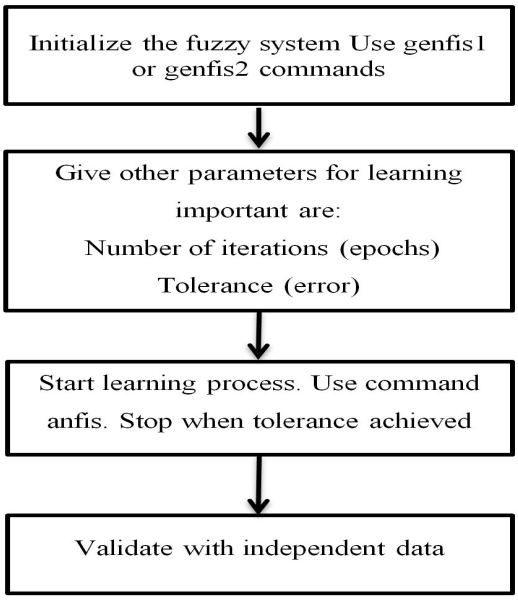

Figure 4.24: Basic flow diagram of computations in ANFIS.

The process of using ANFIS technique involves data generation (hypothesise a model structure) of all possible angles lying within the possible joint range of movement. The forward kinematic formula is used at this stage to a deduce a combination of all theta values. Then, the ANFIS solution is built specifically to address the problem in question. An ANFIS network can only predict angles when they are trained with sample input-output data. After training the network an important step is to validate the network to determine how well the ANFIS network would perform inside a large control system. Until a satisfactory solution is found, different configuration parameters to the ANFIS function should be tried. Finally, in the large control system, the trained ANFIS network is used as a reference to determine what angles of the arm should be given to reach the desired location of the manipulator. The system will apply appropriate force on each joint to make a move once knowledge of desired angles and the current angle are known.

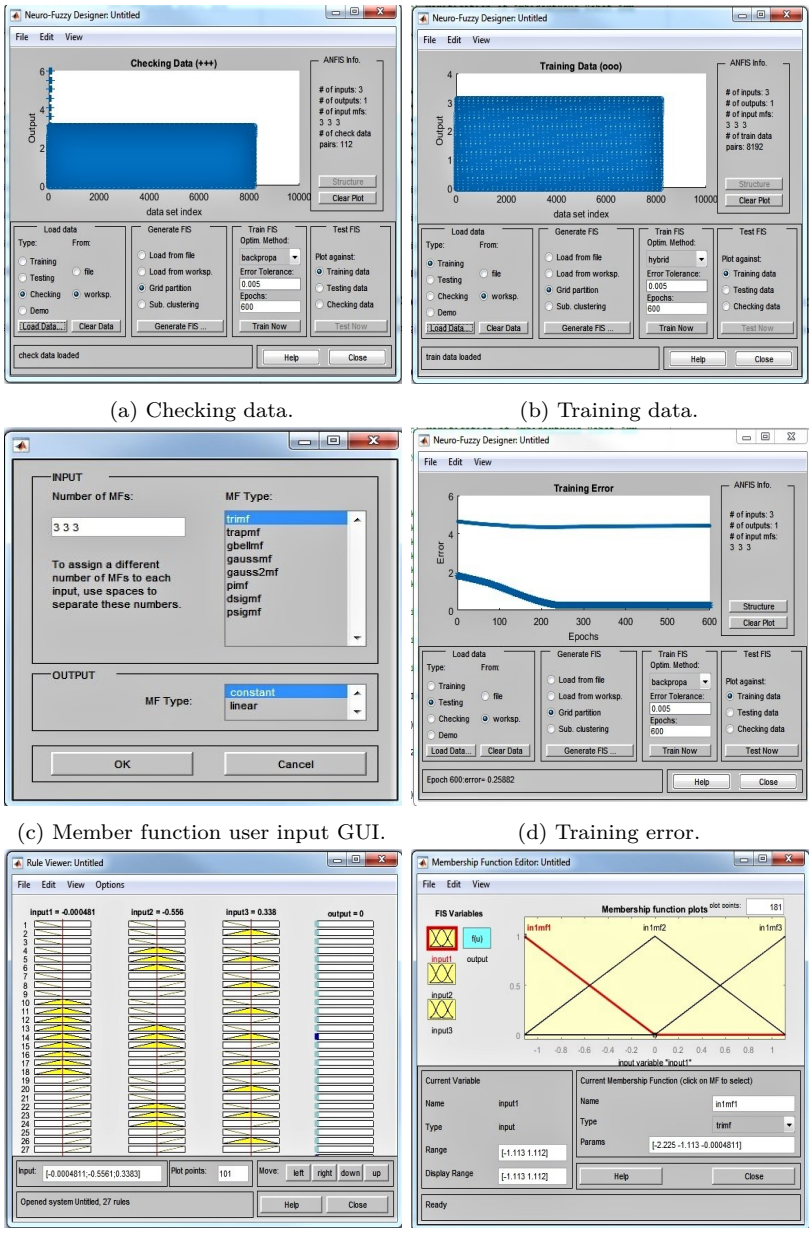

(a) Checking data. (b) Training data.

(c) Member function user input GUI. (d) Training error.

(e) Rule view window. (f) MF Editor.

Figure 4.25: Different stages of ANFIS technique using ANFIS toolbox in MATLAB.

Some of the key stages during training an ANFIS network using ANFIS toolbox in MATLAB including the command window are captured in Figure 4.25. An example is considered to show how the Sugeno type fuzzy system is created trained and tested using the neuro-fuzzy Designer. The neuro-fuzzy designer command is used to open

the neuro-fuzzy designer that lets users number of tasks namely: loading, plotting and clearing the data, generating or loading the initial FIS structure, training the FIS and validating the trained FIS. The training data set that includes the desired input/output is loaded. The data that required modelling is loaded in the form of an array with the data arranged as column vectors and output data in the last column. Similarly testing and checking data can also be loaded in the designer app.

A user is required to specify the data type, and either data from file or a workshop is loaded by clicking Load Data button. After the loading of data, it displays the plot. The training, testing and checking data are shown in blue colour as circles, diamonds and pulses respectively. The user then needs to focus on generating FIS portion in the designer app at the bottom centre of the designer app. There are three options given on the designer app namely: load from file, load from the workshop, grid partition (generates a single-output Sugeno-type FIS by using grid partitioning on the data) and sub-clustering (generates an initial model for ANFIS training by first applying subtractive clustering on the data). After loading the training data and generating the initial FIS structure, the process of training the FIS is started by choosing a hybrid or backpropagate option from drop-down menu optimisation method. Each row of training data is the desired input/output of the target system to be modelled, and each row starts with an input vector that is followed by an output value. The MF parameters are trained using the optimisation method. Stop criteria is set by entering the training Epochs and the training error tolerance. The training error is the difference between the training data output value and the output of the fuzzy interference system. The training process automatically stops when the maximum threshold is reached. The checking data has the same format as the training data, and it is used to test the generalisation capability of FIS at each epoch. After training the FIS, error plots are examined to see overfitting during the training process. The checking error is the difference between the checking output value and the output of the FIS. Model validation is the last step in the whole process.

4.2.4 ANFIS Controller Design for the Ambidextrous Robot Arm

This section describes an ANFIS network developed and trained to control the ambidextrous robot arm. Using ANFIS toolbox in MATLAB, all 5 joints is derived by 5 different ANFIS networks as shown in Figure 4.29. Any application of ANFIS requires detailed knowledge of fuzzy logic as ANFIS demands a careful choice of suitable shape and MFs. Selection of such parameters affects not only the efficiency of the ANFIS model but also computational cost. Various MFs can be used to solve any given problem. A Gaussian shape of the MF is a very popular choice due to its smooth representation of input space. There were number of tests performed to find the suitable ANFIS network. The results are listed in Table 4.4.

Table 4.4: Training and data set validation for θ_1.

Test No. for (Joint) θ_1	Optimisation method	Membership Functions		Training Epoch	Average error		
		Number of MFs	Type of MFs		Training	Testing	Checking
1	Backpropagation	5	Trimf	1200	0.13	0.13	0.48
2	Backpropagation	3	Trimf	1200	0.27	0.27	0.99
3	Hybrid	5	Trimf	1200	0.16	0.17	0.64
4	Hybrid	3	Trimf	1200	0.28	0.27	0.96
5	Hybrid	5	Trapmf	1200	0.14	0.13	0.57
6	Hybrid	5	Gauss2mf	1200	0.11	0.11	0.42
7	Hybrid	5	Gbellmf	1200	0.15	0.15	0.52
8	Hybrid	5	Dimf	1200	0.14	0.14	0.48
9	Hybrid	5	Psigmf	1200	0.12	0.12	0.45
10	Backpropagation	5	Gauss2mf	1200	0.11	0.12	0.44

It is apparent from the results summarised in Table 4.4 that the best result was achieved in test 6. Training plots for θ_1 are shown in Figure 4.26.

Figure 4.26: Training, testing and checking error vs Epochs for θ_1 (Test 6) is plotted.

The same settings of test 6 from Table 4.4 were copied for θ_2, θ_3, θ_4 and θ_5 to achieve satisfactory results. Table 4.5 presents the results of ANFIS training for θ_2, θ_3, θ_4 and θ_5 with the same setting introduced earlier for θ_1.

The ANFIS training methodology is summarised in Figure 4.27. First, the training data set and checking data set are obtained in the form of input-output vectors at the beginning of the process. The membership function is computed based on these vectors. Then, the error between the desired and actual output is determined. Once the membership function is known, system training begins. After this process, final membership function and training error from the training data sets are produced. Finally, results obtained from training are tested, and ANFIS structures can be viewed at the end.

The training error can be reduced by changing the key parameters such as membership function, increasing the number of the input membership function, increasing the number of epochs or increasing the training data. However, the key to determining the most suitable ANFIS network lies in a balancing exercise to find the mean point between network computing time and training error.

Table 4.5: Training and data set validation for θ_1 to θ_5.

Joints	Optimisation method	Membership Functions		Training Epoch	Average error		
		Number of MFs	Type of MFs		Training	Testing	Checking
θ_1	Hybrid	5	Gauss2mf	1200	0.11	0.11	0.42
θ_2	Hybrid	5	Gauss2mf	1200	0.06	0.06	0.24
θ_3	Hybrid	5	Gauss2mf	1200	0.09	0.09	0.28
θ_4	Hybrid	5	Gauss2mf	1200	0.16	0.15	0.32
θ_5	Hybrid	5	Gauss2mf	1200	0.18	0.16	0.34

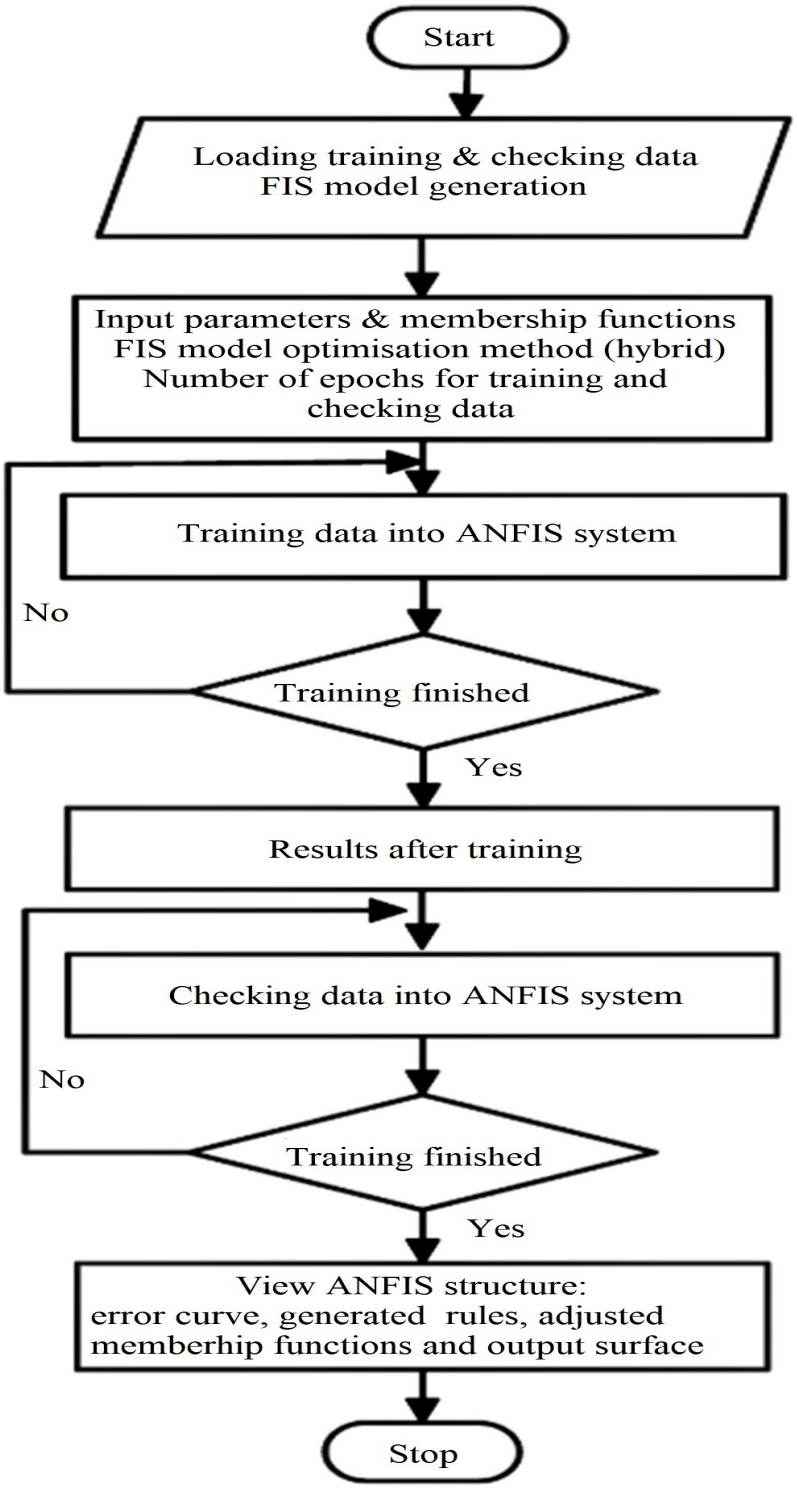

Figure 4.27: ANFIS training methodology.

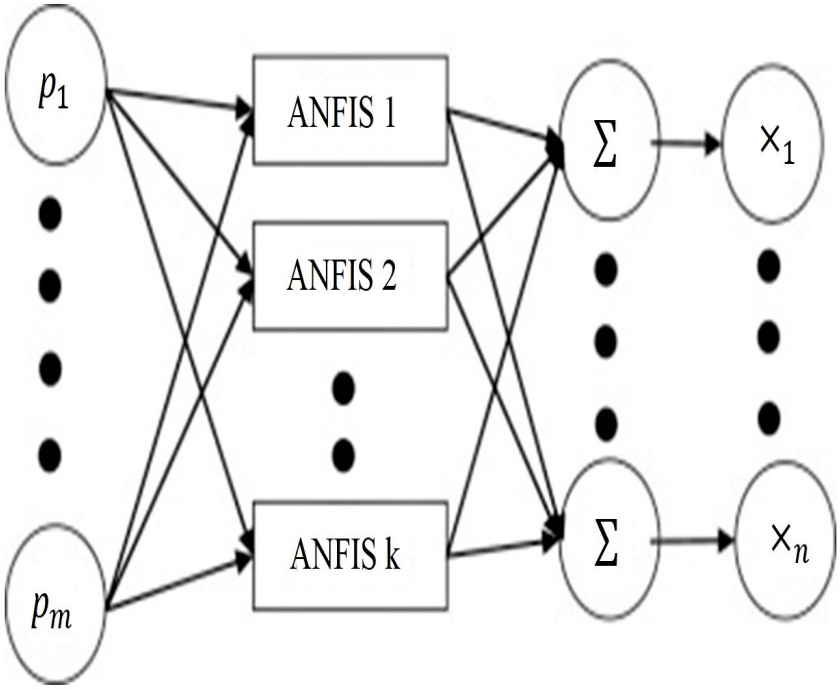

Figure 4.28: General MANFIS architecture.

ANFIS has one output, and in order to move multiple joints, multiple ANFIS networks are required as shown in Figure 4.28. For the ambidextrous robot arm specifically five ANFIS networks namely ANFIS-1, ANFIS-2, ANFIS-3, ANFIS-4, and ANFIS-5 are used to solve the problem of inverse kinematics. Multiple ANFIS also known as (MANFIS) is modelled in Simulink software as shown in Figure 4.29. The MANFIS maps the input in task space to the joint angles in joint space, and joint angles are used to determine the desired trajectory.

Figure 4.29 shows a Simulink diagram for the controller. The controller contains five ANFIS with six inputs (X, Y, Z, Rx, Ry and Rz) and five output (θ_1, θ_2, θ_3, θ_4 and θ_5).

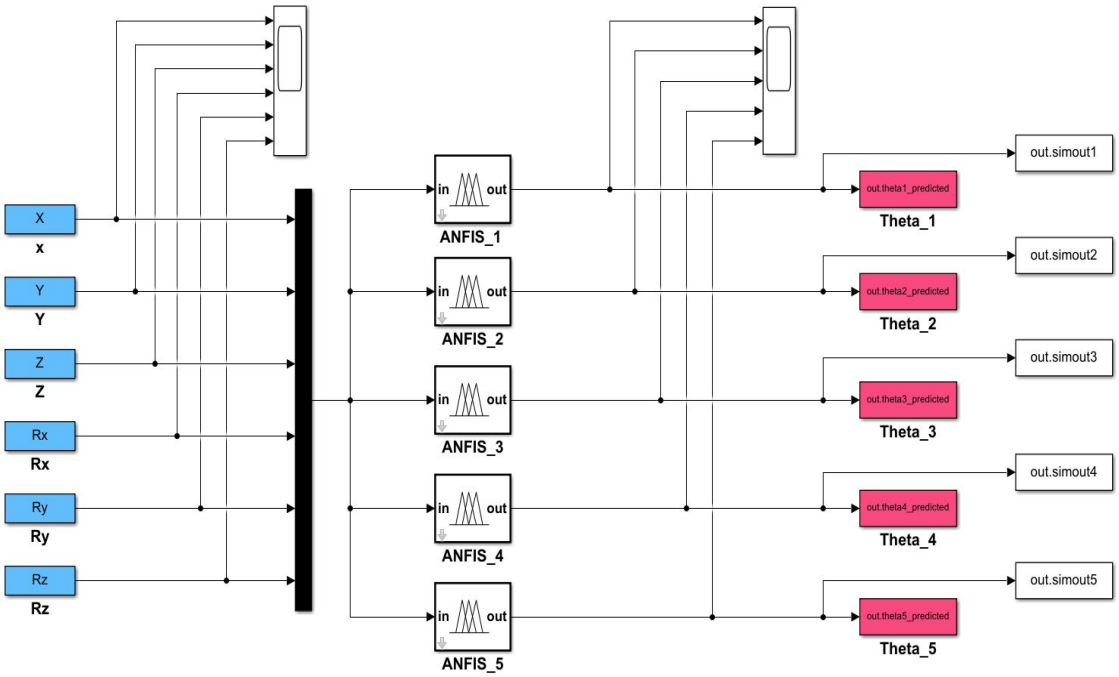

Figure 4.29: MANFIS modelled in Simulink software.

In order to evaluate the ability of the controller to solve the inverse kinematics problem, the controller has been tested with three paths. The first path in 2D plane (Y-Z) and the other paths in 3D space (X-Y-Z) as shown in Figure 4.30.

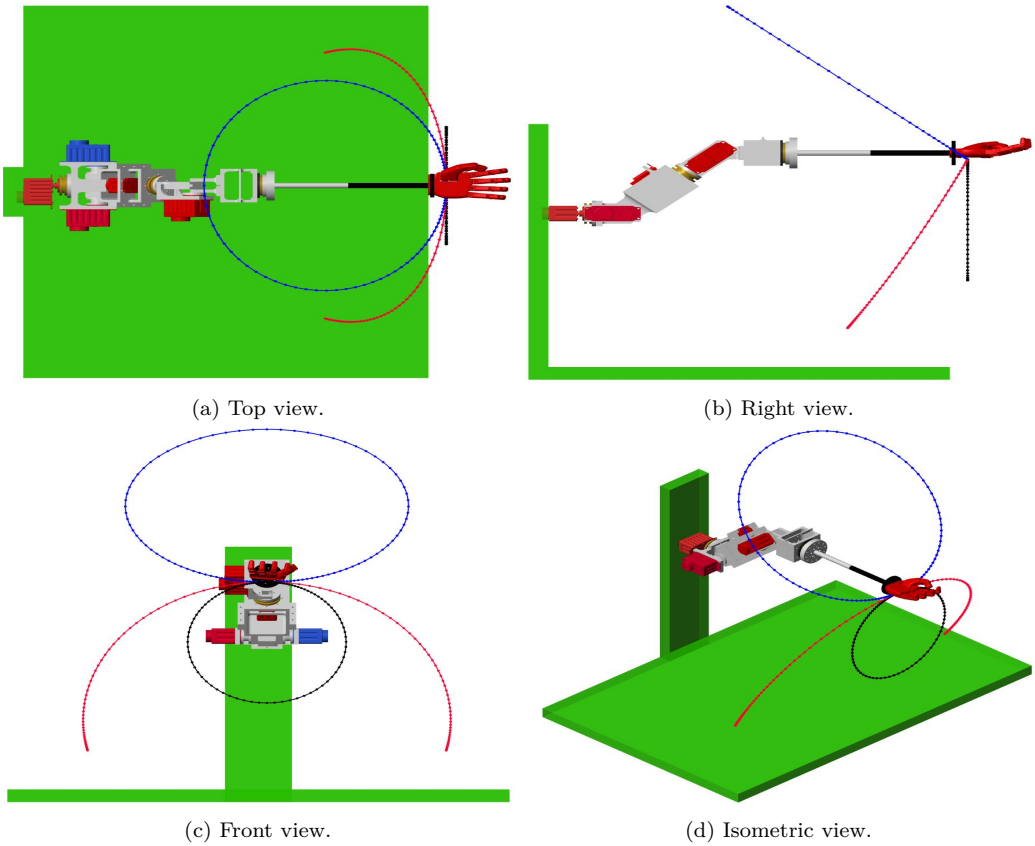

(a) Top view. (b) Right view.

(c) Front view. (d) Isometric view.

Figure 4.30: The desired paths in the task space. The black circle represents a circular path in y-z plane. The two other paths in x, y and z axes are illustrated by a red arc and a blue circle respectively.

The results will be presented in the following figures for both the desired and the response of the controller. Further, the desired path and the predicted one along each axis (x, y and z) combined with difference between the two paths. The first evaluated path will be the circle in y-z plane. Figure 4.31 depicts the desired and the predicted path. The red color path is produced by the robot hand in the operational space. The average difference between the two paths in the y-axis and z-axis are illustrated in Figures 4.32 and 4.33 respectively. The maximum difference is about 0.5 cm in both axes. A short video for this experiment is available in [162].

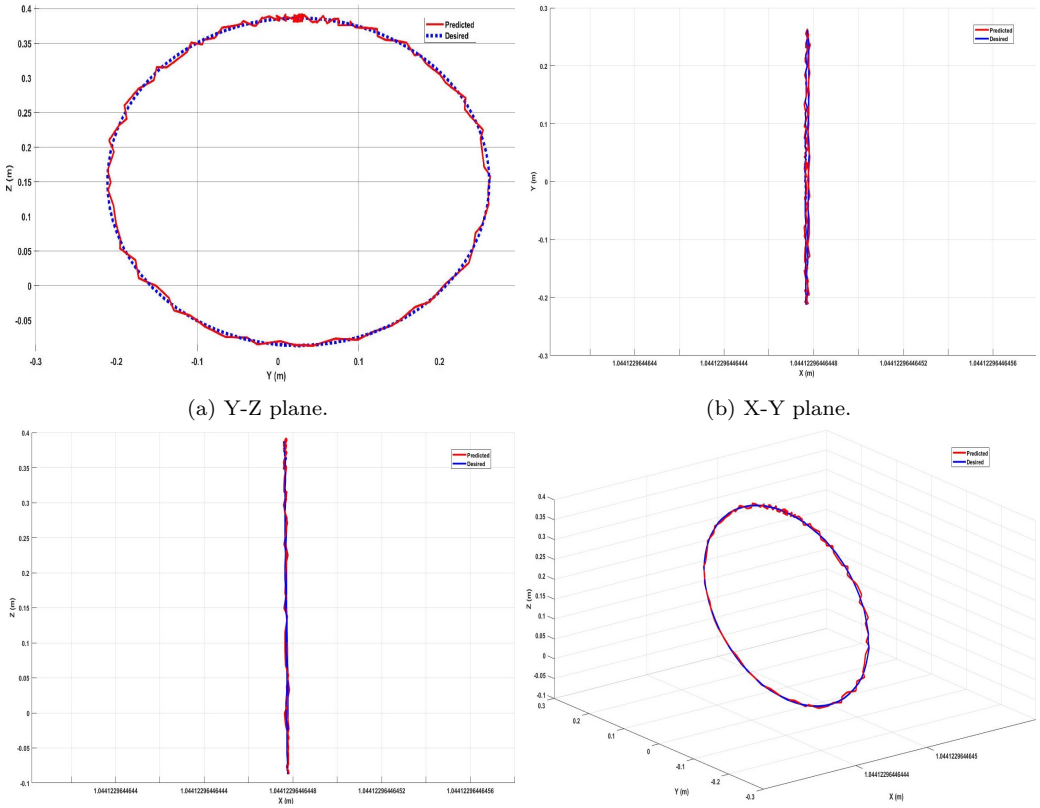

(a) Y-Z plane.

(b) X-Y plane.

(c) X-Z plane.

(d) Three dimension view.

Figure 4.31: The desired path (blue color) and the predicted path (red color) in the task space produced by the robot hand.

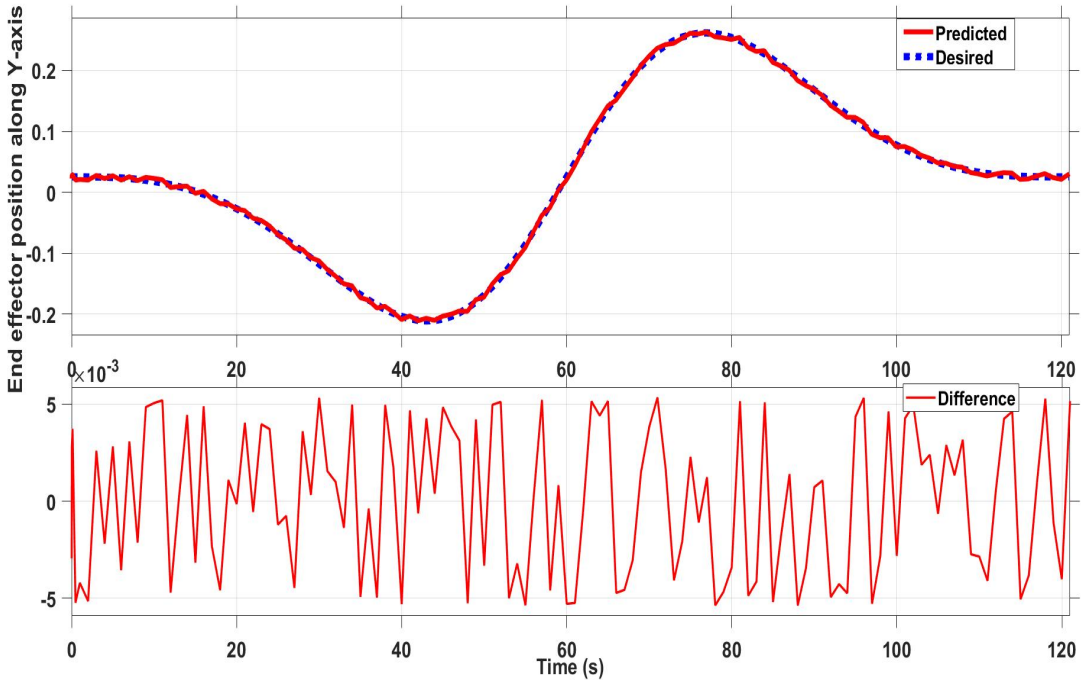

Figure 4.32: The hand position along y-axis for the circle path in y-z plane.

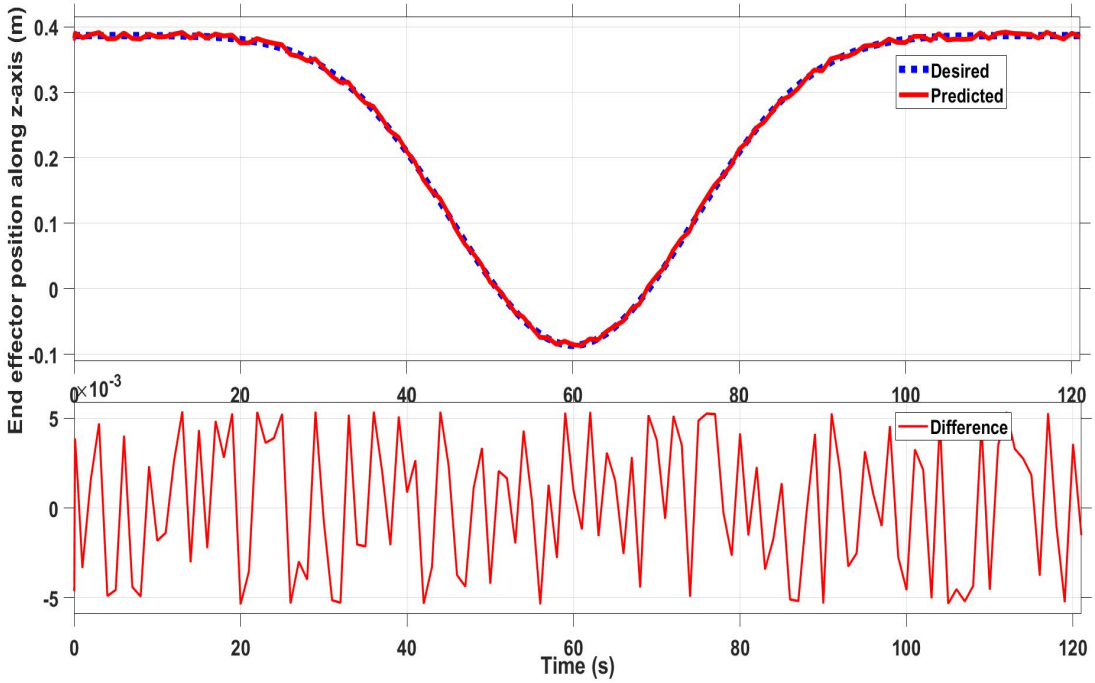

Figure 4.33: The hand position along z-axis for the circle path in y-z plane.

In general, solving inverse kinematic problem in 2D workspace is easy due to the limited effect for the orientation parameters at the end effector of the robot. Therefore, the next evaluation will exploit a circular path in x, y and z axes. Figure 4.34 shows four views for the desired and predicted paths. The difference between the two paths along x, y and z axes are shown in Figures 4.35, 4.36 and 4.37 respectively. The maximum error between the two paths is approximately 0.4 cm. The results of using this type of controller is expected as more constraints are imposed by the orientation parameters.

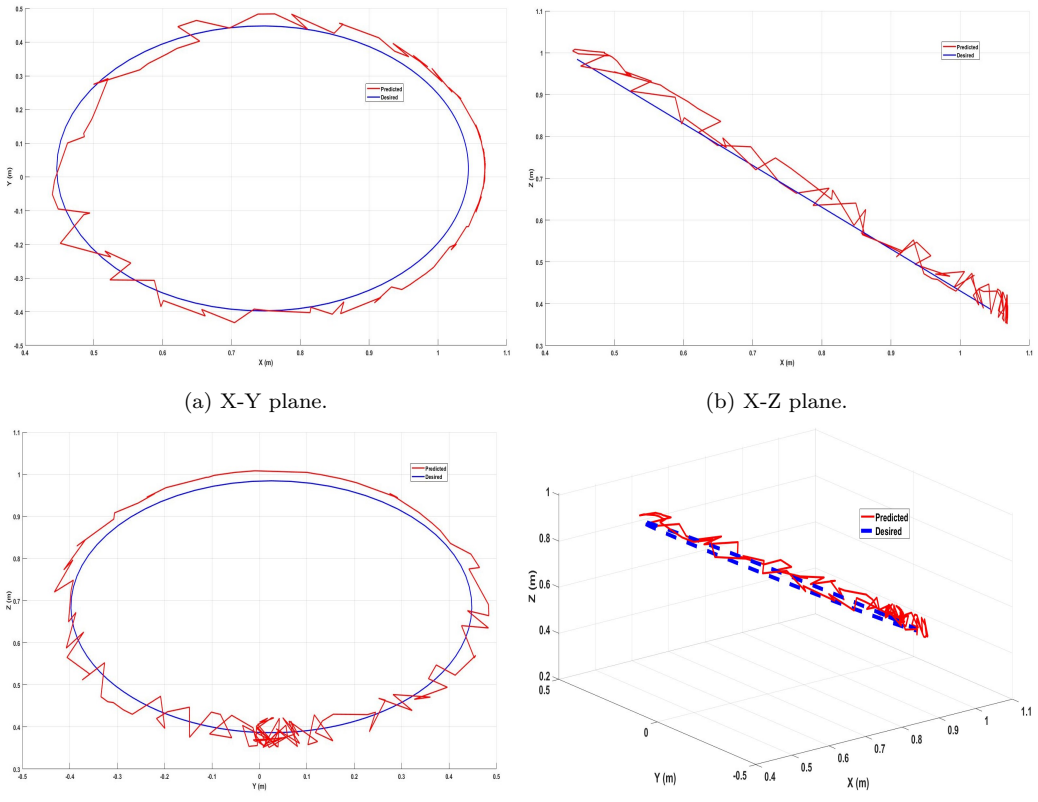

(a) X-Y plane.

(b) X-Z plane.

(c) Y-Z plane.

(d) Three dimension view.

Figure 4.34: The desired path (blue color) and the predicted path (red color) in the task space produced by the robot end effector.

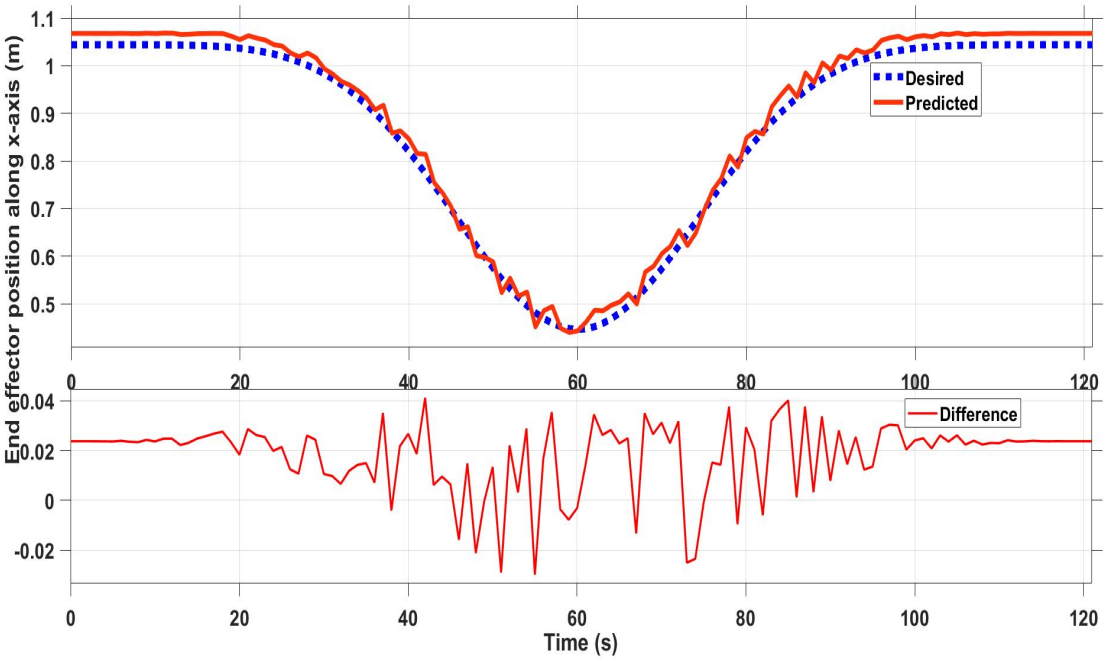

Figure 4.35: The hand position along x-axis for the circle path in x, y and z axes.

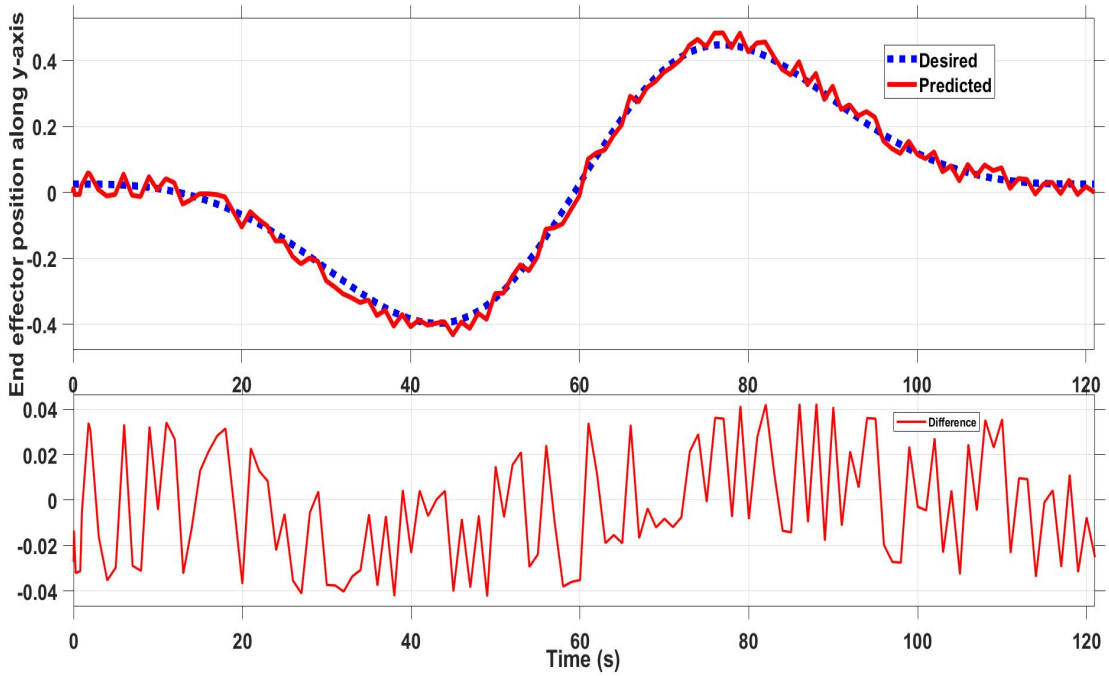

Figure 4.36: The hand position along y-axis for the circle path in x, y and z axes.

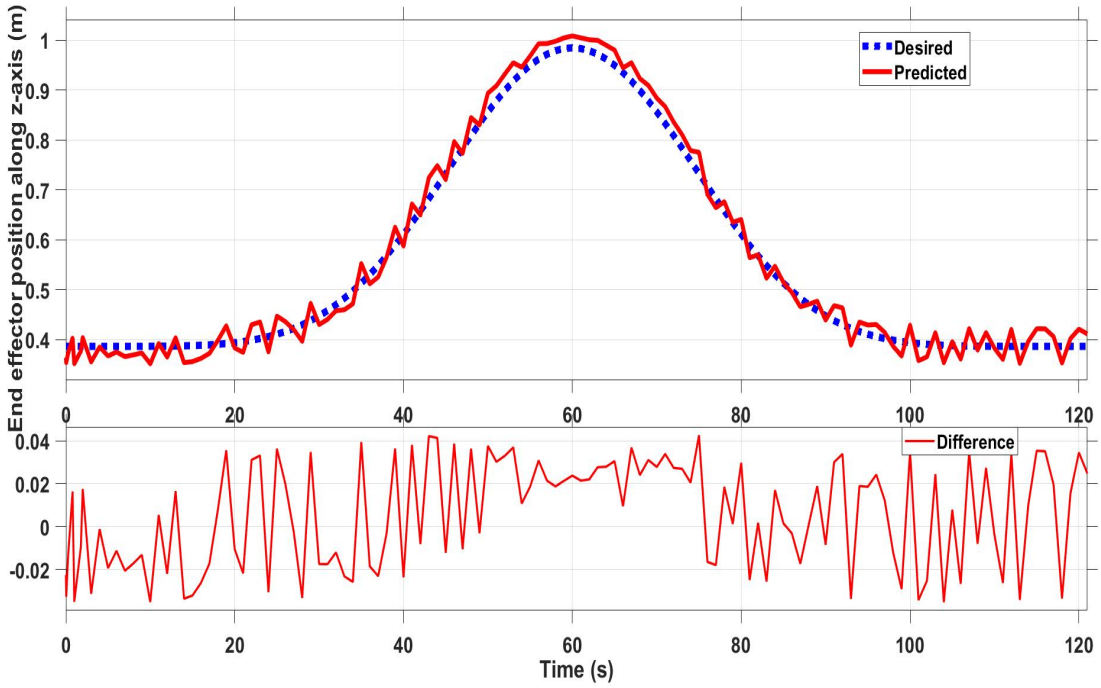

Figure 4.37: The hand position along z-axis for the circle path in x, y and z axes.

From the results shown in Figures 4.35, 4.36 and 4.37 it is apparent that MANFIS-1 controller that is used to produce the robot path did not produce the satisfactory results. It is noted that the controller failed to produce the trajectory in all axes. This suggests a different approach is required for controllers to work efficiently in an ambidextrous environment. Therefore, a new controller (as shown in Figure 4.38) was designed in Simulink to achieve the ambidexterity element. Five ANFIS networks formed each MANFIS and were driven by a selector block. The idea of using if block (selector) comes from the observation of results where the MANFIS-1 controller can produce a satisfactory result within the specified ranges it is trained for, and the same can be applied to the MANFIS-2 controller. So by having a selector, it is possible to select the best possible controller for the given axis.

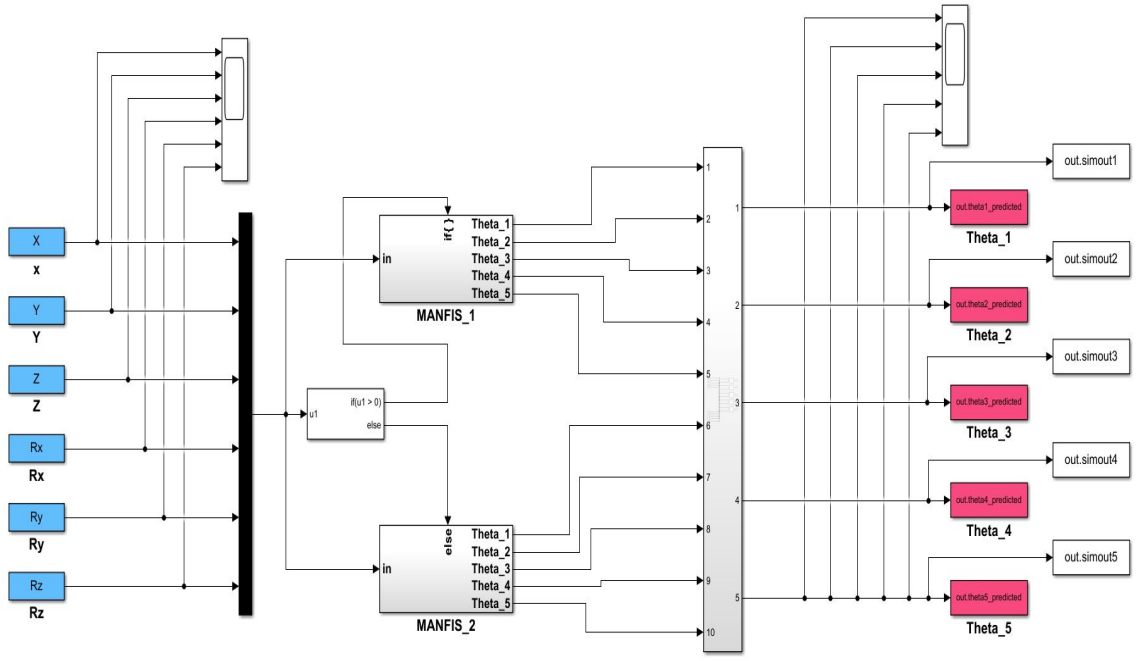

Figure 4.38: Ambidextrous robot arm controller designed in Simulink.

The previous desired path (circular path in 3D) will be utilised to evaluate the proposed controller. Figure 4.39 shows four views for the desired and predicted paths. It's obvious that the controller gave a perfect response to produce the joint angles of the robot arm. The maximum error is about 0.2 cm as shown in Figures 4.40, 4.41 and 4.42. A short video for this experiment is available in [163].

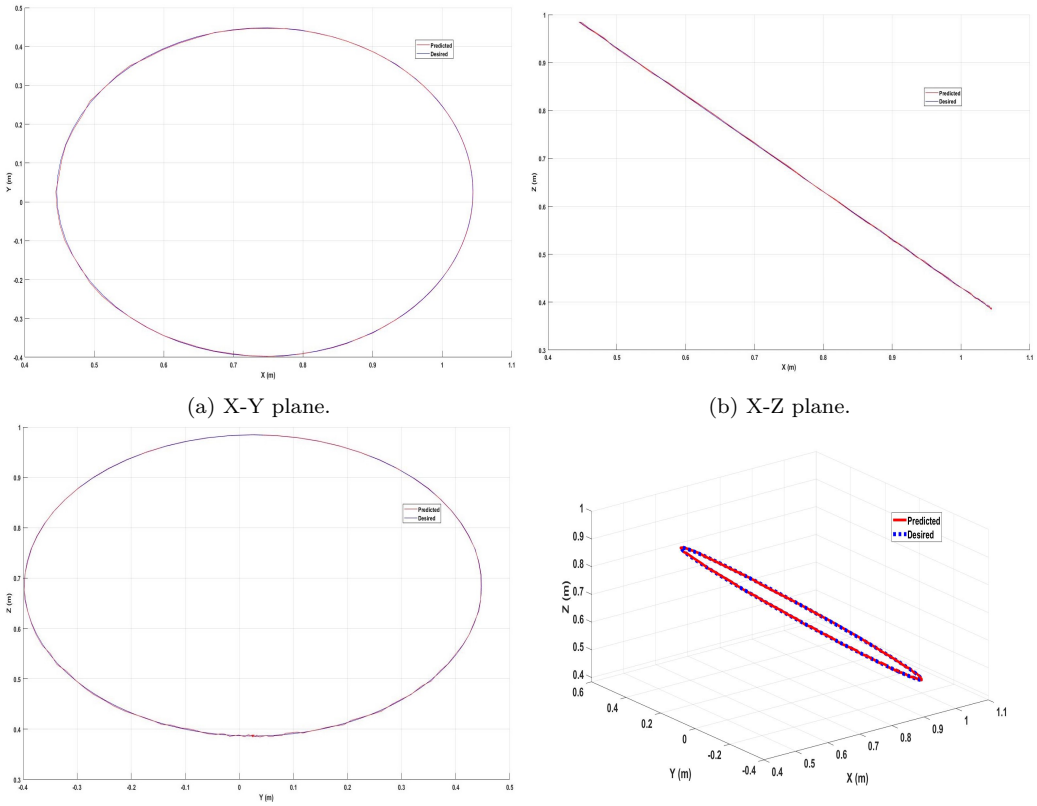

(a) X-Y plane.

(b) X-Z plane.

(c) Y-Z plane.

(d) Three dimension view.

Figure 4.39: The desired path (blue color) and the predicted path (red color) in the task space produced by the robot end effector.

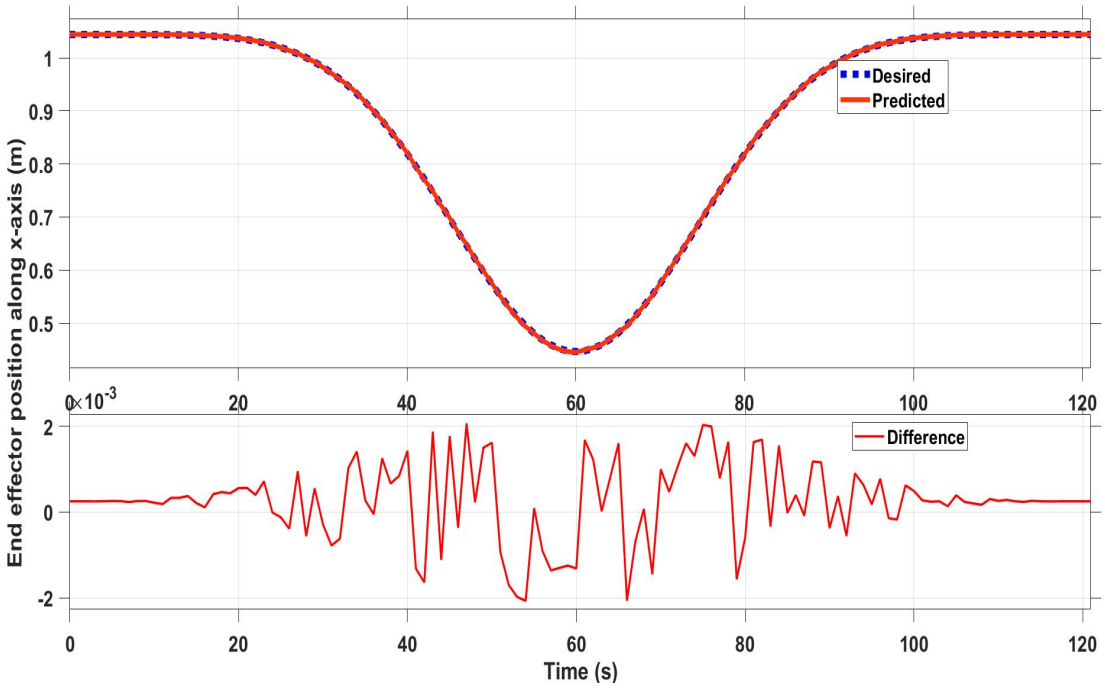

Figure 4.40: The hand position along x-axis for the circular path in x, y and z axes.

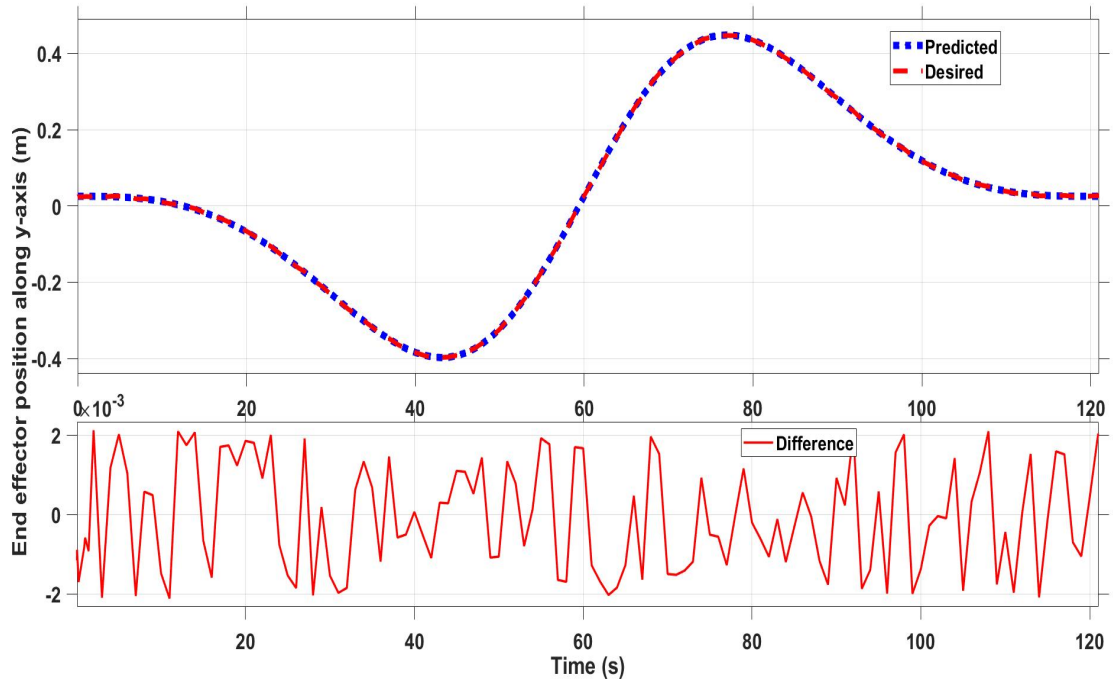

Figure 4.41: The hand position along y-axis for the circular path in x, y and z axes.

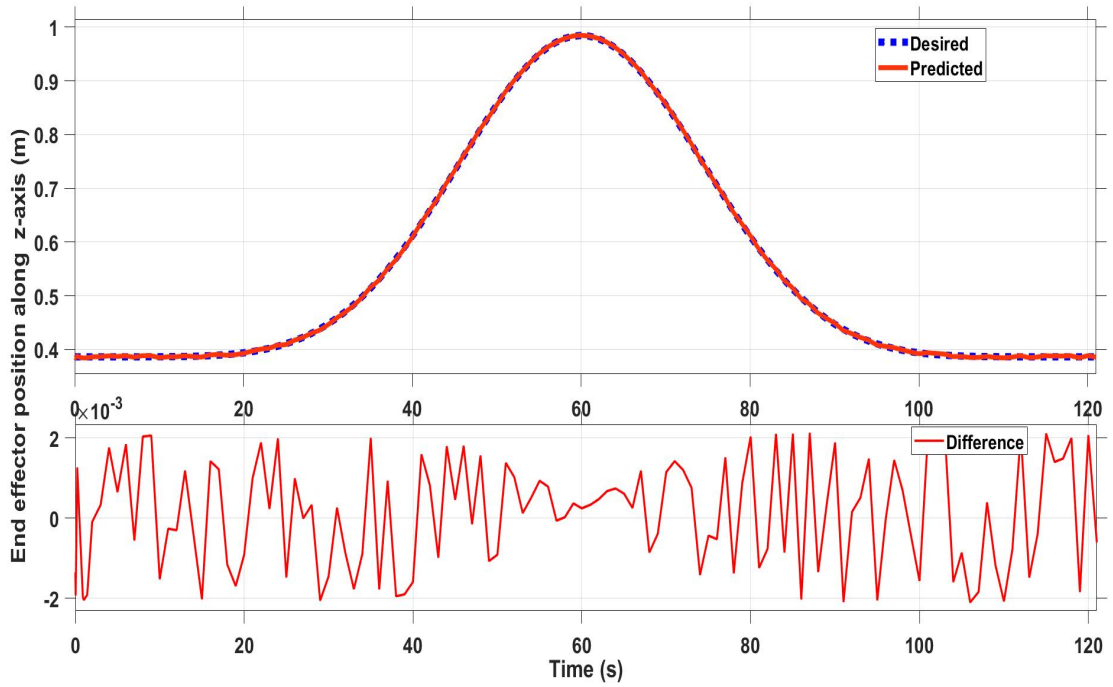

Figure 4.42: The hand position along z-axis for the circular path in x, y and z axes.

To further validate the proposed controller, an arc path in 3D is chosen for this experiment. The diameter of arc path is 105 cm. The wide range of the path impose more complexity on the controller to generate the joints angles. The results of the desired and the predicted path are presented in Figure 4.43. Although the desired path has a wide range of motion, the response of the controller to produce the joints angles of the robot was typical. In term of the difference between the two paths, Figures 4.44, 4.45 and 4.46 clearly illustrate that the maximum error is approximately 0.2 cm which is acceptable in robotic applications. A short video for this experiment is available in [164].

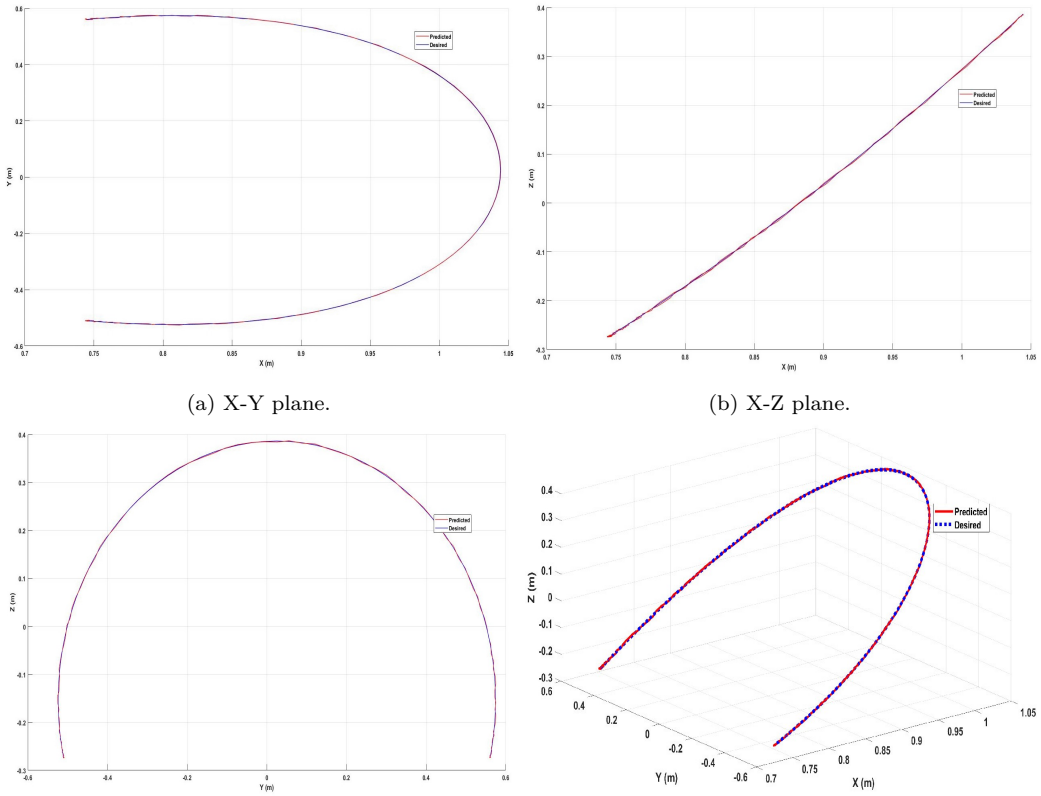

(a) X-Y plane.

(b) X-Z plane.

(c) Y-Z plane.

(d) Three dimension view.

Figure 4.43: The desired path (blue color) and the predicted path (red color) in the task space produced by the robot end effector.

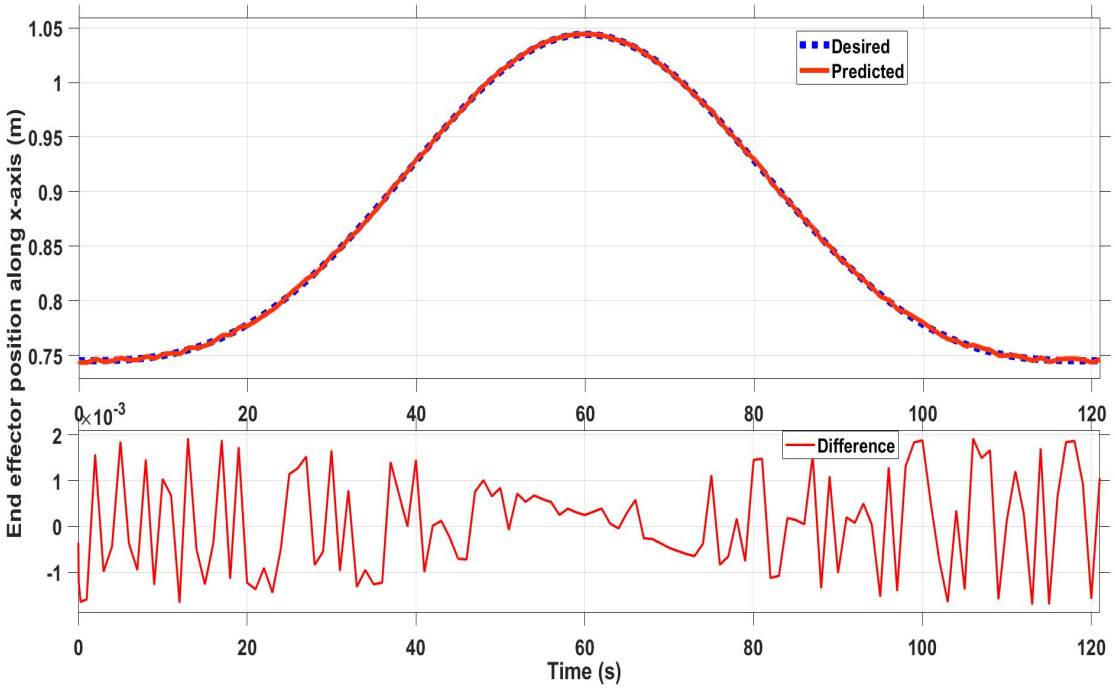

Figure 4.44: The hand position along x-axis for the arc path.

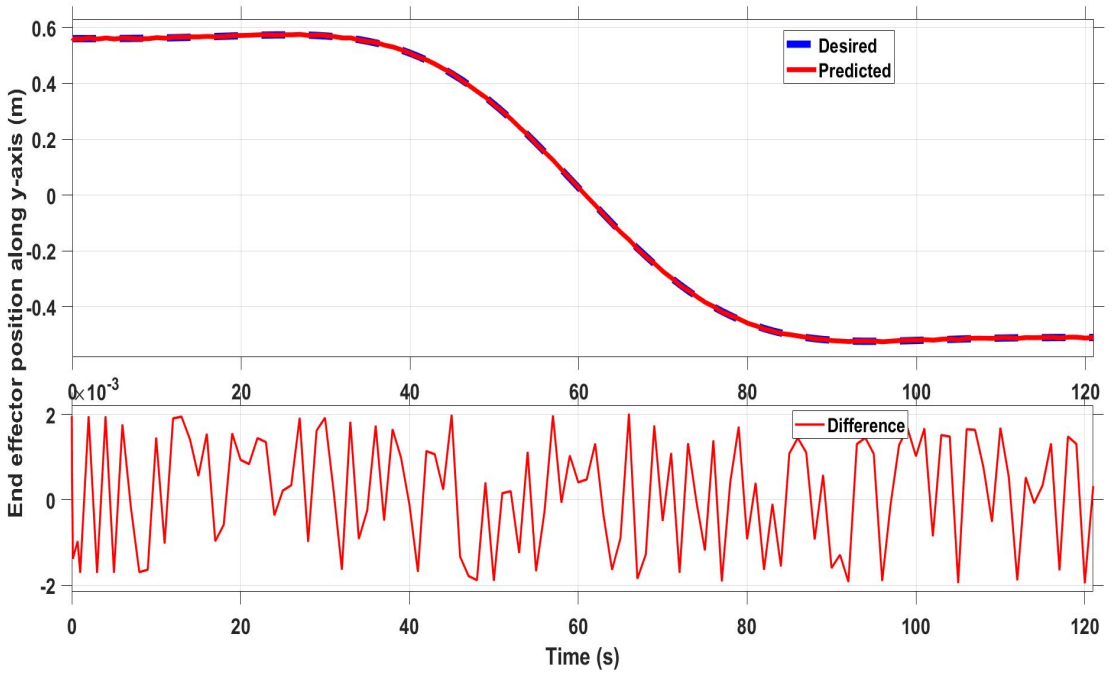

Figure 4.45: The hand position along y-axis for the arc path.

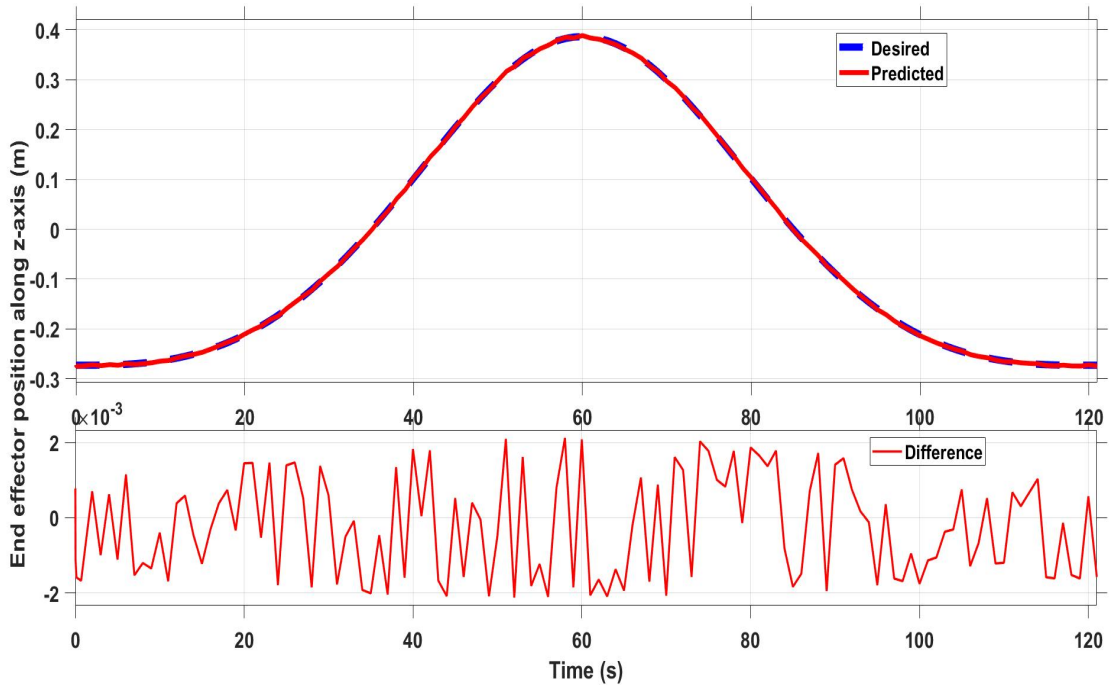

Figure 4.46: The hand position along z-axis for the arc path.

In the following experiment, velocity parameter is inserted to the trajectory by differentiating the input of each ANFIS. The selected path for this evaluation is generated by combining two curves. Figure 4.47 shows four views for the robot environment and the path. The distances between adjacent nodes of the generated path are not same which means the robot will move in different speed along the whole trajectory.

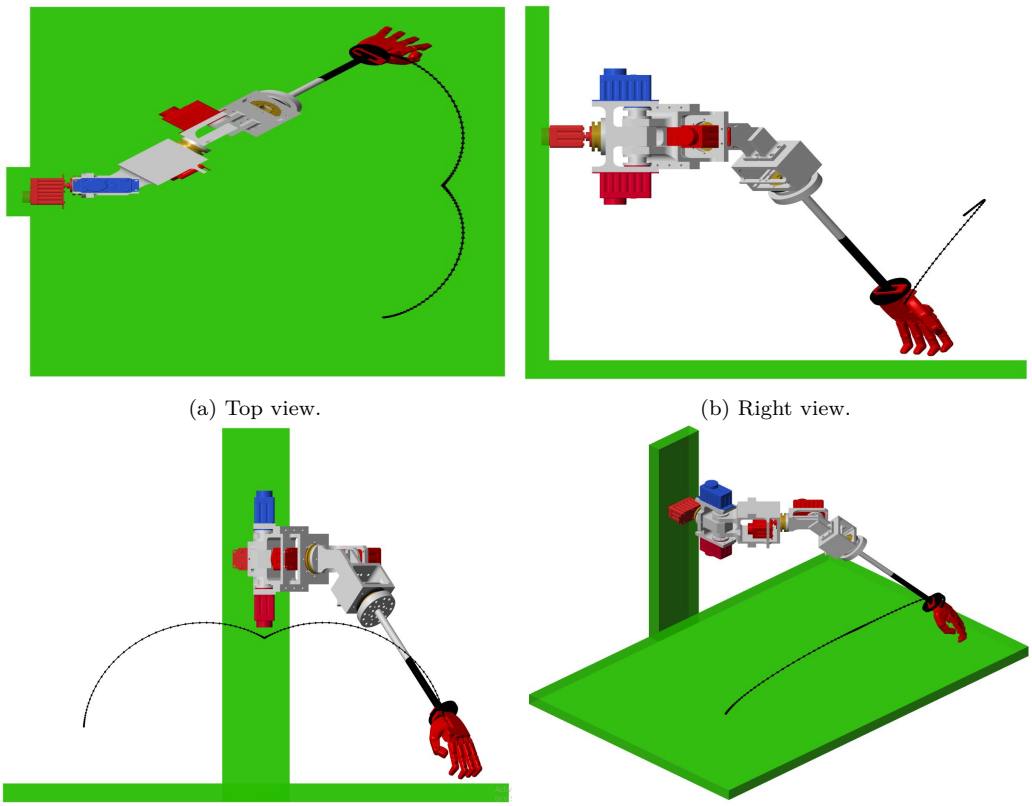

(a) Top view. (b) Right view.

(c) Front view. (d) Isometric view.

Figure 4.47: The desired paths in the task space for the combined curves path.

Figure 4.48 presents the desired and the predicted trajectory for the combined curves path. Although the parameters of the velocity have been added to the controller, the robot followed the desired trajectory perfectly. The maximum difference between the desired and the predicted paths is approximately 0.2 cm. A short video for this experiment is available in [165].

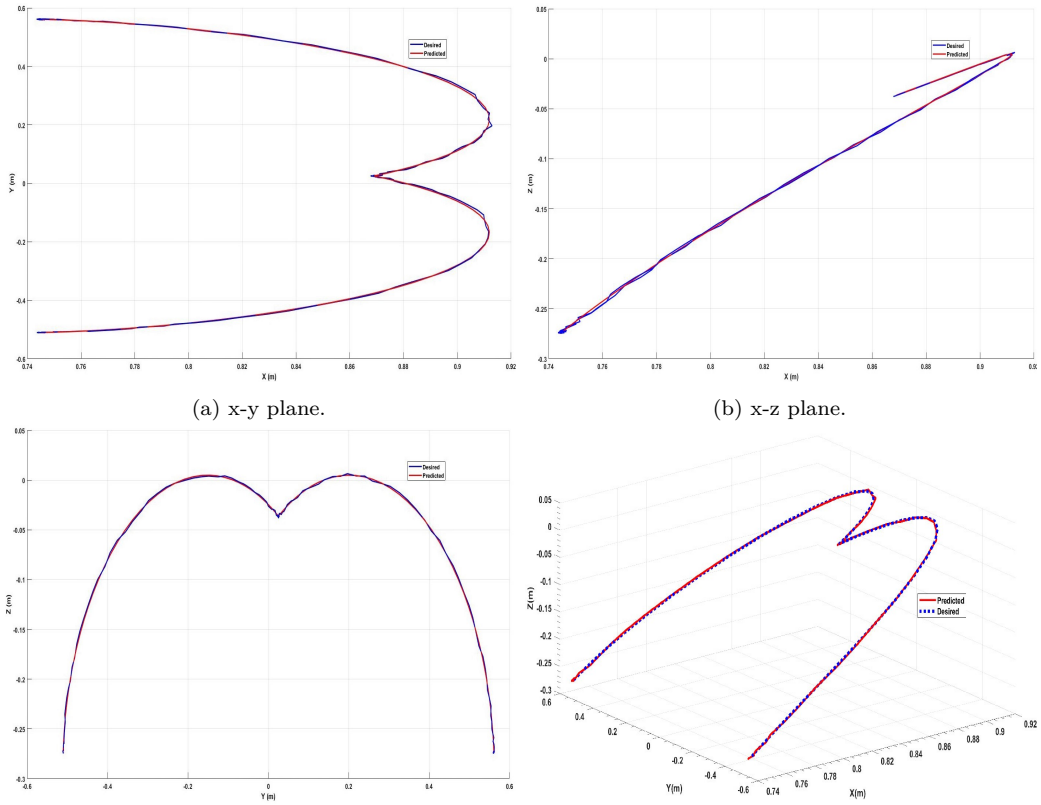

(a) x-y plane.

(b) x-z plane.

(c) y-z plane.

(d) x, y and z axes.

Figure 4.48: The desired paths in the task space for the combined curves path.

Figure 4.52 represents the produced joints angles for the ambidextrous robot arm. The joints transitions are very smooth. Further, its clear from the figure that the velocity of the robot has been drooped slightly after 50 seconds (for about 20 seconds) and then resumed after time 70 seconds. This period represent the space where the two curves have been combined.

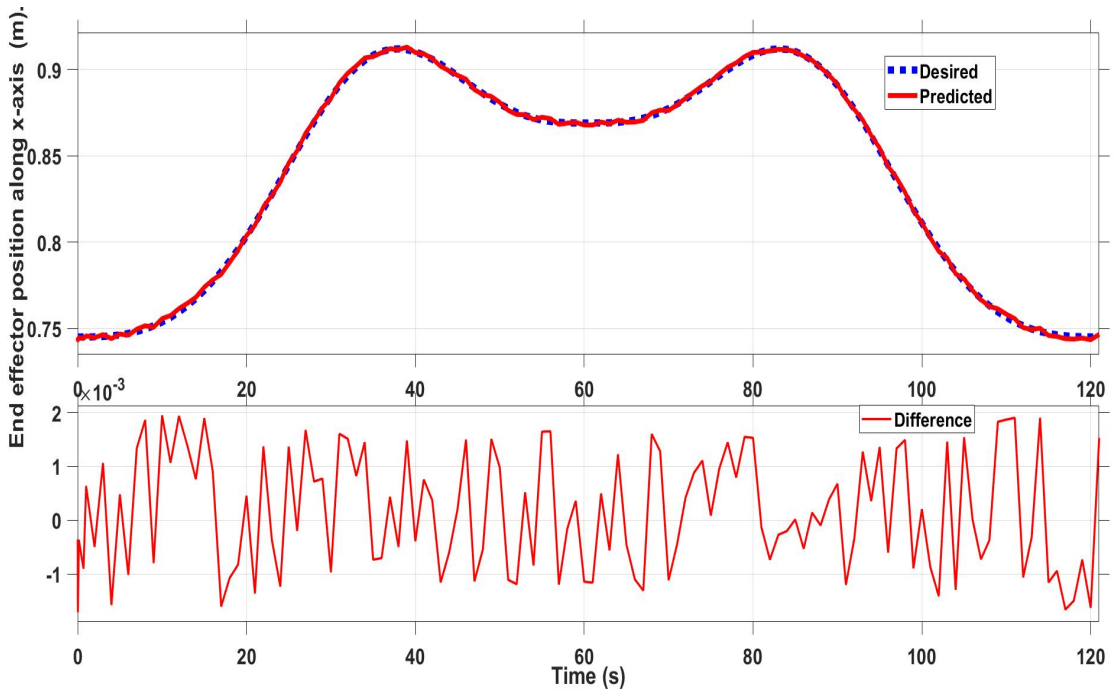

Figure 4.49: The hand position along x-axis for the combined curves path.

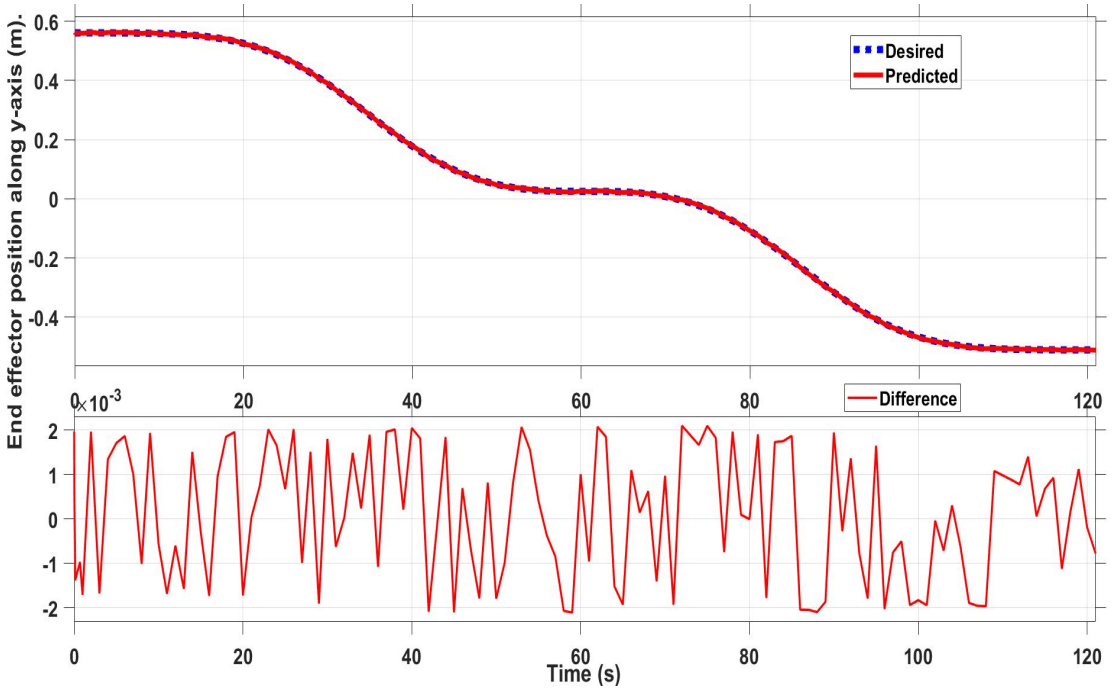

Figure 4.50: The hand position along y-axis for the combined curves path.

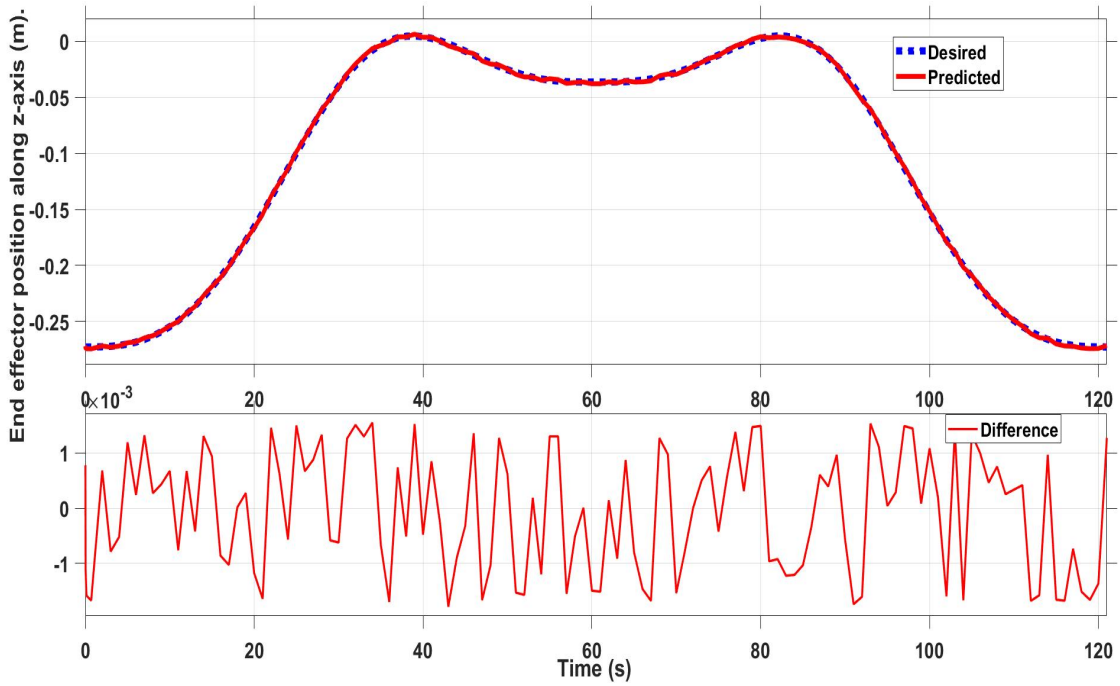

Figure 4.51: The hand position along z-axis for the combined curves path.

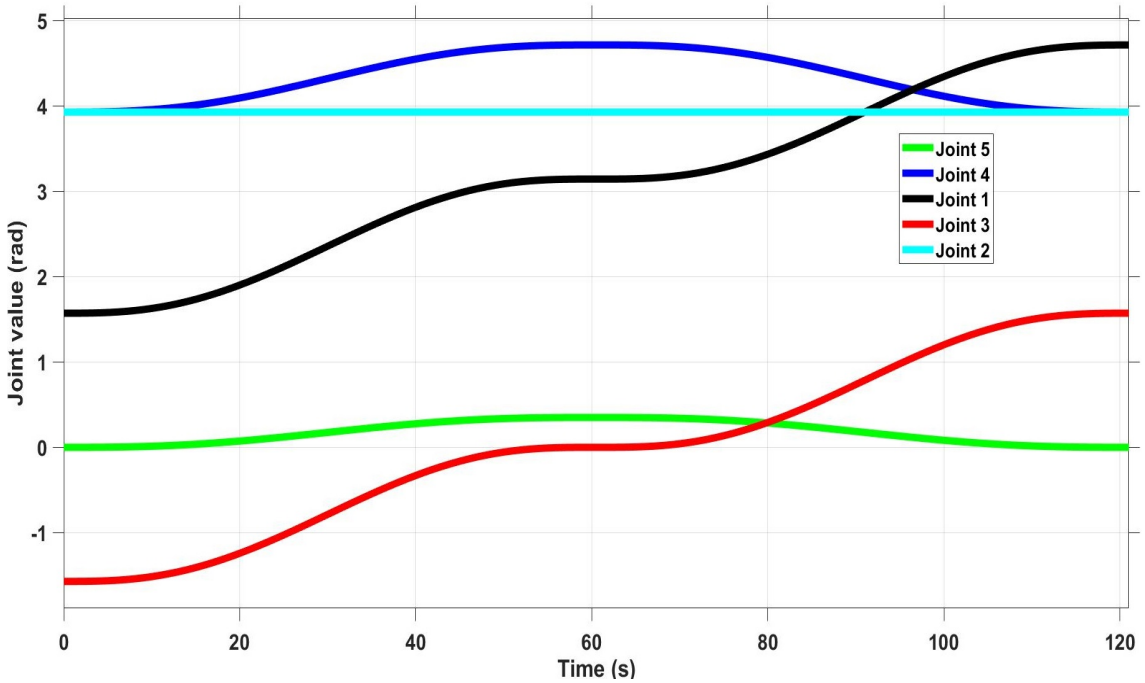

Figure 4.52: The joint values to produce the combined path at the robot hand.

4.2.5 The Efficiency of the Robot Arm

Robots are widely used in industry due to their efficiency and high performance. Many of them are employed in industry where the highest percentage of energy is consumed. Therefore, completing tasks with minimal energy consumption has become point of interest for many researchers [166]. Nevertheless, the optimisation of the power consumption is still a challenging task. In this section, the aim was to verify the efficiency of the robot arm in term of the power consumption. The performance of the ambidextrous robot was compared with a conventional robot. Figure 4.53 shows a robot arm that was used in the experiments and the main specification of this robot has been illustrated in the Appendix C. The model of this robot was designed in SolidWorks 2018 and it was exported to SimMechanics environment.

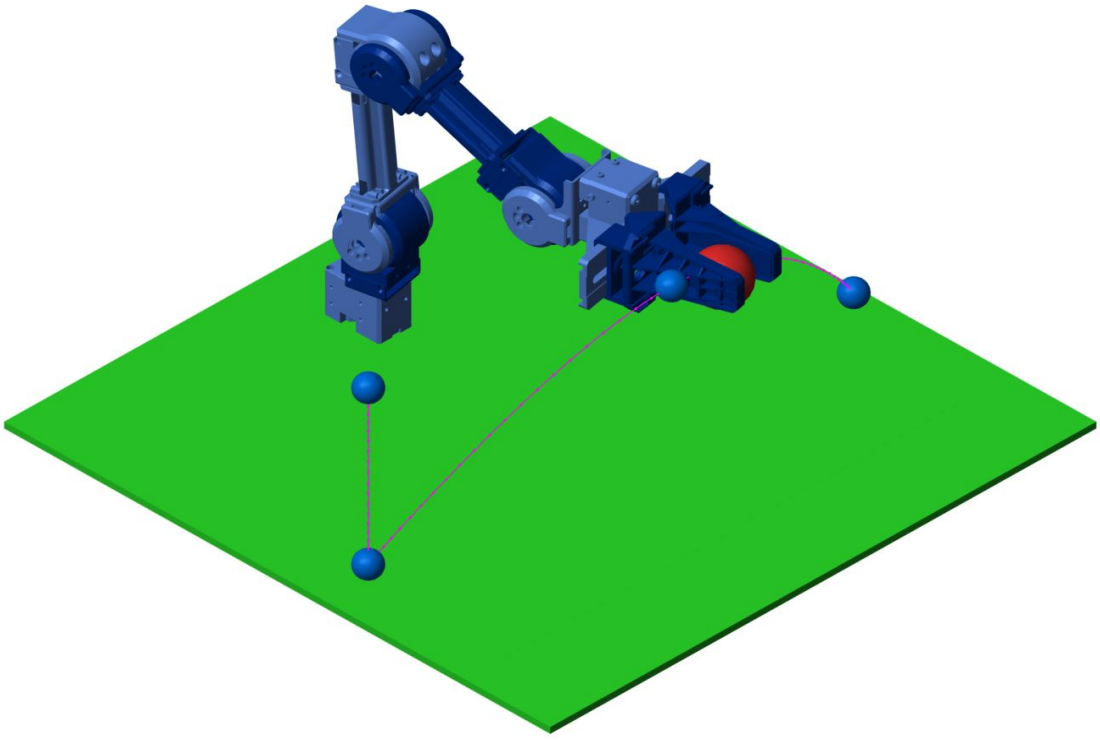

Figure 4.53: A conventional robot arm that was used in the experiments.

The two robots follow a semi-circular path. This path is generated using three points in as xyz plane and the intermediate points have been interpolated using a quantic polynomial to get the continuous velocity and acceleration for both robots [167].

Figure 4.54 and Figure 4.55 show the position of the hand of the ambidextrous arm and the end effector of the conventional arm in all three axis (x, y and z axis) respectively. Short videos of the two robot while performing the tasks are available in [168, 169].

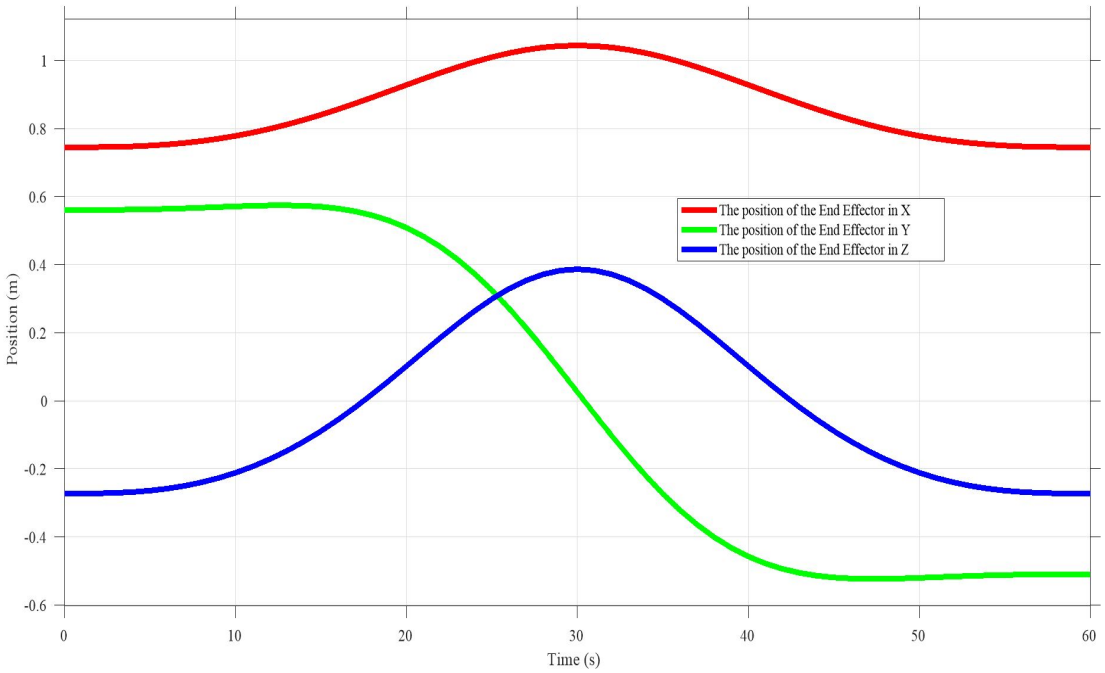

Figure 4.54: The position of the ambidextrous arm in x, y and z axis

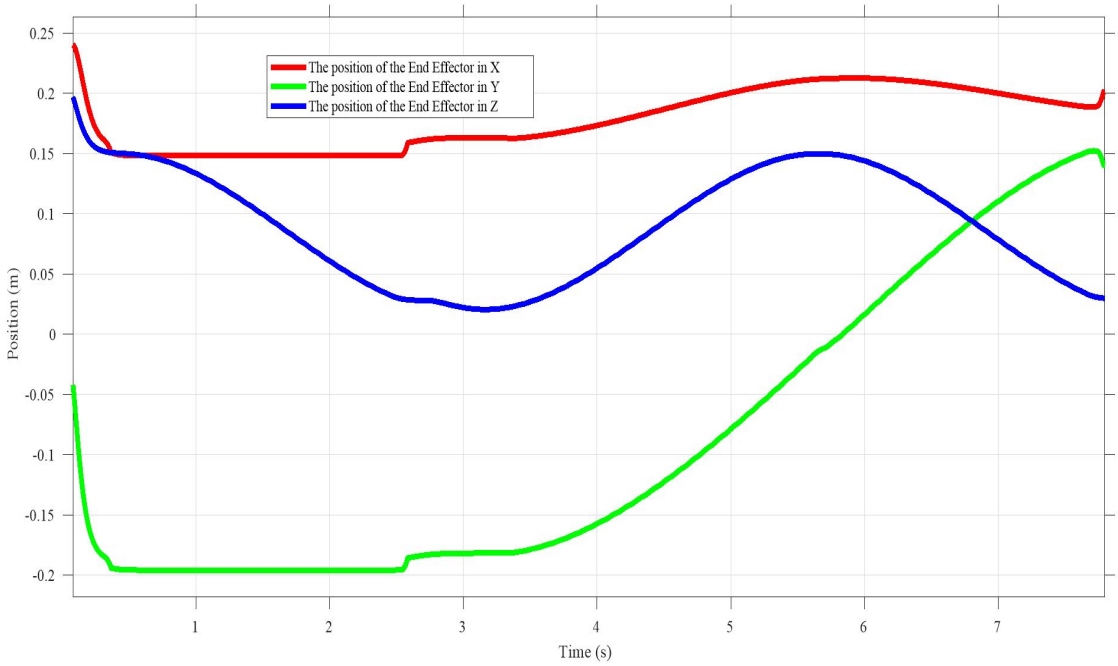

Figure 4.55: The position of conventional arm in x, y and z axis.

The experiment is divided in two parts. The first part each robot follow the specified path with no load. The robots carried a load of 0.5 kg by the hand for the ambidextrous arm and by the gripper for the normal robot in the second part. A snapshot of the ambidextrous arm and the conventional arm while passing through the path is depicted in Figure 4.56.

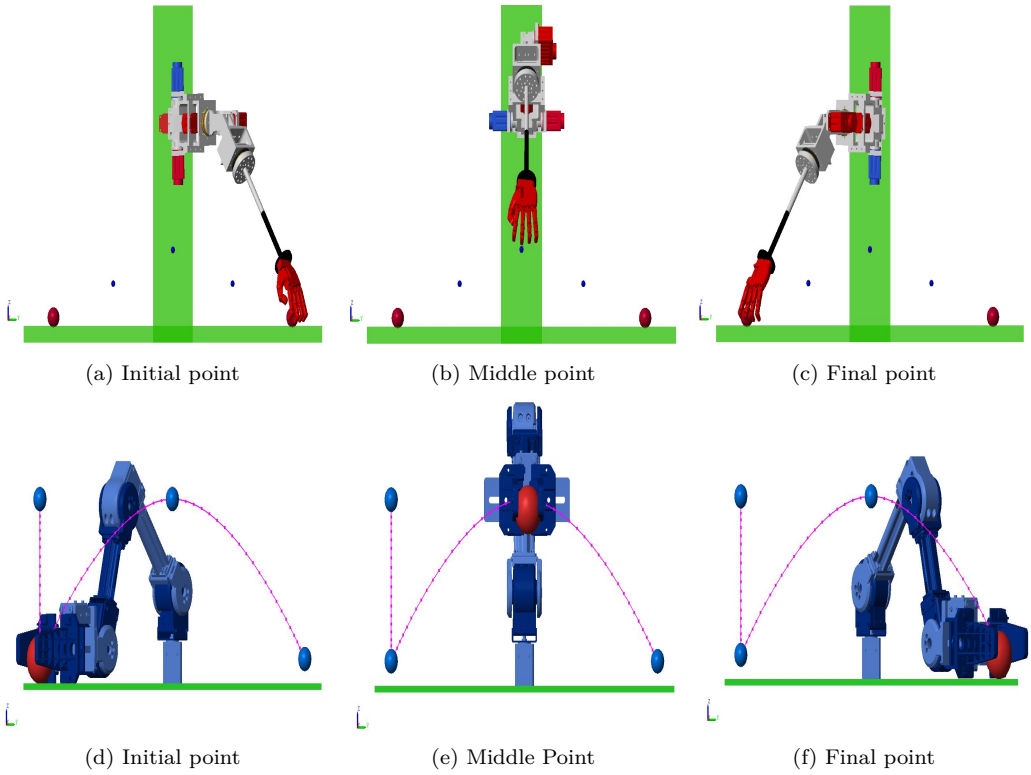

(a) Initial point (b) Middle point (c) Final point

(d) Initial point (e) Middle Point (f) Final point

Figure 4.56: Snapshots while the ambidextrous arm (a) (b) (c) and the conventional arm (d) (e) (f) follow the path.

Two tasks are performed on the ambidextrous arm to validate the design. First the torque exerted by the arm on each joint is noted while no load is placed and then with 0.5 kg load. The purpose of this experiment was to see the torque exerted on each joint and then compare it with the conventional arm performance doing exactly the same tasks. The torque for both robots has been calculated depending on the Euler–Lagrange equation as represented in Equation (4.27) [170].

$$M(\theta)\ddot{\theta} + H(\theta, \dot{\theta})\dot{\theta} + G(\theta) = \tau \tag{4.27}$$

where $M \in \Re^{(5\times5)}$, is the inertia matrix of the system, $\ddot{\theta} \in \Re^{(5\times1)}$is the joint acceleration, $H\ (\theta, \dot{\theta}) \in \Re^{(5\times1)}$ is a vector of Coriolis and centrifugal forces, $G \in \Re^{(5\times1)}$ is vector of gravity forces, $\tau \in \Re^{(5\times1)}$ is vector of joint torques.

Figures 4.57 to 4.61 depict the torque exerted by the ambidextrous arm.

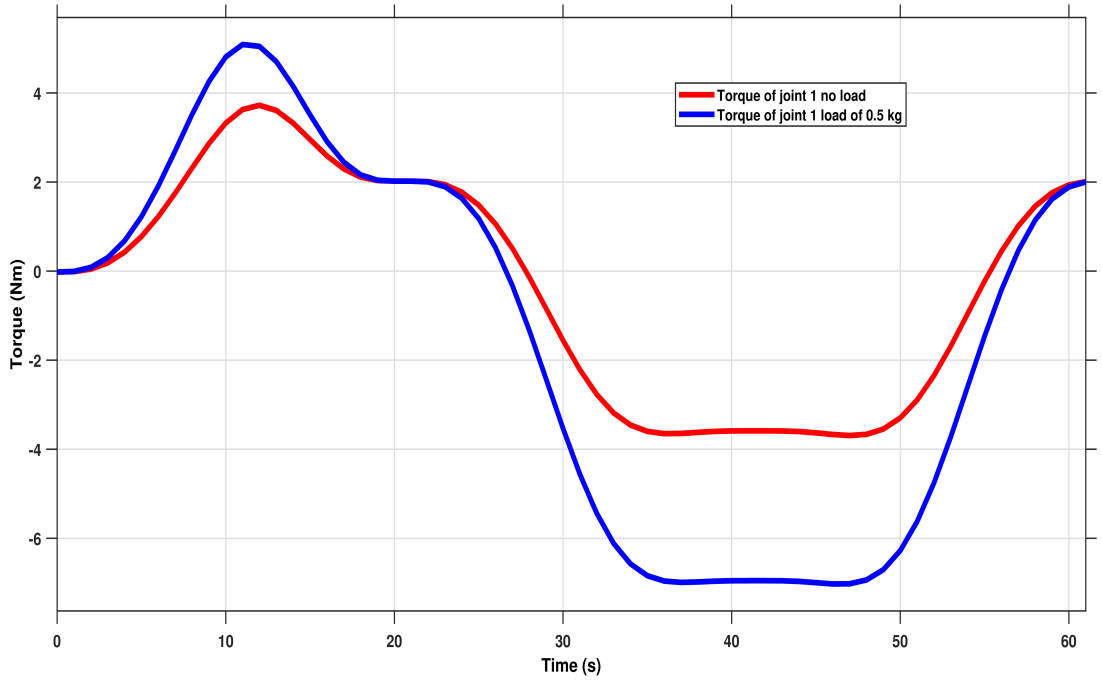

Figure 4.57: The torque exerted by the ambidextrous arm in joint one.

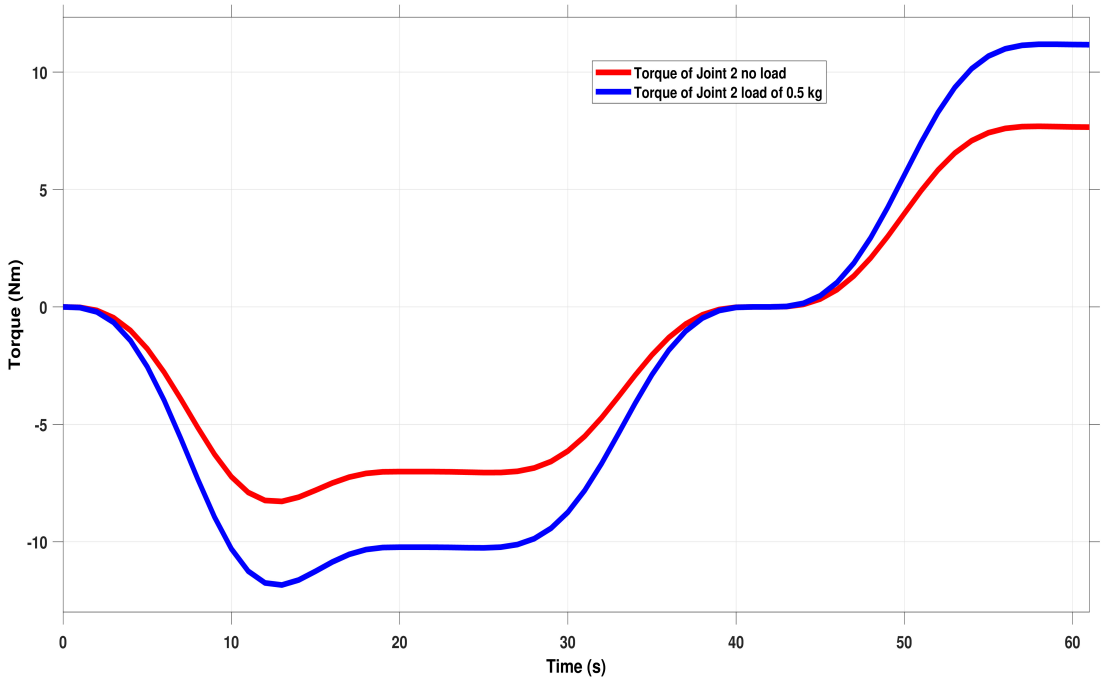

Figure 4.58: The torque exerted by the ambidextrous arm in joint two.

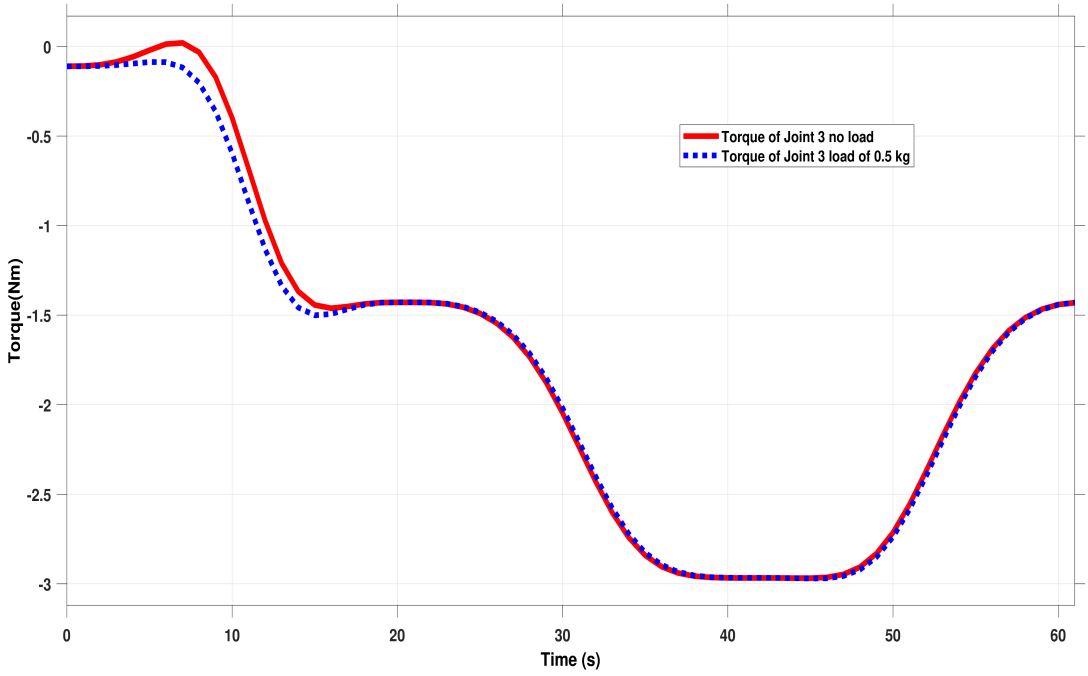

Figure 4.59: The torque exerted by the ambidextrous arm in joint three.

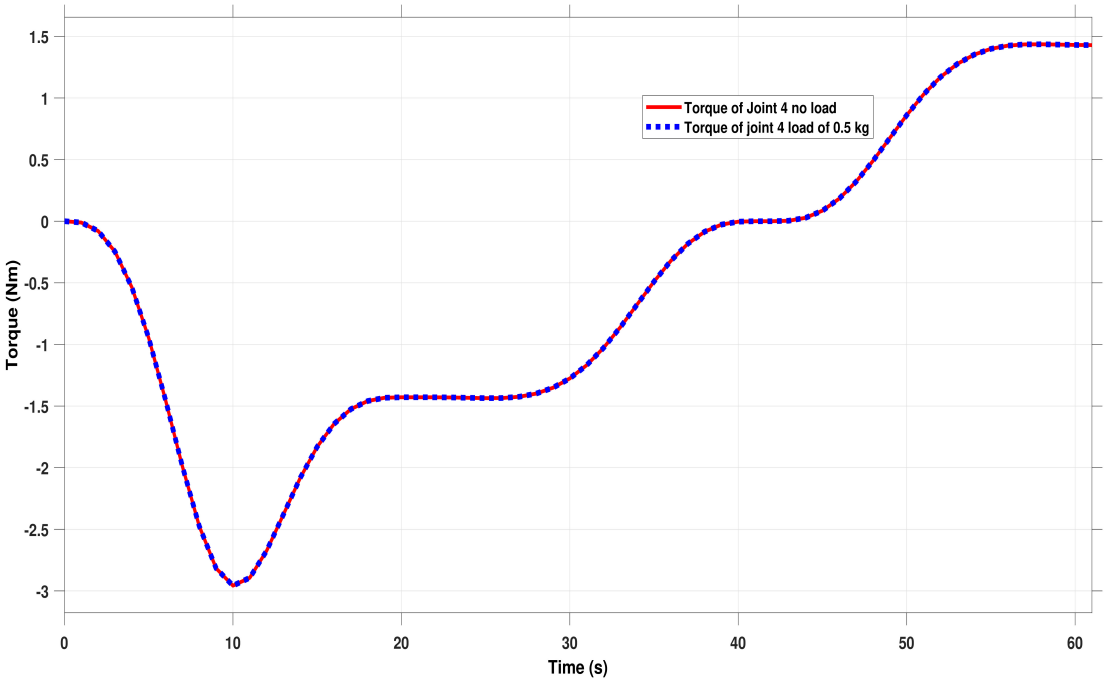

Figure 4.60: The torque exerted by the ambidextrous arm in joint four.

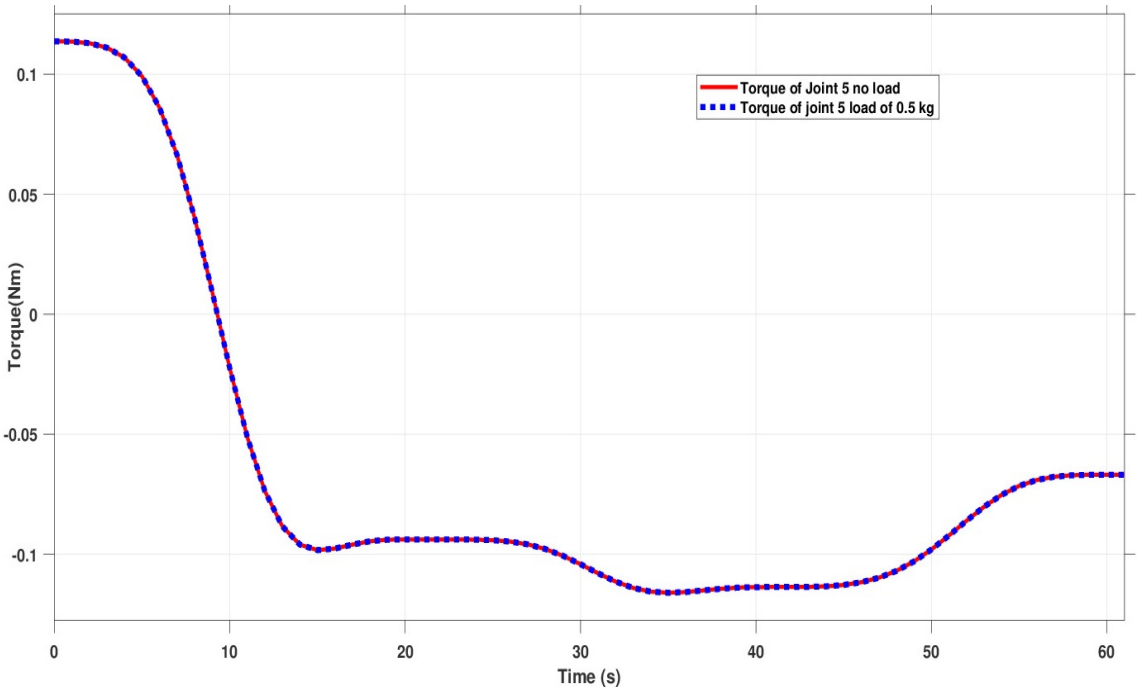

Figure 4.61: The torque exerted by the ambidextrous arm in joint five.

Similarly, the two tasks were assigned to the conventional arm to see the torque exerted on each joint in both scenarios. Figures 4.62 to 4.63 show the torque exerted by the conventional arm while performing the two tasks.

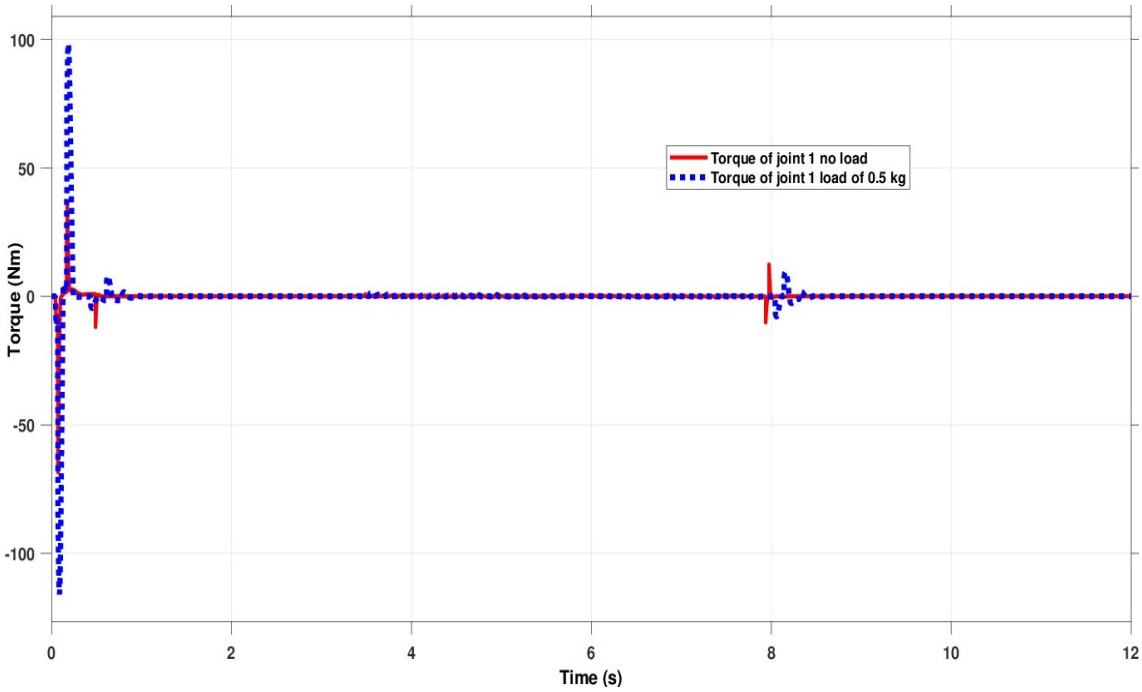

Figure 4.62: The torque exerted by the conventional arm in joint one.

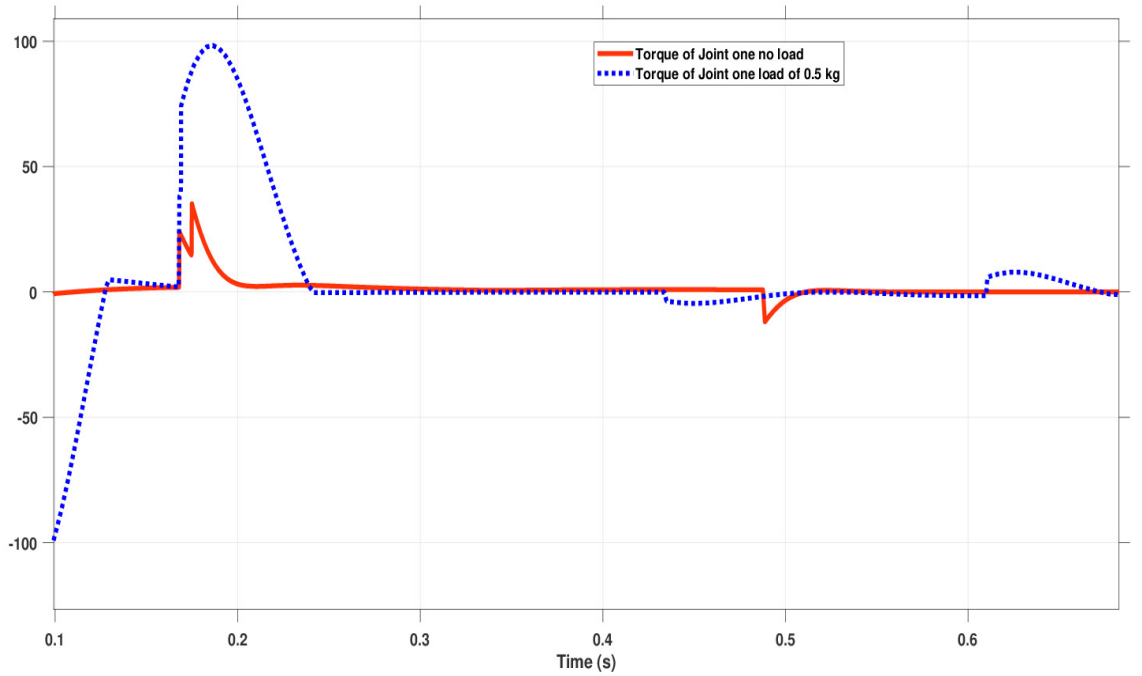

Figure 4.63: Magnified part of the torque exerted in joint one for time from 0-0.7 s.

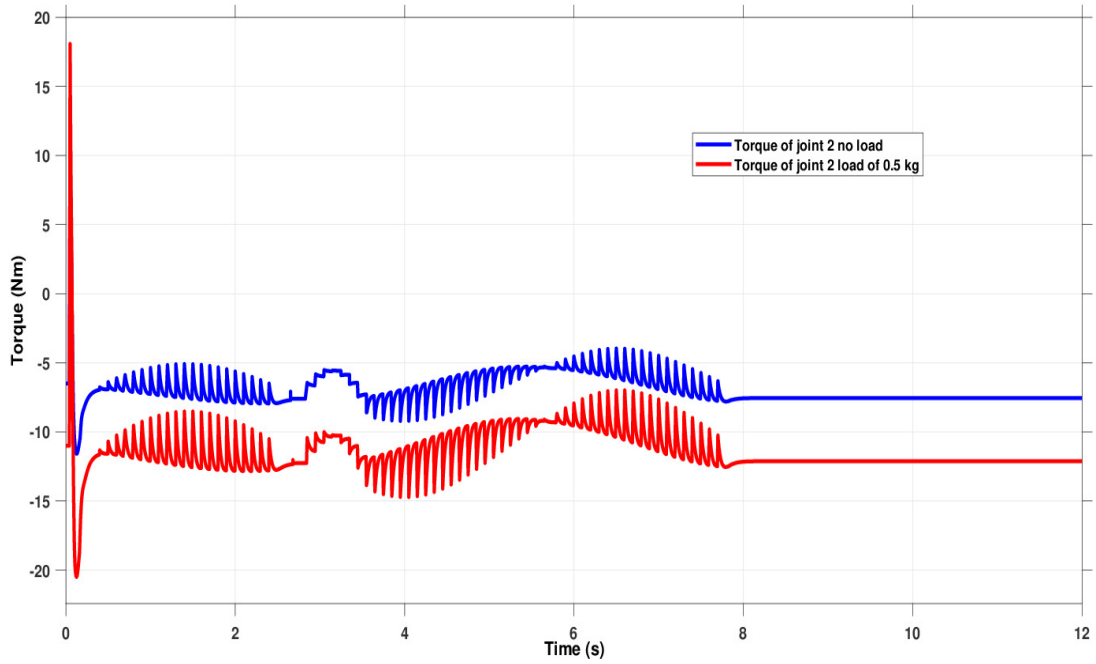

Figure 4.64: The torque exerted by the conventional arm in joint two.

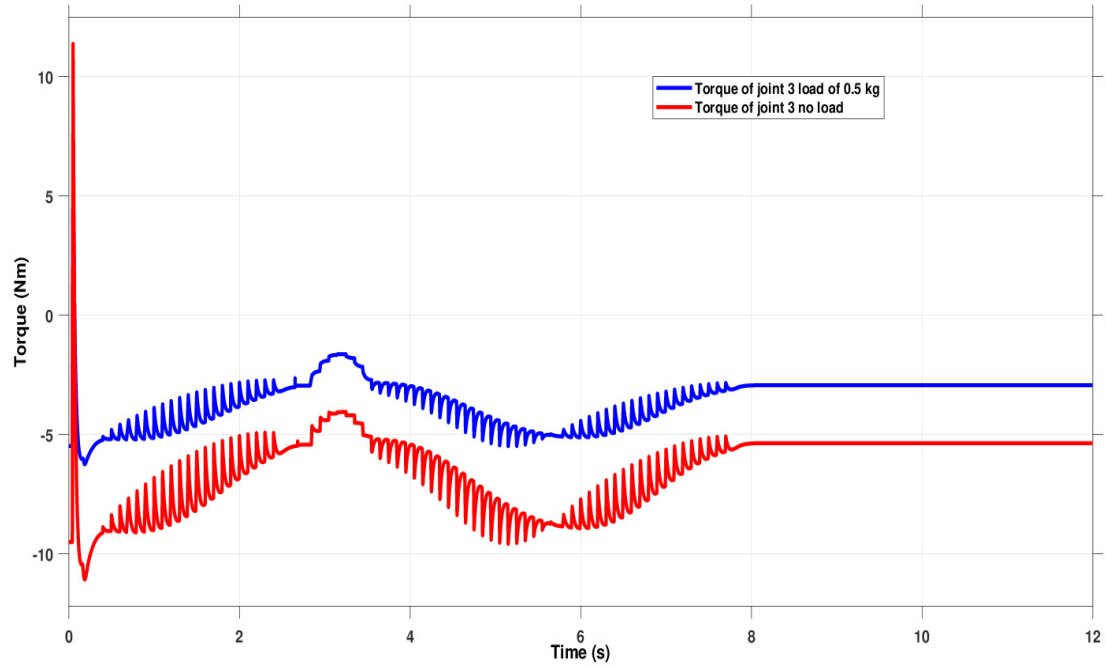

Figure 4.65: The torque exerted by the conventional arm in joint three.

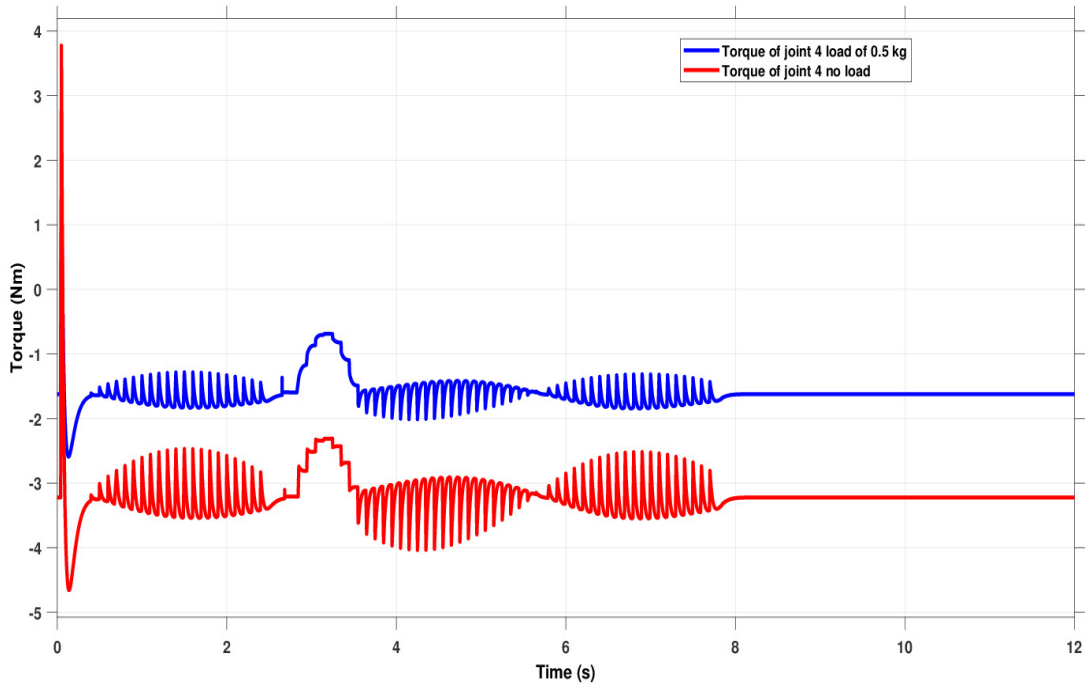

Figure 4.66: The torque exerted by the conventional arm in joint four.

It is clear from this experiment that the exerted torque at only joint one and two in the ambidextrous arm have been changed when carrying a load. Whereas, the exerted torque at every joint of the conventional robot arm has been changed. This verifies the effectiveness of the ambidextrous arm design.

In order to verify the efficiency of the ambidextrous arm design, acceleration graphs are obtained through experiment. If acceleration stays the same in both scenarios (without load and with load) it proves the efficiency of the design. By comparing the results of how the arm behaves with load and without load, the efficiency of the design can be deduced. The acceleration of the ambidextrous arm in the x-axis and y-axis is shown in Figures 4.67 and 4.68 respectively.

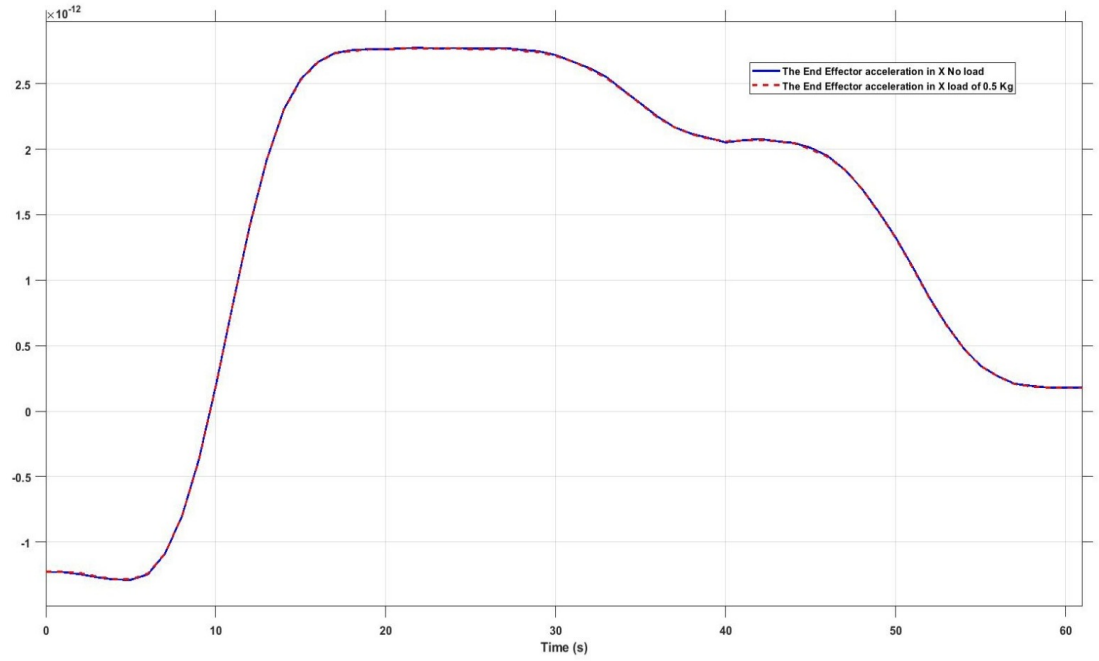

Figure 4.67: The acceleration of the EE in x-axis (The ambidextrous arm).

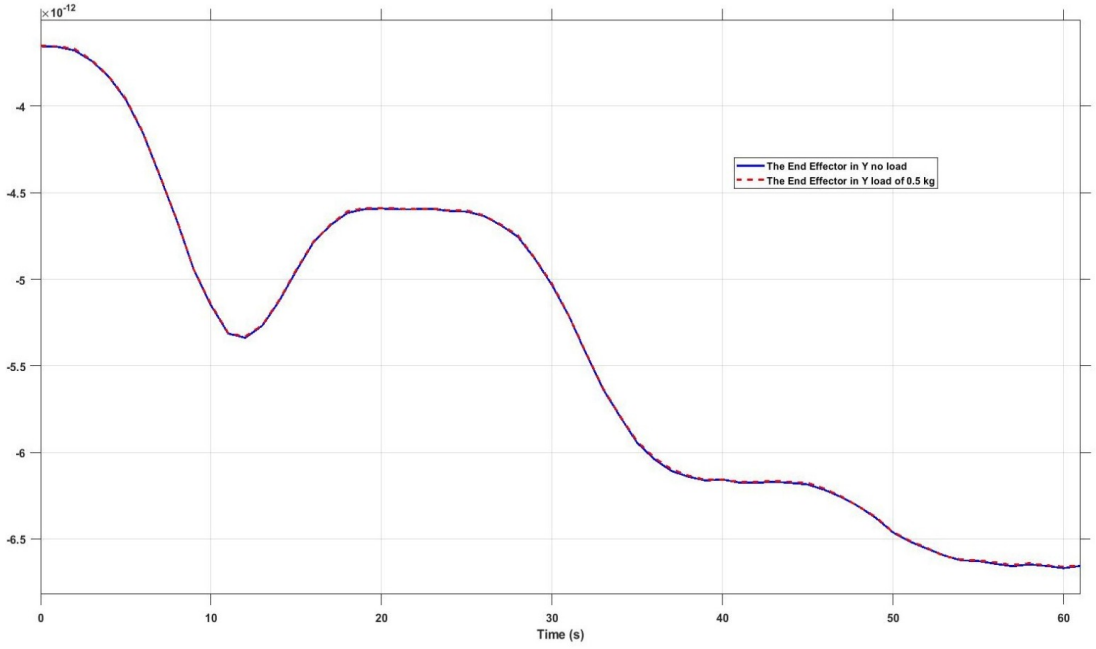

Figure 4.68: The acceleration of the EE in y-axis (The ambidextrous arm).

Similarly, the acceleration of the conventional arm in the x-axis and y-axis is shown in Figure 4.69 and Figure 4.70 respectively. The conventional arm is also tested in both scenarios first without load then with 0.5 kg load. It can be observed from both figures that acceleration has changed.

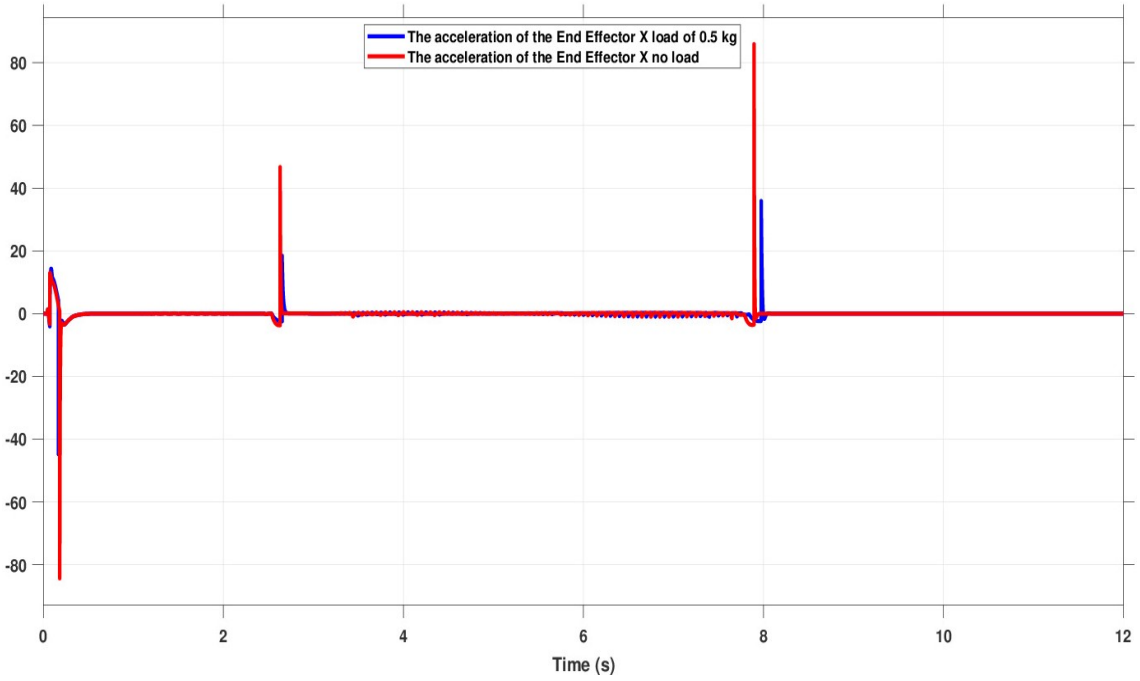

Figure 4.69: The acceleration of the EE in x-axis (The conventional arm).

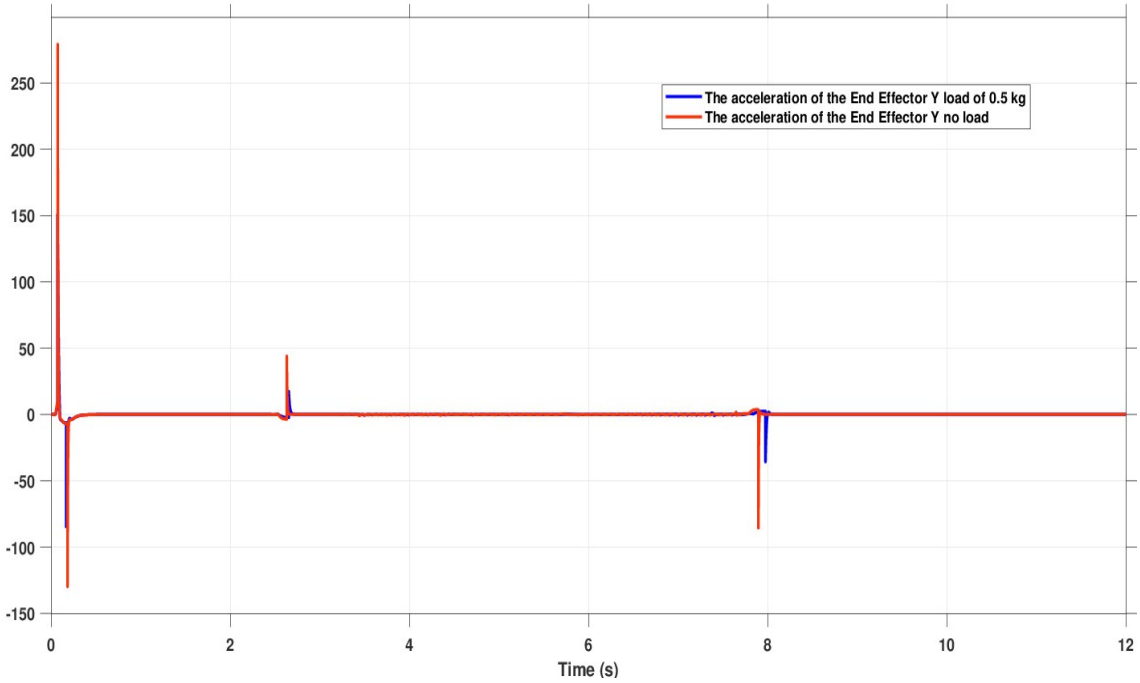

Figure 4.70: The acceleration of the EE in y-axis (The conventional arm).

By comparing Figure 4.67 and Figure 4.68 with Figure 4.69 and Figure 4.70, efficiency of ambidextrous design is evident.

4.3 Chapter Summary

In section 4.1.2, a feasibility analysis for combining conventional controllers with neural networks was presented. While conventional methods such as PID control are widely used and reliable, combining them with artificial intelligence approaches offers better accuracy rates. All the tests were carried out on a novel 3D printed multi-finger ambidextrous robot hand. Force sensors were used to trigger the algorithm. The grasping trajectory of each finger was combined with data from the adjacent fingers to improve accuracy.

In section 4.2, modelling of the ambidextrous robotic arm was presented. First, links and joints were identified, DH convention for frame assignment introduced,

and forward kinematics calculated. Furthermore, the inverse kinematic problem was discussed in great detail. Due to the complexity of computing inverse kinematics for an ambidextrous robot arm, an artificial neural fuzzy interference system (ANFIS) was employed. When ANFIS failed to produce satisfactory results due to the nature of ambidextrous design, Multiple ANFIS was then used to improve accuracy. Use of an 'IF' block as a selector to switch between appropriate MANFIS was implemented. A model for an ambidextrous robot arm was designed, modelled and tested to confirm the validity of the results. From the results, it was confirmed that the use of MANFIS may be the most appropriate solution in controlling ambidextrous systems. The efficiency of the ambidextrous arm was tested by comparing its performance with a traditional robot arm. Both the exerted torque and the acceleration of the end effector (in x and y direction) have been used to accomplish the tasks in two cases (load and no load). The experiments have proved the effectiveness of the ambidextrous arm in terms of power consumption and stability.

CHAPTER 5

Conclusion

This thesis was related to successful design, development and control of the ambidextrous robot arm. It offered greater range of movement than conventional dexterous arms. In addition to the design, combined use of PAMs with motors in the project was unlike any other robotic arm. Literature review chapter compiled the references of existing work and confirmed none of the arms found in literature offered an ambidextrous feature of this nature as proposed in the thesis. Therefore, the novel design of the ambidextrous robotic arm was proposed. Since design of the arm was unique, naturally it required a new approach to control the arm. When existing controllers failed to drive the arm, modified MANFIS controller was proposed.

The concept of the ambidextrous robot hand was originally proposed by Dr Emre Akyürek in 2015 [40]. The existing design was good enough to prove the basic ambidextrous design concept of hand, but it was not possible to interlink the hand with the arm without improvements. Therefore, number of changes were done to improve the existing hand (see section 3.1). These changes were addition of wrist movement offering another degree of freedom, re-routing of the tendons (for greater strength), complete replacement of tendon string material (polythene string is used to avoid breaking issues), replacement of 4 mm hose tail barb to 8mm for better

speed of system, incorporation of force sensors on the thumb to offer better control, complete re-design of electronic circuit to avoid short-circuit and poor connection issues, replacing all metal parts to the newly designed 3D printed parts in a bid to reduce weight from 3.2 kg to 2.3 kg. By making these changes, the new design met the requirement of being a fully 3D printed ambidextrous robot hand offering 14 DOF with improved control. Being complex, non-linear and coupled system, the ambidextrous robot hand could not be effectively controlled using classical controllers such as PID. To enhance the effectiveness of the conventional controllers for the nonlinear and uncertain systems, gains of the PID controller was conservatively tuned and adapted to the process parameter variations. This addition offered better results than using simple classic controllers. Therefore, for stable control of the ambidextrous robot hand, number of conventional controllers were tested with Neural network approach. The result comparison of these controllers confirmed combined use of PID with NN was the best controller to drive the ambidextrous hand. Also, five fingers were used for sensory feedback to better reflect the scenarios being experiment.

The ambidextrous robot arm was designed in SOLIDWORKS (step by step process was discussed in section 3.2) and 3D printed at Brunel university London. Since the design of the arm broke the dexterous arm constraints, it became quite challenging to control the arm. First, the problem of forward kinematics and inverse kinematics was introduced. Then, an ANFIS controller was trained to control a simple dexterous arm effectively. After satisfactory results were obtained, the difficulty level was increased to control the ambidextrous arm. It was apparent that ambidextrous trajectories could not be performed using a simple ANFIS based controller. In the end, it was decided to combine two simple ANFIS controllers to form a controller design for both right and left arm movements. A conventional ANFIS network failed to work alone in a space where the ambidextrous movement was required. Multiple ANFIS were then used and merged with each other for better accuracy. A Simulink/MATLAB based model specifically for an ambidextrous robot arm was designed, modelled

and tested to confirm the efficency of work (see section 4.2.4). From the trajectory simulation analysis, it was confirmed that the combined use of modified MANFIS controller was the most appropriate controller for controlling ambidextrous systems in general. The efficiency of the ambidextrous arm was tested further by comparing its performance with a conventional robot arm. The results shown in section 4.2.5 proved the efficiency of the ambidextrous arm when compared with conventional arm in term of power consumption and the stability.

5.1 Recommendations for Further Study

As with every project, there is always a room for improvement and the ambidextrous robot arm was no exception. A few things were identified for further researchers to look into. The ambidextrous robot arm was interlinked to the re-designed version of the ambidextrous robot hand. It is noted that the length of PAMs is far more than what is needed in reality. For instance, through experiments, it was established that while performing the tasks the PAMs never contracted more than 3.5 bar, but it offered up to 8 bar. Having said that such PAMs were designed to be lengthier and extra weight gets added to mechanical structure. Since 3.5 bar was the maximum required for the majority of the tasks, shorter and more lightweight PAMs should be added to the structure for better speed. Reduction in weight not only increases the efficiency of the ambidextrous robot arm but also makes robot arm design lighter and easy to control. Hence, this will allow the designer to expand the range of movement of the current ambidextrous robot arm.

From the control side, conventional controllers were tested, and their performances were compared to find the most appropriate one. The modified MANFIS controller was the best option to control ambidextrous trajectories. The training time increases when the ANFIS architecture has more than five MFs per each input. Future research should focus on using ANFIS with multiple outputs.

Furthermore, a balanced approach needs to be identified in future research that could help the arm to use the shortest possible route to reach the desired point while energy consumption is kept to a minimum.

Future of robotic arms looks promising. Robotic arms will have a profound effect on the workplace of the future. "Robots will take our jobs!" is perhaps the most common fear surrounding robotics development. Yes, technology is changing fast and it does have economic ramifications. AI driven robotic arms, for instance, are highly likely to replace key chain workers in manufacturing in the future. The industrial robotic arm has several advantages for the manufacturer. Once a robotic arm is integrated into a production line, the production speed increases as the robot reduces the cycle time between each work piece. Robot industrial arms also decrease work-related injuries and accidents. With these robots in place, along with their necessary safety packages, workers are kept clear of hazardous environments, toxic fumes and tedious, sometimes injury-inducing work. In my view, robotic arms will most likely replace tasks, not jobs. In-fact, it will also create new market and jobs. We might need additional education and re-training for those jobs, but the opportunities will be there.

Bibliography

[1] R. Miller, "Robots in Industry," in *Industrial Robot Handbook*. Springer US, 1989, pp. 1–9.

[2] M. Edwards, "Robots in industry: An overview," *Applied Ergonomics,Elsevier*, vol. 15, no. 1, pp. 45–53, 1984.

[3] "Robotics: A Brief History." [Online]. Available: https://cs.stanford.edu/people/eroberts/courses/soco/projects/1998-99/robotics/history.html

[4] Y. Koren, *Robotics for engineers*. McGraw- Hill Book Company, 1985.

[5] D. Gama Melo, Erika Nathalia and Aviles Sanchez, Oscar Fernando and Amaya Hurtado, "Anthropomorphic robotic hands: a review," *Ingeniería y Desarrollo*, vol. 32, no. 2, pp. 279–313, 2014.

[6] B. H and M. Wassink, "Evolution of Robotic Hands," University of Twente, Tech. Rep., 2010.

[7] Y. Tsuneo, "Multifingered robot hands: Control for grasping and manipulation," *Annual Reviews in Control*, vol. 34, pp. 199–208, 2010.

[8] B. Antonio and K. Vijay, "Robotic Grasping and Manipulation: Chapter 1, pp. 1-22," 2000. [Online]. Available: http://www.centropiaggio.unipi.it/sites/default/files/surveys-ramsete01.pdf

[9] S. Park, J. Bae, J. Park, and H. Baeg, "Development of an anthropomorphic robot hand aimed at practical use for wide service robot application," in *IEEE International Conference on Automation Science and Engineering (CASE)*, Seoul, South Korea, 2012.

[10] R. Balasubramanian and V. Santos, *The Human Hand as an Inspiration for Robot Hand Development.* Switzerland: Springer International Publishing, 2014, vol. 95.

[11] G. Bekey, R. Tomovic, and I. Zeljkovic, "Control architecture for the belgrade/usc hand." *T. Iberall S.T. Venkataraman, editor, Dexterous Robot Hands. Springer-Verlag*, 1990.

[12] S. Jacobsen, E. Iversen, D. Knutti, R. Johnson, and K. Biggers, "Design of the Utah/MIT Dexterous Hand," in *Proceedings of the 1986 IEEE International Conference on Robotics and Automation*, 1986, pp. 1520–1532.

[13] C. Lovchik and M. Diftler, "The Robonaut Hand: a Dexterous Robot Hand for Space," in *Proceedings of the IEEE International Conference on Robotics and Automation*, Detroit, MI, 1999, pp. 907–912.

[14] Y. Zhang, Z. Han, H. Zhan, X. Shang, and T. Wang, "Design and Control of the BUAA Four fingered Hand," in *Proceeding of International Conference in Robotics and Automation*, 2001, pp. 2517–2522.

[15] J. Ueda, Y. Ishida, M. Kondo, and T. Ogasawara, "Development of the NAIST-Hand with Vision-based Tactile Fingertip Sensor," in *Proc. of the 2005 IEEE International Conference on Robotics and Automation, Barcelona, Spain,*, 2005, pp. 2332–2337.

[16] J. Gazeau, S. Zeghloul, M. Arsicualt, and J. Lallemand, "The lms hand: force and position controls in the aim of fine manipulation of objects." in *IEEE International Conference on Robotics and Automation, ICRA01, Seoul, Korea*, 2001, pp. 2642–2648.

[17] A. Caffaz and G. Cannata, "The design and development of the dist-hand dextrous gripper." in *Proc. IEEE int. Conf. on Robotics and Automation, ICRA98*, 1998, pp. 2075–2080.

[18] G. Cannata and M. Maggiali, "An Embedded Tactile and Force Sensor for Robotic Manipulation and Grasping," in *Proc. of the IEEE-RAS Int. Conf. on Humanoids, Humanoids,Tsukuba, Japan*, 2005, pp. 80–85.

[19] H. Kawasaki, T. Komatsu, and K. Uchiyama, "Dexterous anthropomorphic robot hand with distributed tactile sensor: Gifu hand II," *IEEE/ASME Transactions on Mechatronics,*, vol. 7, no. 3, pp. 296–303, 2002.

[20] J. Butterfass, M. Grebenstein, H. Lieu, and G. Hirzinger, "DLR-Hand II: Next Generation of a Dextrous Robot Hand," in *Proceedings of the 2001 IEEE International Conference on Robotics and Automation*, 2001, pp. 109–114.

[21] R. Howe, A. Dollar, and M. Claffee, "Robots Get a Grip." *IEEE Spectrum*, vol. 51, no. 12, pp. 42–47, 2014. [Online]. Available: https://spectrum.ieee.org/robotics/humanoids/inexpensive-durable-plastic-hands-let-robots-get-a-grip/?utm_source=techalert&utm_medium=email&utm_

[22] M. Zecca, G. Cappiello, F. Sebastiani, S. Roccella, F. Vecchi, M. C. Carrozza, and P. Dario, "Experimental analysis of the proprioceptive and exteroceptive sensors of an underactuated prosthetic hand," in *Advances in Rehabilitation Robotics*, 2004, pp. 233–242.

[23] A. Deshpande, "Mechanisms of the anatomically correct testbed hand," *IEEE/ASME Transactions on Mechatronics,*, vol. 18, no. 1, pp. 238–250, 2013.

[24] A. Kargov, T. Asfour, C. Pylatiuk, R. Oberle, H. Klosek, S. Schulz, K. Regenstein, G. Bretthauer, and R. Dillmann, "Development of an anthropomorphic hand for a mobile assistive robot," in *9th International Conference on Rehabilitation Robotics, ICORR*, 2005, pp. 182–186.

[25] A. Namiki and M. Ishikawa, "The analysis of high-speed catching with a

multifingered robot hand," in *Proceedings of the 2005 IEEE International Conference on Robotics and Automation.* IEEE, 2005, pp. 2655–2660.

[26] L. Zollo, S. Roccella, R. Tucci, B. Siciliano, E. Guglielmelli, M. Carrozza, and P. Dario, "BioMechatronic Design and Control of an Anthropomorphic Artificial Hand for Prosthetics and Robotic Applications," in *The First IEEE/RAS-EMBS International Conference on Biomedical Robotics and Biomechatronics, 2006. BioRob.*, 2006.

[27] E. Akyürek, T. Kalganova, M. Mukhtar, L. Paramonov, L. Steele, M. Simko, L. Kavanagh, A. Nimmo, and A. Huynh, "A novel design process of low cost 3D printed ambidextrous finger designed for an ambidextrous robotic hand," *WSEAS Transactions on Circuits and Systems*, pp. 1109–2734, 2015.

[28] "How to Give Industry a Hand," 2016. [Online]. Available: https://www.siemens.com/innovation/en/home/pictures-of-the-future/digitalization-and-software/autonomous-systems-piezoelectric-robotic-hand.html

[29] F. Spadafora, M. Muzzupappa, F. Bruno, D. Ribas, and P. Ridaob, "Design and Construction of a Robot Hand Prototype for Underwater Applications," in *IFAC (International Federation of Automatic Control)*, 2015.

[30] I. Godler and T. Sonoda, "A Five Fingered Robotic Hand Prototype by using Twist Drive," in *ISR / ROBOTIK*, 2010, pp. 1–6.

[31] L. Kelion, "Open Bionics robotic hand for amputees wins Dyson Award," 2015. [Online]. Available: http://www.bbc.co.uk/news/technology-34044453

[32] "Moley Robotics - Fully Automated Cooking robot." [Online]. Available: http://www.moley.com/about-us/

[33] P. Kyberd, O. Holland, P. Chappell, S. Smith, R. Tregidgo, P. Bagwell, and J. Snaith, "ARCUS: A two degree of freedom hand prosthesis with hierarchical

grip control," *IEEE Transactions on Rehabilitation Engineering*, vol. 3, no. 1, pp. 70–76, 1995.

[34] J. Chu, D. Jung, and Y. Lee, "Design and control of a multifunction myoelectric hand with new adaptive grasping and self-locking mechanisms," in *2008 IEEE International conference on robotics and automation*. IEEE, 2008, pp. 743–748.

[35] M. Carrozza, C. Chiara, and S. Giovanni, "A cosmetic prosthetic hand with tendon driven under-actuated mechanism and compliant joints: ongoing research and preliminary results," in *Proceedings of the 2005 IEEE International Conference on Robotics and Automation*, 2005, pp. 2661–2666.

[36] J. Pons, E. Rocon, R. Ceres, D. Reynaerts, B. Saro, S. Levin, and W. Moorleghem, "The MANUS-HAND Dextrous Robotics Upper Limb Prosthesis: Mechanical and Manipulation Aspects," *Autonomous Robots*, vol. 16, no. 2, pp. 143–163, 2004.

[37] G. Catalano, Mand Grioli, E. Farnioli, A. Serio, C. Piazza, and A. Bicchi, "Adaptive synergies for the design and control of the Pisa/IIT SoftHand," *The International Journal of Robotics Research*, vol. 33, no. 5, pp. 768–782, 2014.

[38] S. Immanuel and G. Schulz, "A New Anthropomorphic Robotic Hand," in *Humanoids 2008-8th IEEE-RAS International Conference on Humanoid Robots*, 2008, pp. 418–422.

[39] J. Iqbal, O. Ahmad, and A. Malik, "HEXOSYS II - Towards realization of light mass robotics for the hand," in *IEEE*. IEEE, 2011.

[40] E. Akyürek, A. Dilly, F. Jourdan, Z. Liu, S. Chattoraj, I. B. Juandeaburre, M. Heinrich, L. Paramonov, P. Turner, Stelarc, and T. Kalganova, " Remote-Controlled Ambidextrous Robot Hand Concept," *Computer Technology ans Application (CTA)*, vol. 4, pp. 569–574, 2013.

[41] E. Akyürek, A. Huynh, and T. Kalganova, "Control of an Asymmetrical Design of a Pneumatically Actuated Ambidextrous Robot Hand," *International Journal of Electrical, Electronics, Communication, Energy Science and Engineering, vol. 8, no. 5,*, 2014.

[42] J. Pertin-Troccaz, "The robotics review 1, chapter grasping: a state of the art." in *The Robotics Review I, O. Khatib, J.J. Craig, and T. LozanoPerez, eds.* Cambridge (MA): MIT Press, 1989, pp. 71–98.

[43] K. Shimoga, "Robot grasp synthesis algorithms: A survey," *The International Journal of Robotics Research*, vol. 15, no. 3, pp. 230–236, 1996.

[44] J. Pons, R. Ceres, F. Pfeiffer, "Multifingered dextrous robotics hand design and control: a review," *Robotica*, vol. 17, no. 6, pp. 661–674, 1999.

[45] M. T. Mason and J. K. Salisbury, "Robot hands and the mechanics of manipulation," in *The MIT Press, Cambridge, MA*, 1985.

[46] S. T. Venkataraman, and T. Iberall, *Dextrous robot hands.* Springer Science & Business Media, 2012.

[47] M. Bianchi and A. Moscatelli, *Human and robot hands.* Springer, 2016.

[48] L. Marchal-Crespo and D. Reinkensmeyer, "Review of control strategies for robotic movement training after neurologic injury," *Journal of NeuroEngineering and Rehabilitation*, vol. 6, no. 1, 2009.

[49] T. C. Hsia, "Adaptive control of robot manipulators - A review," in *Proceedings of IEEE International Conference on Robotics and Automation.* USA: IEEE, 1986, pp. 183–189.

[50] K. Hashimoto, "A review on vision-based control of robot manipulators," *Advanced Robotics,*, vol. 17, no. 10, pp. 969–991, 2003.

[51] C. Abdallah, D. Dawson, P. Dorato, and M. Jamshidi, "Survey of robust control for rigid robots," *Control Systems Magazine*, vol. 11, no. 2, pp. 24–30, 1991.

[52] L. Sciavicco and B. Siciliano, *Modelling and Control of Robot Manipulators 2nd Edition*. Springer, 2000.

[53] H. Ali, S. Noor, and S. Bashi, "A Review of Pneumatic Actuators (Modeling and Control)," *Australian Journal of Basic and Applied Sciences*, vol. 3, no. 2, pp. 440–454, 2009.

[54] A. Ollero and L. Merino, "Control and perception techniques for aerial robotics," *Annual Reviews in Control, Elsevier*, vol. 28, no. 2, pp. 167–178, 2004.

[55] C. Lauretti, F. Cordella, A. L. Ciancio, E. Trigili, J. M. Catalan, F. J. Badesa, S. Crea, S. M. Pagliara, S. Sterzi, N. Vitiello *et al.*, "Learning by demonstration for motion planning of upper-limb exoskeletons," *Frontiers in neurorobotics*, vol. 12, p. 5, 2018.

[56] B. Nagaraj and N. Murugananth, "A comparative study of pid controller tuning using ga, ep, pso and aco," in *2010 International Conference On Communication Control And Computing Technologies*. IEEE, 2010, pp. 305–313.

[57] J. Armendariz, V. Parra-Vega, R. García-Rodríguez, and S. Rosales, "Neuro-fuzzy self-tuning of pid control for semiglobal exponential tracking of robot arms," *Applied Soft Computing*, vol. 25, pp. 139–148, 2014.

[58] A. Belkadi, H. Oulhadj, Y. Touati, S. A. Khan, and B. Daachi, "On the robust pid adaptive controller for exoskeletons: A particle swarm optimization based approach," *Applied Soft Computing*, vol. 60, pp. 87–100, 2017.

[59] S. Jung, S. Yim, and T. Hsia, "Experimental studies of neural network impedance force control for robot manipulators," in *Proceedings 2001 ICRA.*

IEEE International Conference on Robotics and Automation (Cat. No. 01CH37164), vol. 4. IEEE, 2001, pp. 3453–3458.

[60] B. Rudall, "World Robotics 2003," in *131 United Nations Economic Commission for Europe and International Federation of Robotics*, 2003.

[61] Z. Deutsches, "Robotic Hand Powered By Brushless DC Servo Motors." [Online]. Available: https://www.micromo.com/applications/robotics-factory-automation/sensitive-4-finger-hand

[62] M. Bélanger-Barrette, "Top 5 Robotic Applications in the Automotive Industry," 2014. [Online]. Available: https://blog.robotiq.com/bid/69722/Top-5-Robotic-Applications-in-the-Automotive-Industry

[63] S. Choi, G. Zhang, and T. Fuhlbrigge, "Applications and Requirements of Industrial Robots in Meat Processing," in *2013 IEEE International Conference on Automation Science and Engineering (CASE), 2013*, 2013.

[64] T. Ueno and M. Oda, "Robotic hand developed for both space missions on the International Space Station and commercial applications on the ground," in *The 2009 IEEE/RSJ International Conference on Intelligent Robots and Systems October 11-15, 2009 St. Louis, USA*, 2009.

[65] K. Lee and I. Shimoyama, "A skeletal framework articial hand actuated by pneumatic articial muscles." in *Proc. IEEE International Conference on Robotics and Automation,ICRA99, Detroit, Michigan*, 1999.

[66] J. Sancho-Bru, A. Pérez-González, M. Vergara, and D. Giurintano, "A 3D Biomechanical Model of the Hand for Power Grip," *Journal of Biomechanical engineering, vol. 125, pp. 78-83, 2001*, vol. 125, pp. 78–83, 2001.

[67] D. Wilkinson, M. Weghe, and Y. Matsuoka, "An Extensor Mechanism for an Anatomical Robotic Hand," *"Proc. IEEE International Conference on Robotics and Automation,*, vol. 1, pp. 238–243, 2003.

[68] "Festo Exo-hand," 2012, accessed on 05.10.2014. [Online]. Available: http://www.festo.com/cms/en_corp/12713.htm.

[69] T. Laliberté, L. Birglen, and C. Gosselin, "Underactuation in robotic grasping hands," *Japanese Journal of Machine Intelligence and Robotic Control*, vol. 4, no. Special Issue on Underactuated Robots, pp. 77–87, 2002.

[70] G. Stellin, C. Cipriani, F. Zaccone, M. C. Carrozza, C. Laschi, and P. Dario, "Design of an anthropomorphic dexterous hand for a 2-years-old humanoid : ongoing work," in *Proc. RoManSy, Tokyo, Japan,*, 2008.

[71] M. Moran, "Evolution of robotic arms," *Journal of robotic surgery*, vol. 1, no. 2, pp. 103–111, 2007.

[72] H. Paul, Richard P and Rong, Ma and Zhang, "The dynamics of the PUMA manipulator," in *American Control Conference*. IEEE, 1983, pp. 491–496.

[73] D. Gow, W. Douglas, C. Geggie, E. Monteith, and D. Stewart, "The development of the Edinburgh modular arm system," in *Proceedings of the Institution of Mechanical Engineers Part H Journal of Engineering in Medicine*, 2001, pp. 291–298.

[74] D. Bluethmann, William and Ambrose, Robert and Diftler, Myron and Askew, Scott and Huber, Eric and Goza, Michael and Rehnmark, Fredrik and Lovchik, Chris and Magruder, "Robonaut: A robot designed to work with humans in space," *Autonomous robots*, vol. 14, no. 2, pp. 179–197, 2003.

[75] P. Corke, *Robot arm kinematics*. Springer, 2017.

[76] T. Austin-Morgan, "Delft robot arm wins Amazon Picking Challenge," 2016, accessed on 05.11.2017. [Online]. Available: http://www.eurekamagazine.co.uk/design-engineering-news/delft-robot-arm-wins-amazon-picking-challenge/142971/

[77] A. Quigley, Morgan and Asbeck, Alan and Ng, "A low-cost compliant 7-DOF robotic manipulator," in *2011 IEEE International Conference on Robotics and Automation*, 2011, pp. 6051–6058, accessed on 15.10.2015. [Online]. Available: http://mindtrans.narod.ru/pdfs/A_Low_Cost_Compliant_7_DOF_Robotic_Manipulator.pdf

[78] "WAM Arm," 2011, accessed on 04.10.2018. [Online]. Available: http://web.barrett.com/CustomerDocuments/WAMDataSheet_02.2011.pdf

[79] "Benfits of a dual arm robotic system," 2016, accessed on 09.04.2018. [Online]. Available: https://static1.squarespace.com/static/5293f0f7e4b096d144796cd1/t/5a0b2b5a8165f51313791777/1510681436937/Benefits+of+Dual+Arm+Robotic+System.pdf

[80] "SCHUNK Mobile Gripping Systems for higher Productivity in your Service Robotics Application." 2016, accessed on 23.05.2019. [Online]. Available: http://www.schunk-modular-robotics.com/en.html

[81] "S. Robotics, "R17 5-axis robot arm," 2010." 2010, accessed on 05.01.2018. [Online]. Available: http://www.strobotics.com/

[82] "KR 1000 titan," 2013, accessed on 11.12.2018. [Online]. Available: https://www.kuka.com/en-gb/products/robotics-systems/industrial-robots/kr-1000-titan

[83] "Hero Arms," 2018, accessed on 01.07.2019. [Online]. Available: https://openbionics.com/press/

[84] C. Trout, "AMO Arm pneumatic prosthetic does mind-control on the cheap," 2011, accessed on 05.10.2019. [Online]. Available: https://www.engadget.com/2011/04/05/amo-arm-pneumatic-prosthetic-does-mind-control-on-the-cheap/?guccounter=1

[85] Z. Lu, A. Chauhan, F. Silva, and L. Lopes, "A Brief Survey of Commercial Robotic Arms for Research on Manipulation," in *IEEE Symposium on Robotics and Applications(ISRA)*. IEEE, 2012, pp. 986–991.

[86] O. Bas, "Robotic arm by Onur Bas," 2012, accessed on 02.08.2018. [Online]. Available: https://grabcad.com/library/robotic-arm--8

[87] L. Orejel, "Robotic arm by Luis Orejel," 2013, accessed on 07.10.2020. [Online]. Available: https://grabcad.com/library/robotic-arm-7

[88] R. Guyser, "Simple robotic arm-Airbrush," accessed on 13.03.2018. [Online]. Available: https://grabcad.com/library/simple-robotic-arm-airbrush

[89] E. Rodriguez, "Robot Arm for Airbrushing," accessed on 23.11.2018. [Online]. Available: https://grabcad.com/library/robotic-arm-airbrushing-1

[90] R. Rhonda, "NASA, Main System Integration Standards, 1(3), Anthropometry and Biomechanics," accessed on 24.09.2020. [Online]. Available: http://msis.jsc.nasa.gov/sections/section03.htm

[91] Y. Nakamura and H. Hanafusa, "Inverse Kinematic Solutions With Singularity Robustness for Robot Manipulator Control," *ASME. J. Dyn. Sys., Meas., Control*, vol. 108, no. 3, pp. 163–171, 1986.

[92] M. W. Walker, "Adaptive Control of Manipulators Containing Closed Kinematic Loops," *IEEE Transactions on Robotics and Automation*, vol. 6, no. 1, 1990.

[93] J. Liu and K. Abdel, "Robust Control of Planar Dual-Arm Cooperative Manipulators," *Robotics and Computer-Integrated Manufacturing*, vol. 16, no. 2-3, pp. 109–119, 2000.

[94] C. Cheah, C. Liu, and J. Slotine, "Adaptive Jacobian Tracking Control of Robots With Uncertainties in Kinematic, Dynamic and Actuator Models," *IEEE Transactions on Automatic Control*, vol. 51, no. 6, 2006.

[95] B. Tondu, V. Boitier, and P. López., "Naturally Compliant Robot-Arms Actuated By Mckibben Artificial Muscles," in *IEEE International Conference*, 1994, pp. 2635–2637.

[96] B. Tondu and P. López, "Modeling and Control of Mckkiben Artificial Muscle Robot Actuators," in *IEEE Control Systems Magazine*, 2000, pp. 22–29.

[97] K. Ahn and P. Ho, "Design and implementation of an adaptive recurrent neural networks (ARNN) controller of the pneumatic artificial muscle (PAM) manipulator," *Mechatronics*, vol. 19, no. 6, pp. 816–828, 2009.

[98] J. B. Christoph Hartmann, O. Obst, S. Ikemoto, and M. Asada, *Real-Time Inverse Dynamics Learning for Musculoskeletal Robots based on Echo State Gaussian Process Regression.* Springer, 2012.

[99] B. Tondu, S. Ippolito, J. Guiochet, and A. A. Daidie., "Seven Degrees of Freedom Robot Arm Driven by Pneumatic Artificial Muscles for Humanoid Robots," *The International Journal of Robotics Research*, pp. 268–272, 2005.

[100] A. Caballero and P. Cortés, "Prototipo Experimental para la Identificación y Control de Actuadores por Músculo Neumático, Elsevier -Revista Iberoamericana de Automática," *Informática Industrial*, vol. 7, no. 8, pp. 1–3, 2003.

[101] A. Al-Jodah and L. Khames, "Second Order Sliding Mode Controller Design for Pneumatic Artificial Muscle," *Journal of Engineering (IASJ)*, vol. 1, no. 24, pp. 159–172, 2018.

[102] C. Lee, K. Jeong, and H. Lee, "Motion control of mobile manipulator based on neural networks and error compensation," *Proceedings - IEEE International Conference on Robotics and Automation*, vol. 5, no. 5, pp. 4627–4632, 2004.

[103] Y. Kung and G. Shu, "Development of a FPGA-based motion control IC for robot arm," in *IEEE International Conference on Industrial Technology*, 2006, pp. 1397–1402.

[104] A. Tunwannarux and S. Tunwannarux, "Design of a 5-Joint Mechanical Arm with User Friendly Control Program," *World Academy of Science, Engineering and Technology,International Journal of Mechanical, Aerospace, Industrial, Mechatronic and Manufacturing Engineering*, vol. 2, no. 1, 2008.

[105] G. Huang, C. Tung, C. Lin, and S. Hsiao, "Inverse kinematics analysis trajectory planning for a robot arm," in *8th Asian Control Conference (ASCC)*, 2011.

[106] R. Szabo and A. Gontean, "Remotely commanding the lynxmotion AL5 type robotic arms," in *21st Telecommunications Forum (TELFOR)*, 2013.

[107] A. Gontean and R. Szabo, "Robotic Arm Control Algorithm Based on Stereo Vision Using RoboRealm Vision," *Advances in Electrical and Computer Engineering*, vol. 15, no. 2, pp. 65–74, 2015.

[108] J. D. Greer, T. K. Morimoto, A. M. Okamura, and E. W. Hawkes, "Series Pneumatic Artificial Muscles (sPAMs) and Application to a Soft Continuum Robot," in *IEEE Int Conf Robot Autom*, 2017, pp. 5503–5510.

[109] M. Ariyanto, R. Ismail, A. Nurmiranto, W. Caesarendra, and J. Paryanto, "Development of a Low Cost Anthropomorphic Robotic Hand Driven by Modified Glove Sensorand Integrated with 3D Animation," in *IEEE EMBS Conference on Biomedical Engineering and Sciences (IECBES)*, 2016.

[110] "8-bit Atmel Microcontroller Datasheet," 2014, accessed on 21.01.2019. [Online]. Available: http://www.atmel.com/Images/Atmel-2549-8-bit-AVR-Microcontroller-ATmega640-1280-1281-2560-2561_datasheet.pdf

[111] E. Roche, "Pneumatic Artificial Muscles," accessed on 18.04.2020. [Online]. Available: https://softroboticstoolkit.com/book/pneumatic-artificial-muscles

[112] "The difference between ABS and PLA for 3D printing," accessed on 05.07.2016. [Online]. Available: http://www.protoparadigm.com/news-updates/the-difference-between-abs-and-pla-for-3d-printing/

[113] E. Ackerman, "Dex-Net 4.0 Enables 'Ambidextrous' Robots to Choose Best Gripper for the Job," accessed on 19.07.2020. [Online]. Available: https://spectrum.ieee.org/automaton/robotics/artificial-intelligence/a-choice-of-grippers-helps-dualarm-robot-pick-up-objects-faster-than-ever

[114] J. Mahler, M. Matl, V. Satish, M. Danielczuk, B. DeRose, S. McKinley, and K. Goldberg, "Learning ambidextrous robot grasping policies," *Artificial Intelligence (Science Robotics)*, vol. 4, no. 26, 2019.

[115] "Scientists develop novel 'ambidextrous' approach for self-learning robot," 2019, accessed on 05.10.2020. [Online]. Available: https://www.theweek.in/news/sci-tech/2019/01/17/Scientists-develop-novel-ambidextrous-approach-for-self-learning-robots.html

[116] B. W. Kraft, "Ambidextrous robotic master controller," USA, 2007.

[117] M. Mukhtar, E. Akyürek, T. Kalganova, and N. Lesne, "Control of 3D printed ambidextrous robot hand actuated by pneumatic artificial muscles," in *SAI Intelligent Systems Conference (IntelliSys), 2015. IEEE*, 2105.

[118] "Elbow-joint-movement." [Online]. Available: http://www.imagekb.com/elbow-joint-movement

[119] K. Young, C. Warren, R. Budynas, and S. Gordon, *Roark's formulas for stress and strain.* McGraw-hill New York, 2011, vol. 7.

[120] K. Yong, "A Multi-sensor System Applied to Control an Intelligent Robotic Hand for Underwater Environment." in *2009 International Conference on Mechatronics and Automation*, 2009, pp. 513–518.

[121] A. D. Deshpande, J. Ko, D. Fox, and Y. Matsuoka, "Anatomically Correct Testbed Hand Control: Muscle and Joint Control Strategies," in *IEEE International Conference on Robotics and Automation, , pp. 4416-4422.*, 2009.

[122] "Shadow Dexterous Hand E1M3R, E1M3L." Shadow, accessed on 17.11.2018. [Online]. Available: http://www.shadowrobot.com/products/dexterous-hand/

[123] N. Tsujiuchi, T. Koizumi, H. Kan, H. Takeda, T. Kudawara, and M. Hirano, "Modeling and control of a joint driven by pneumatic actuator," in *Industrial Electronics IECON '09. 35th Annual Conference of IEEE*, 2009, pp. 2271–2276.

[124] X. Jiang, C. Xiong, R. Sun, and Y. Xiong, "Characteristics of the Robotic Arm of a 9-DoF Upper Limb Rehabilitation Robot Powered by Pneumatic Muscles," *ICIRA*, vol. LNAI 6425, pp. 463–474, 2010.

[125] N. Tsujiuchi, T. Koizumi, S. Nishino, H. Komatsubara, T. Kudawara, and M. Hirano, "Development of Pneumatic Robot Hand and Construction of Master-Slave System," *Journal of System Design and Dynamics*, vol. 2, no. 6, pp. 1306–1315, 2008.

[126] J. Wang, J. Pu, and P. Moore, "Accurate position control of servo pneumatic actuatorsystems: an application to food packaging," *Control Engineering Practice*, vol. 7, pp. 699–706, 1999.

[127] K. Ahn and H. Anh, "Design and Implementation an Adaptive Takagi-Sugeno Fuzzy Neural Networks Controller for the 2-Links Pneumatic Artificial Muscle(PAM) Manipulator using in Elbow Rehabilitation," in *First International Conference on Communications and Electronics*, 2006, pp. 356–361.

[128] J. Wu, J. Huang, and Y. Wang, "RLS-ESN based PID control for rehabilitation robotic arms driven by PM-TS actuators," in *The 2010 International Conference on Modelling, Identification and Control (ICMIC)*, 2010, pp. 511–516.

[129] H. Anh and K. Ahn, "Hybrid control of a pneumatic artificial muscle (PAM) robot arm using an inverse NARX fuzzy model," *Journal Engineering Applications of Artificial Intelligence*, vol. 24, no. 4, pp. 697–716, 2011.

[130] G. Xiang and J. F. Zheng, "Design study of an adaptive fuzzy-PD controller for pneumatic servo system," *Control Engineering Practice*, vol. 13, pp. 55–65, 2005.

[131] D. Tu and K. Kyoung, "Nonlinear PID control to improve the control performance of 2 axes pneumatic artificial muscle manipulator using neural network," *Mechatronics*, vol. 16, pp. 577–587, 2006.

[132] T. Yanbing and W. Xiaoxin, "Parameter self-tuning of PID in pneumatic artificial muscle joint based on PSO algorithm," in *29th Chinese Control Conference (CCC)*, 2010, pp. 3205–3208.

[133] R. Guyser, B. Verrelst, F. Daerden, and D. Lefeber, "Pressure Control with On-Off Valves of Pleated Pneumatic Artificial Muscles in a Modular One-Dimensional Rotational Joint," in *International Conference on Humanoid Robots*, 2003, pp. 761–768.

[134] B. Vanderborght, R. Verrelst, R. Ham, V. Damme, P. Beyl, and D. Lefeber, "Torque and compliance control of the pneumatic artificial muscles in the biped "Lucy""," *Robotics and Automation, 2006. ICRA 2006. Proceedings 2006 International Conference*, pp. 842–847, 2006.

[135] G. Andrikopoulos, G. Nikolakopoulos, and S. Manesis, "Advanced Non-linear PID Based Antagonistic Control for Pneumatic Muscle Actuators," *IEEE Transactions on Industrial Electronics*, pp. 1–12, 2014.

[136] Z. Bingul, H. Ertunc, and C. Oysu, "Applying neural network to inverse kinematic problem for 6r robot manipulator with offset wrist," in *Adaptive and Natural Computing Algorithms*. Springer, 2005, pp. 112–115.

[137] A. T. Hasan, H. Al-Assadi, A. A. M. Isa, and K. Suzuki, "Neural networks' based inverse kinematics solution for serial robot manipulators passing through singularities," in *Artificial Neural Networks. Industrial and Control Engineering Applications.* InTech, 2011.

[138] S. Oltean, D. Şoaita, M. Dulau, and T. Jovrea, "Aspects of interdisciplinarity in the mrip 02 system design," in *International Conference "Optimization of the Robots and Manipulators" OPTIROB*, 2007, pp. 121–125.

[139] C. Secară and L. Vlădăreanu, "Iterative genetic algorithm based strategy for obstacles avoidance of a redundant manipulator," in *Proceedings of the 2010 American conference on Applied mathematics.* World Scientific and Engineering Academy and Society (WSEAS), 2010, pp. 361–366.

[140] H. Cao, G. Si, Y. Zhang, and X. Ma, "A hybrid controller of self-optimizing algorithm and anfis for ball mill pulverizing system," in *2007 International Conference on Mechatronics and Automation.* IEEE, 2007, pp. 3289–3294.

[141] N. Courty and E. Arnaud, "Inverse kinematics using sequential monte carlo methods," in *International Conference on Articulated Motion and Deformable Objects.* Springer, 2008, pp. 1–10.

[142] C. S. Dumitriu *et al.*, "Direct search based strategy for obstacle avoidance of a redundant manipulator." *Analele Universitatii'Eftimie Murgu'*, vol. 17, no. 1, 2010.

[143] L. Wang and C. Chen, "A combined optimization method for solving the inverse kinematics problems of mechanical manipulators," *IEEE Transactions on Robotics and Automation*, vol. 7, no. 4, pp. 489–499, 1991.

[144] P. Kalra, P. Mahapatra, and D. Aggarwal, "An evolutionary approach for solving the multimodal inverse kinematics problem of industrial robots," *Mechanism and machine theory*, vol. 41, no. 10, pp. 1213–1229, 2006.

[145] R. KOuml *et al.*, "A neuro-genetic approach to the inverse kinematics solution of robotic manipulators," *Scientific Research and Essays*, vol. 6, no. 13, pp. 2784–2794, 2011.

[146] J. Ramirez, A. Rubiano *et al.*, "Optimization of inverse kinematics of a 3r robotic manipulator using genetic algorithms," *World Academy of Science, Engineering and Technology*, vol. 59, pp. 1425–1430, 2011.

[147] S. Tabandeh, C. Clark, and W. Melek, "A genetic algorithm approach to solve for multiple solutions of inverse kinematics using adaptive niching and clustering," in *2006 IEEE International Conference on Evolutionary Computation*. IEEE, 2006, pp. 1815–1822.

[148] B. Daya, S. Khawandi, M. Akoum *et al.*, "Applying neural network architecture for inverse kinematics problem in robotics," *Journal of Software Engineering and Applications*, vol. 3, no. 03, p. 230, 2010.

[149] J. F. Gardner, A. Brandt, and G. Luecke, "Applications of neural networks for coordinate transformations in robotics," *Journal of Intelligent and Robotic Systems*, vol. 8, no. 3, pp. 361–373, 1993.

[150] H. Jack, D. Lee, R. Buchal, and W. H. Elmaraghy, "Neural networks and the inverse kinematics problem," *Journal of intelligent manufacturing*, vol. 4, no. 1, pp. 43–66, 1993.

[151] B. Vanderborght, B. Verrelst, R. V. Ham, J. Vermeulen, and D. Lefeber, "Dynamic Control of a Bipedal Walking Robot actuated with Pneumatic Artificial Muscles," in *Proceedings of the 2005 IEEE International Conference on Robotics and Automation*, 2005, pp. 1–6.

[152] M. Zinn, O. Khatib, B. Roth, and J. Salisbury, "Towards a human centered intrinsically-safe robotic manipulator," *In Proc. of IARP/IEEERAS Joint Workshop Toulouse, France*, 2002.

[153] F. Salem and A. Rashed, "PID Controllers and Algorithms:Selection and Design Techniques Applied in Mechatronics Systems Design - Part II," in *International Journal of Engineering Sciences,*, 2013, pp. 191–203.

[154] "Bang–bang control," 2014, accessed on 18.04.2020. [Online]. Available: http://en.wikipedia.org/wiki/Bang\T1\textendashbang_control

[155] M. Aware, A. Kothari, and S. Choube, "Application of adaptive neuro-fuzzy controller (anfis) for voltage source inverter fed induction motor drive," in *Proceedings IPEMC 2000. Third International Power Electronics and Motion Control Conference (IEEE Cat. No. 00EX435)*, vol. 2. IEEE, 2000, pp. 935–939.

[156] C. Lee and J. Lee, "Multiple neuro-adaptive control of robot manipulators using visual cues," *IEEE transactions on industrial electronics*, vol. 52, no. 1, pp. 320–326, 2005.

[157] R. Swasti and P. Sidhartha, "Anfis approach for tcsc-based controller design system stability improvement design for power," *IEEE ICCCCT-10*, pp. 149–154, 2010.

[158] M. Jasim, "Solution of inverse kinematics for scara manipulator using adaptive neuro-fuzzy network," *International Journal on Soft Computing*, vol. 2, no. 4, p. 59, 2011.

[159] M. F. Queen, M. SasiKumar, and P. BabuAurtherson, "Inverse kinematics solution of 4 dof industrial manipulator using neuro-fuzzy network," *International Journal of Emerging Technology and Advanced Engineering*, vol. 2, no. 8, pp. 276–280, 2012.

[160] R. Pérez-Rodríguez, A. Marcano-Cedeño, Ú. Costa, J. Solana, C. Cáceres, E. Opisso, J. M. Tormos, J. Medina, and E. J. Gómez, "Inverse kinematics of a 6 dof human upper limb using anfis and ann for anticipatory actuation

in adl-based physical neurorehabilitation," *Expert Systems with Applications*, vol. 39, no. 10, pp. 9612–9622, 2012.

[161] G. Strang, *Introduction to linear algebra*. Wellesley-Cambridge Press Wellesley, MA, 1993.

[162] M. Mukhtar, "Ambidextrous robot arm follow a circuler path in Y-Z plane." 2020, accessed on 23.12.2020. [Online]. Available: https://youtu.be/Zs0Hu-36v1U

[163] ——, "Ambidextrous robot arm follow a circuler path in X-Y-Z," 2020, accessed on 23.12.2020. [Online]. Available: https://youtu.be/cylZKJxEQmo

[164] ——, "Ambidextrous robot arm follow an Arc path in X-Y-Z." 2020, accessed on 23.12.2020. [Online]. Available: https://youtu.be/LCLuUSQlPRw

[165] ——, "Ambidextrous robot arm follow a combined curves path in X-Y-Z." 2020, accessed on 23.12.2020. [Online]. Available: https://youtu.be/J-TC2Tavzb0

[166] A. Mohammed, B. Schmidt, L. Wang, and Gao, "Minimizing energy consumption for robot arm movement," *Procedia Cirp*, vol. 25, no. 25, pp. 400–405, 2014.

[167] T. Kroger, "Online trajectory generation: Straight-line trajectories," *IEEE Transactions on Robotics*, vol. 27, no. 5, pp. 1010–1016, 2011.

[168] M. Mukhtar, "Conventional Arm," 2019, accessed on 18.04.2020. [Online]. Available: https://www.youtube.com/watch?v=HqWU3t8559o

[169] ——, "Ambidextrous Robot Arm," 2019, accessed on 18.04.2020. [Online]. Available: https://www.youtube.com/watch?v=RSA_T472_hA

[170] V. Falkenhahn, T. Mahl, A. Hildebrandt, R. Neumann, and O. Sawodny, "Dynamic modeling of constant curvature continuum robots using the Euler-

Lagrange formalism," in *2014 IEEE/RSJ International Conference on Intelligent Robots and Systems*. IEEE, 2014, pp. 2428–2433.

APPENDIX A

Transformation Matrix of the Robot

$$r_{11} = [(C\theta_1 C\theta_2 C\theta_3 - S\theta_1 S\theta_3)C\theta_4 - (C\theta_1 S\theta_2 S\theta_4)]C\theta_5 + (-C\theta_1 C\theta_2 S\theta_3 - S\theta_1 C\theta_3)S\theta_5 \tag{A.1}$$

$$r_{12} = [(C\theta_1 C\theta_2 C\theta_3 - S\theta_1 S\theta_3)C\theta_4 - (C\theta_1 S\theta_2 S\theta_4)](-S\theta_5) + (-C\theta_1 C\theta_2 S\theta_3 - S\theta_1 C\theta_3)C\theta_5 \tag{A.2}$$

$$r_{13} = -(C\theta_1 C\theta_2 C\theta_3 - S\Theta_1 S\theta_3)S\theta_4 - (C\theta_1 S\theta_2 C\theta_4) \tag{A.3}$$

$$r_{21} = [(S\theta_1 C\theta_2 C\theta_3 + C\theta_1 S\theta_3)C\theta_4 - (S\theta_1 S\theta_2 S\theta_4)]C\theta_5 + (-S\theta_1 C\theta_2 S\theta_3 - C\theta_1 C\theta_3)S\theta_5 \tag{A.4}$$

$$r_{22} = [(S\theta_1 C\theta_2 C\theta_3 + C\theta_1 S\theta_3)C\theta_4 - (S\theta_1 S\theta_2 S\theta_4)](-S\theta_5) + (-S\theta_1 S\theta_2 S\theta_3 - C\theta_1 C\theta_3)C\theta_5 \tag{A.5}$$

$$r_{23} = -(S\theta_1 C\theta_2 C\theta_3 + C\theta_1 S\theta_3)S\theta_4 - (S\theta_1 S\theta_2 C\theta_4) \tag{A.6}$$

$$r_{31} = (S\theta_2 C\theta_3 C\theta_4 + S\theta_4 C\theta_2)C\theta_5 - (S\theta_2 S\theta_3 S\theta_5) \tag{A.7}$$

$$r_{32} = (S\theta_2 C\theta_3 C\theta_4 + S\theta_4 C\theta_2)(-S\theta_5) - (S\theta_2 S\theta_3 S\theta_5) \tag{A.8}$$

$$r_{33} = -S\theta_2 C\theta_3 C\theta_4 + C\theta_2 C\theta_4 \tag{A.9}$$

$$d_x = [-(C\theta_1 C\theta_2 C\theta_3 + S\theta_1 S\theta_3)S\theta_4 - (C\theta_1 S\theta_2 C\theta_4)](l_4 + l_5) - (l_2 + l_3) - (C\theta_1 S\theta_2) \tag{A.10}$$

$$d_y = [-(S\theta_1 C\theta_2 C\theta_3 + C\theta_1 S\theta_3)S\theta_4 + (S\theta_1 S\theta_2) - (C\theta_4)](l_4 + l_5) - (l_2 + l_3) - (S\theta_1 S\theta_2) \tag{A.11}$$

$$d_z = -(S\theta_2 C\theta_3 S\theta_4 + C\theta_2 C\theta_4)(l_4 + l_5) + (l_2 + l_3)(C\theta_2) + l_1 \tag{A.12}$$

APPENDIX B

Simulink Environment

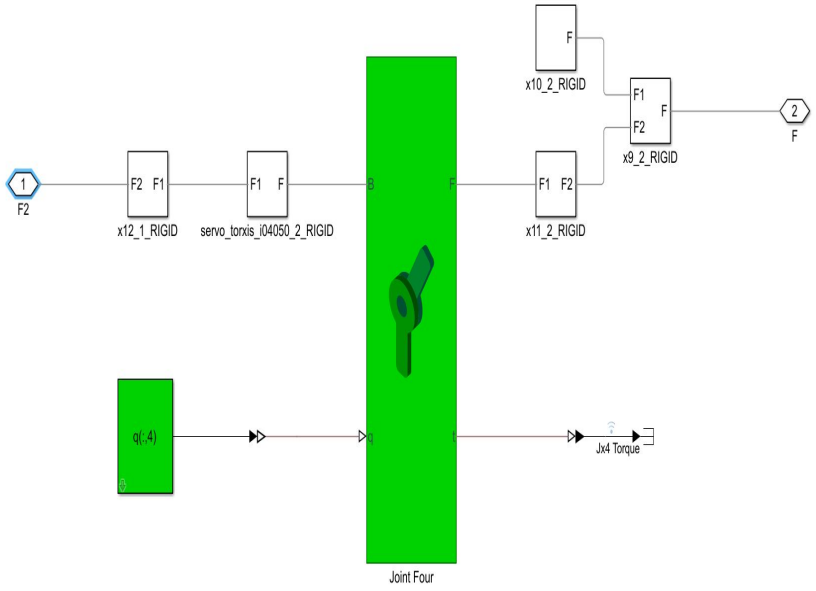

Figure B.1: Simulink block diagram for joint four of the ambidextrous arm.

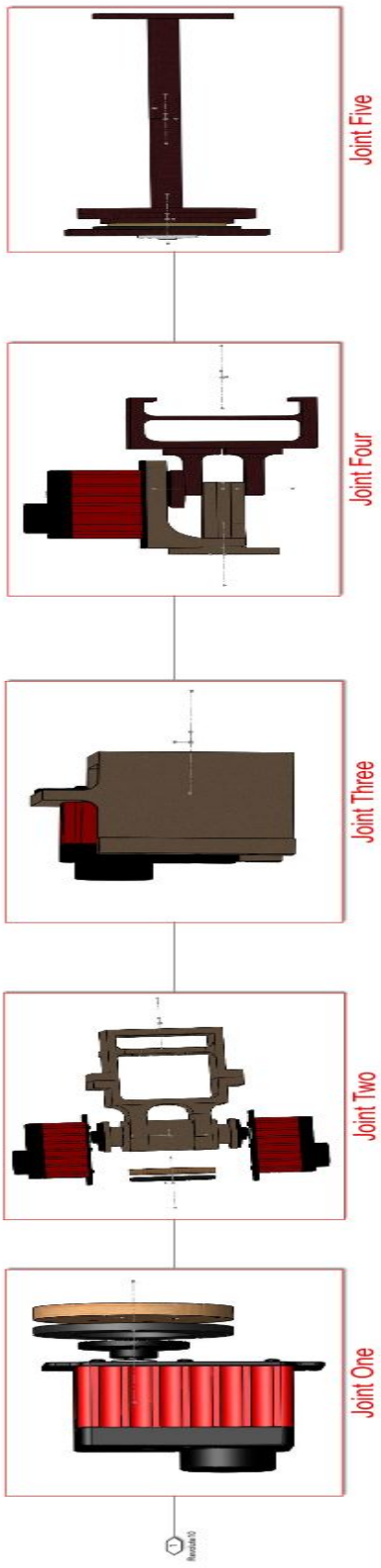

Figure B.2: Simulink block diagram for the ambidextrous arm.

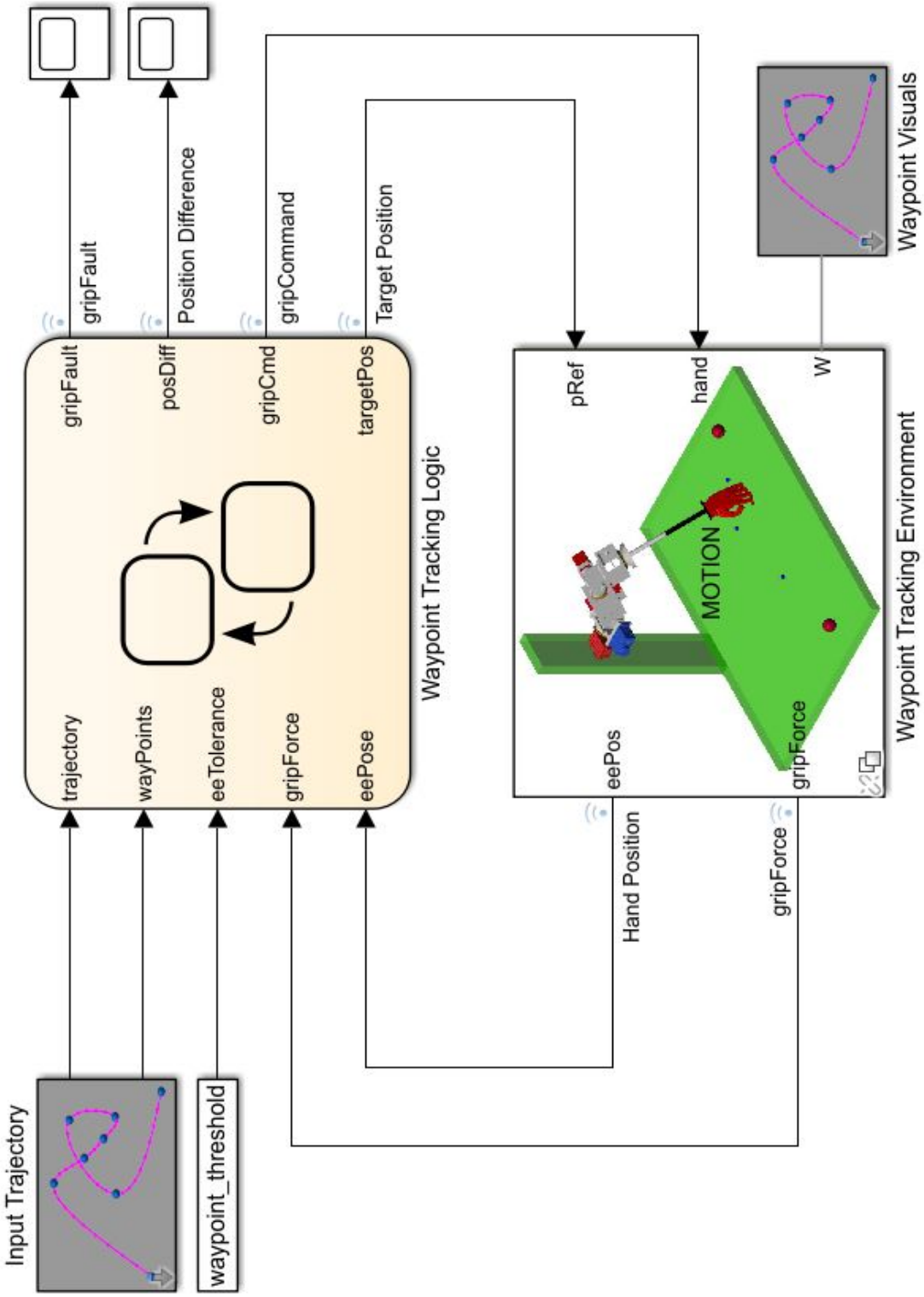

Figure B.3: Simulink block diagram for the controller of the ambidextrous arm.

APPENDIX C

The Robot Specification

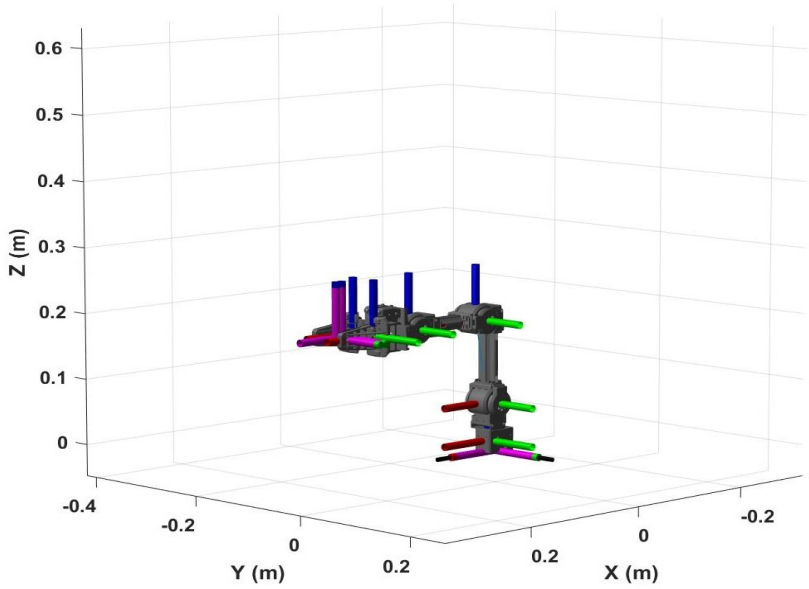

Figure C.1: The coordinate system in each joint for the conventional robot arm.

Table C.1: The conventional robot specifications.

Idx	Body Name	Joint Name	Joint Type	Parent Name	Children Name
1	link1	World fixed	fixed	world	link1
2	link2	joint1	revolute	link1	link2
3	link3	joint2	revolute	link2	link3
4	link4	joint3	revolute	link3	link4
5	link5	joint4	revolute	link4	link5
6	link6	joint5	revolute	link5	link6

Table C.2: DH parameter of the conventional robot arm.

Link	a_i(cm)	d_i(m)	α_i(deg)	θ_i(deg)
1	2.5	0	0	θ_1
2	5.0	0	0	θ_2
3	12.5	0	0	θ_3
4	12.5	0	90	θ_4
5	15.0	0	0	θ_5

APPENDIX D

Finite Element Analysis

FEA of Elbow Design: As a result of the finite element analysis for an applied force of 40 N at the moved point, a value of maximum stress of 5.592 MPa was obtained which offers an acceptable safety coefficient of 1.43. The downside is the hole deformation that needs to be reduced on future designs. This can be done by moving the hole upwards, leaving more space for material below it, what should help to alleviate the tension at the critical red region of Figure D.1.

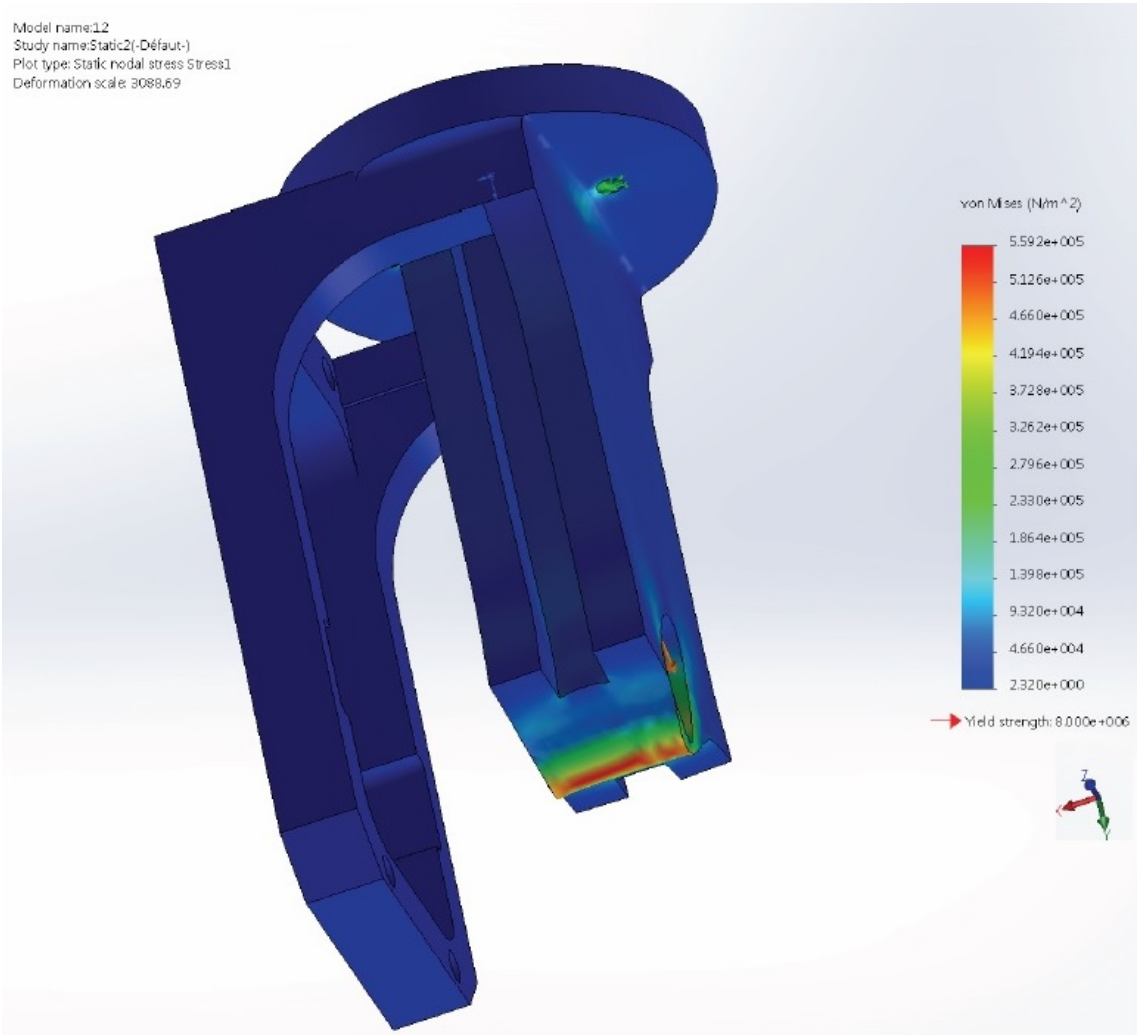

Figure D.1: FEA for the new elbow flexion joint design.

FEA of Shoulder Design: The redesign and addition of material at the critical middle hole that supports the weight of the structure resulted in an acceptable maximum active tension of 2.016 MPa, almost four times less than the material yield value (Figure D.2). This proves the abovementioned materials ability to deliver an excellent tensile mechanical resistance with relatively low weight and also the efficiency of FEA based design.

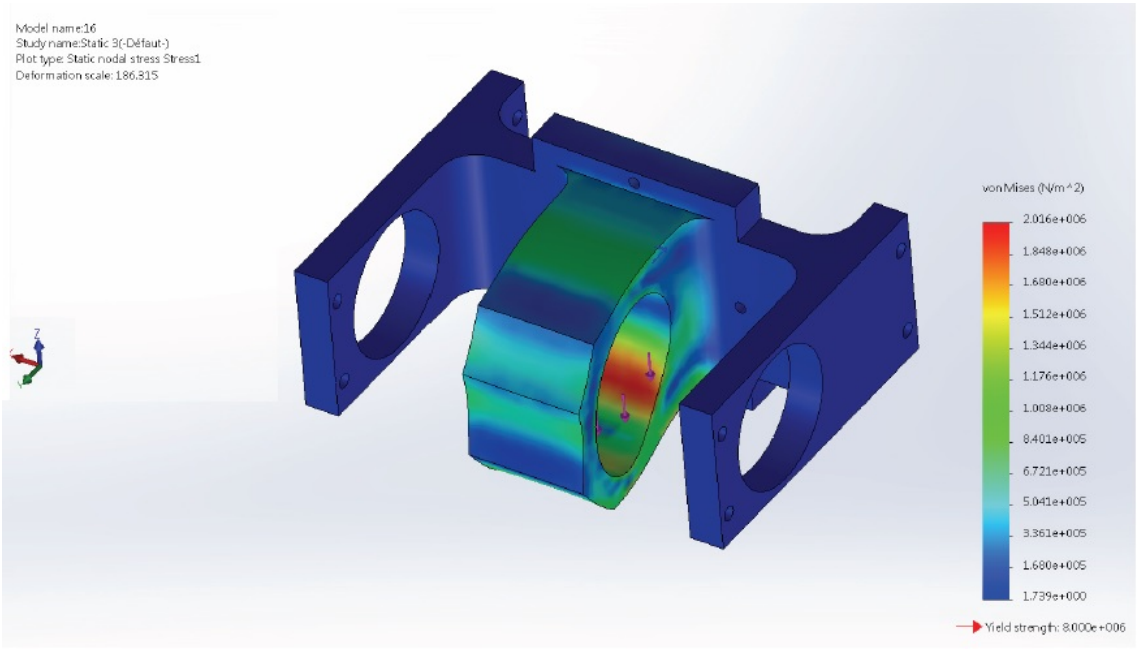

Figure D.2: Shoulder joint, new hole part design.

Despite the big red area of the stress diagram on Figure D.3, the maximum active tension of 1.581 MPa on the new shaft part design is also way below the 8 MPa yield strength for the P430-ABSplus material, providing reliability in terms of plastic deformation and fatigue. As in the other cases, attention should be paid to the deformation and future work done on minimising it, both using FEA analysis based design and looking for new 3D printing alternatives that use better materials.

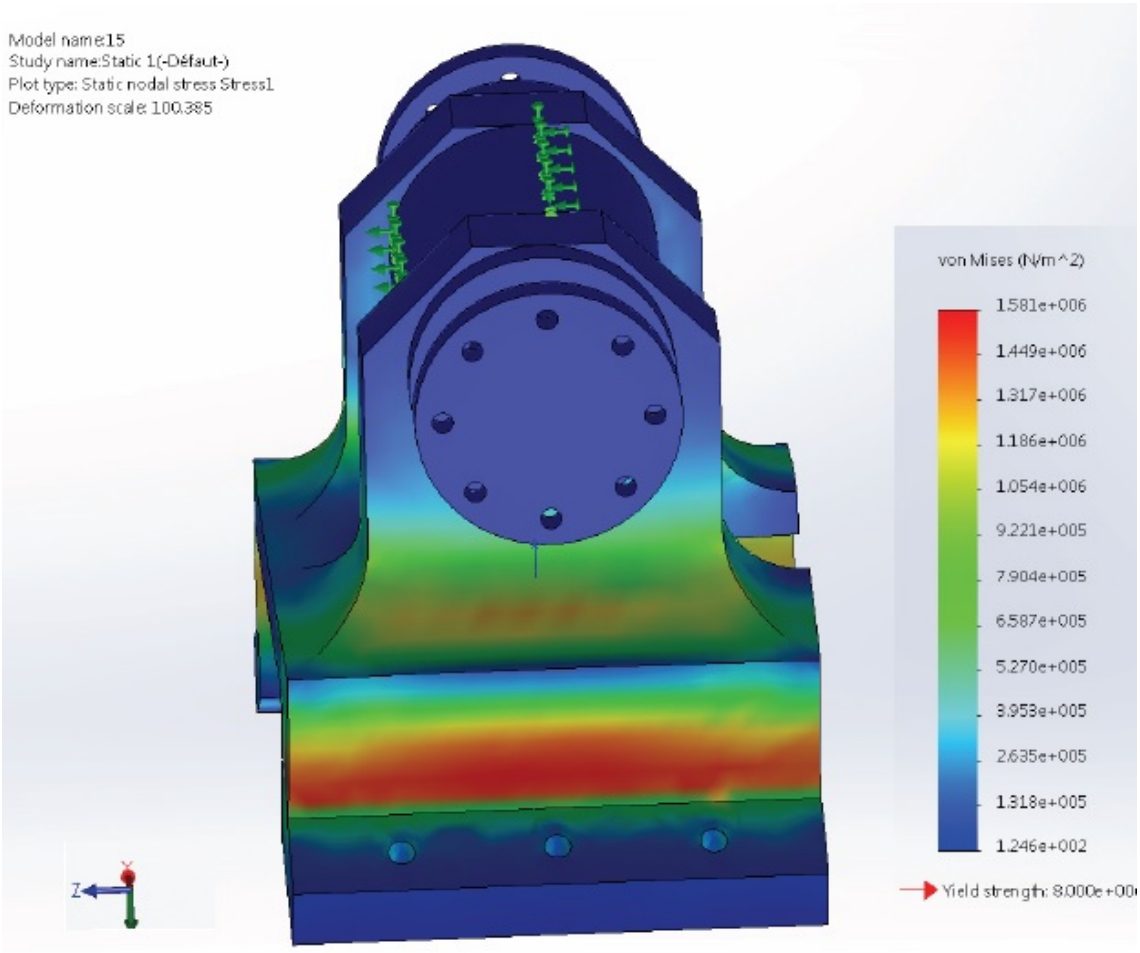

Figure D.3: Shoulder joint, the new shaft part design.

APPENDIX E

Comparison of Existing Ambidextrous Hand and Modified Version

Comparison of existing ambidextrous hand and modified version is shown in Table E.1. For detail steps of hand modification process please refer to 3.1.

Table E.1: Comparison of existing ambidextrous hand and modified version.

-	Existing hand	Modified hand
Year	2015	2018
Mass	3.2 kg	2.3 kg
3D printed solution	No, forearm and base was made of metal making system bulky and difficult to interlink with arm.	Yes, completely 3D printed (lightweight solution)
Use of adapters for efficient distribution of air flow.	No	Yes, (Ambidextrous movements of wrist able to move 0° - 180°).
Wrist movements	No	Yes, (Ambidextrous movements at both elbow and shoulder joints).
Arm movements	No	Yes, (Ambidextrous movements at both elbow and shoulder joints).

-	Existing hand	Modified hand
Controllers implemented	PPSC (Phasing Plane Switch Control), Bang-bang, SMC (Sliding Mode Control), Proportional-integral-derivative (PID) and Backstepping (All controllers implemented on 4 fingers).	Combined use of PID with Neural Networks, Backstepping and Bang-bang (All controllers implemented on 5 fingers).
Thumb control	No	Yes, (force sensors incorporated and data is driven to better reflect the efficiency of controllers tested).
Hose tail connector (between pneumatic circuit and air compressor)	4 mm	8 mm (offers better speed than existing systems).
Electronic and valves interface	Poor design (risk of short circuit, less efficient air flow and risk of wrong connections). See Figure E.1	Re-designing of complete circuit by designing new electronic circuit on printed circuit board (PCB) and use of valve adapter. See Figure E.2

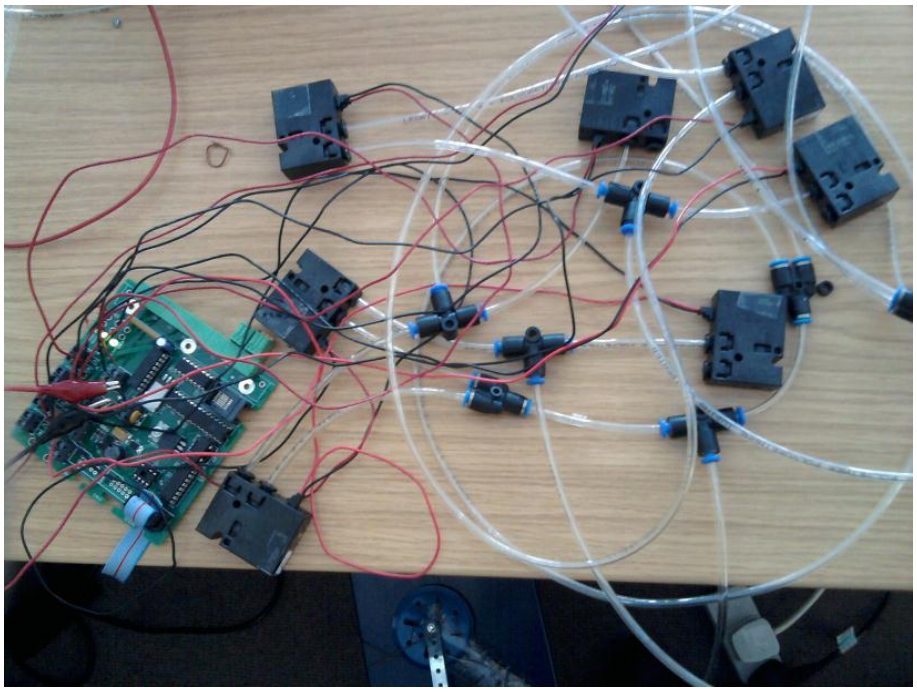

Figure E.1: Existing circuit

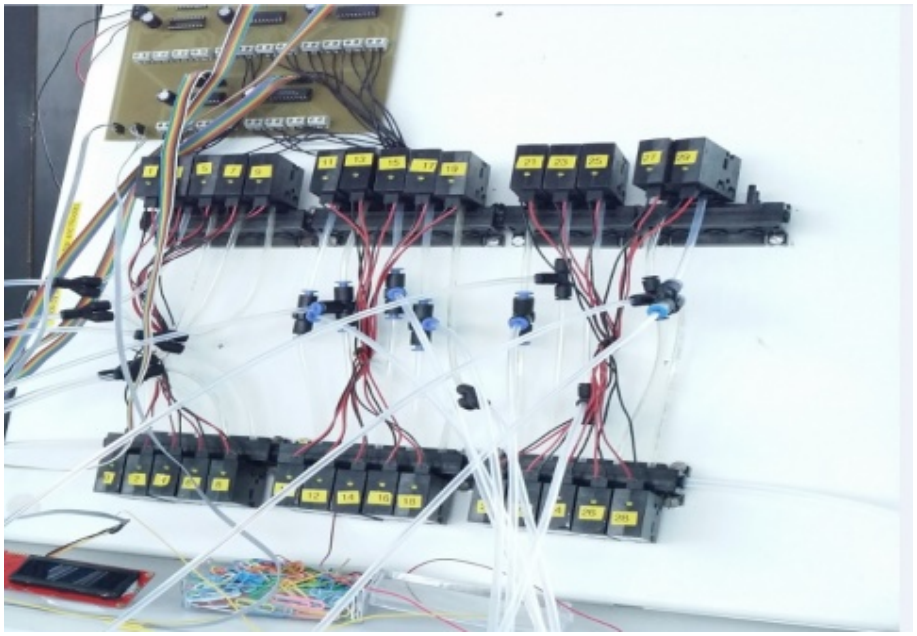

Figure E.2: New circuit